August 2016

An Evaluation of Paleomagnetic Techniques to Determine Emplacement Temperatures of Pyroclastic Density Currents at Mount St. Helens

Devin Gerzich
University of Wisconsin-Milwaukee

AN EVALUATION OF PALEOMAGNETIC TECHNIQUES TO DETERMINE EMPLACEMENT TEMPERATURES OF PYROCLASTIC DENSITY CURRENTS AT MOUNT ST. HELENS

by

Devin Gerzich

A Thesis Submitted in

Partial Fulfillment of the

Requirements for the Degree of

Master of Science

in Geosciences

at

The University of Wisconsin-Milwaukee

August 2016

ABSTRACT

AN EVALUATION OF PALEOMAGNETIC TECHNIQUES TO DETERMINE EMPLACEMENT TEMPERATURES OF PYROCLASTIC DENSITY CURRENTS AT MOUNT ST. HELENS

by

Devin Gerzich

The University of Wisconsin-Milwaukee, 2016
Under the Supervision of Assistant Professor Julie Bowles

During a volcanic eruption, pyroclastic density currents (PDCs) deposit new pumice and ash and rip out and transport lithic fragments from past eruptions. Magnetic minerals in the lithic fragments, such as titanomagnetite, may be partially or completely remagnetized, depending on their emplacement temperature with respect to their Curie and blocking temperatures. By finding the temperature at which this remagnetized overprint is removed, the emplacement temperature of the pyroclastic flow is estimated. This method assumes that the rock magnetic properties that govern magnetic unblocking are constant given a specific magnetic mineral composition, but recent studies demonstrate that Curie temperatures (T_c) in many natural titanomagnetites are a strong function of thermal history. Such variations in Curie temperature may bias estimates of PDC emplacement temperature. The purpose of this study is to evaluate the extent to which this is true.

In 2014, ash, pumice, and lithic clasts from pyroclastic debris containing titanomagnetite were collected from the pumice fields north of Mount St. Helens in order to satisfy the three goals of this study. The goals of this study were to (1) examine how the temperature at which magnetization is removed varies with thermal history; (2) determine to what extent this might

bias emplacement temperature estimates; and (3) to examine how stratigraphic variations in magnetic properties might be used to estimate emplacement temperature.

In reference to goal #1, it has already been found that Curie temperatures in at least one section of the May 18th, 1980 flow increase with depth, in accordance with variations in cooling rates (Bowles et al., 2013). Unoriented pumice samples from the same section were thermally demagnetized, and it was found that blocking temperatures also increase with depth. The maximum unblocking temperature increased from ~415°C at the surface to ~465°C at 90 cm depth, suggesting that paleomagnetically-determined emplacement temperatures may be biased by up to ~50°C. This increase in unblocking temperature with depth is most plausibly explained by cation reordering. Cation reordering is a process in which the cations in the mineral titanomagnetite are allowed to move into a preferred alignment during slow cooling, which can increase the Curie temperature and, therefore, the emplacement temperature estimate.

For goal #2, emplacement temperature estimates were made from lithic and pumice samples from sites 2, 4, 5, and 6 and were compared to measured emplacement temperatures of pyroclastic debris from the May 18, 1980 eruption (Banks and Hoblitt, 1996). The lithic samples were proven to provide more accurate results than the pumice, and the most robust deposit temperature estimate exceeded the measured emplacement temperature by ~40°C. Results overall demonstrate that overestimations of emplacement temperature estimates in samples with titanomagnetite do occur.

To satisfy goal #3, analysis of the Curie temperature vs. depth from several locations allowed for qualitative assessments of emplacement temperatures. Because this can be conducted on ash matrix, it provides a means of crudely estimating temperature when no lithics are present. An elevated T_{c1} (dominant T_c) or T_c that increases with depth is consistent with emplacement at

temperatures above ~300°C, which is the minimum temperature at which cation reordering begins. This allows flows to be classified as emplaced at above 300°C or below 300°C, and the first four May 18th PDCs were found to oscillate about this temperature.

TABLE OF CONTENTS

LIST OF FIGURES

LIST OF TABLES

ACKNOWLEDGEMENTS

I would like to thank my thesis advisor Dr. Julie Bowles of the Geosciences Department at the University of Wisconsin-Milwaukee for her support, helpful edits of my thesis, and for patiently teaching me about paleomagnetism, as the subject was quite new to me. I would also like to thanks Dr. Sophie-Charlotte Lappe and Dr. Julie Bowles for their help with my experiments, such as starting the oven and switching samples in the Kappabridge for me. This project was supported using funds from the National Science Foundation (Grant #1315971) that Dr. Julie Bowles had applied for before I accepted the position as her graduate student and the Department of Geosciences at the University of Wisconsin-Milwaukee. I would also like to express my gratitude to Dr. Barry Cameron and Dr. Lindsay McHenry for helping me to improve my thesis with their edits and comments.

During the course of my Master's thesis, I received aid from outside of the department as well. I would like to thank the parents of Dr. Julie Bowles for lending their camper during our fieldwork at Mount St. Helens, and I would like to thank Peter Solheid, Dr. Sophie-Charlotte Lappe, and Dr. Julie Bowles for their help in collecting samples at Mount St. Helens. I would also like to recognize the Institute of Rock Magnetism (IRM) at the University of Minnesota for contributing to my knowledge of paleomagnetism. Finally, I would like to acknowledge the support of my family and friends for their constant support and encouragement.

Chapter 1: Introduction

Pyroclastic density currents (PDCs) often result from explosive volcanic eruptions. According to Sulpizio et al. (2014), PDCs are clouds containing mixtures of pyroclastic particles and gas that gravity forces to move down a volcano's slope. PDCs are among the most dangerous hazards a volcano can produce, and determining their emplacement temperatures can reveal certain aspects about a particular volcano, such as locations of past vents, modes of emplacement, and average temperature ranges. There are several ways to determine a PDC's emplacement temperature: satellite remote sensing during an eruption (Denniss et al., 1998), conditions of bone and teeth found at the site (Mastrolorenzo et al., 2001), reflectance of charcoal (Pensa et al., 2015), H/C ratio of carbonized wood (Sawada et al., 2000), melting of plastic (Voight and Davis, 2000), and paleomagnetism, which involves studying the magnetic properties of certain rocks (e.g. Hoblitt and Kellogg, 1979). Satellite remote sensing offers an opportunity to collect data from current eruptions that are inaccessible and/or dangerous to sample. However, it does not provide information on historic eruptions, is limited in spatial resolution, and thermal signatures can be covered by ash fall deposits (Denniss et al., 1998). Bone and teeth are not always commonplace at the site of a volcanic eruption and require the loss of human and animal life, but approximations of emplacement temperatures can be found by examining patterns of cracks in the dental enamel and bone coloration of past victims (Mastrolorenzo et al., 2001). The reflectance of charcoal has a direct correlation with its charring temperature, such that the higher the reflectance of the charcoal, the higher the emplacement temperature. Similarly, the H/C ratio of carbonized wood varies with temperature and has been calibrated for temperatures greater than 300°C (Sawada et al., 2000). Unfortunately, methods relying on charcoal suffer the same limitation as the method of examining the bones and teeth at

volcanic sites, in that charcoal is not commonplace. Paleomagnetism typically uses the magnetic remanence directions of lithic clasts incorporated into PDCs. Although lithics are not present in every PDC, they are relatively common compared to bones, teeth, or charcoal. Therefore, paleomagnetism would be the more consistently applicable method for finding the emplacement temperature.

During a volcanic eruption, molten lava is erupted onto the surface and is intrusively cooled as magma beneath the surface. As the lava/magma cools into volcanic/plutonic rock, the magnetic minerals it contains, such as titanomagnetite ($Fe_{3-x}Ti_xO_4$, where $0 \leq x \leq 1$), record the orientation and intensity of the Earth's magnetic field. This is called the primary magnetization of a rock. When another eruption occurs, previously deposited volcanic rock or intrusive clasts may be blown away as pyroclastic debris and/or incorporated in PDCs as lithic clasts. During this process, the rock is reheated and deposited in a new area, with its primary magnetization now randomly oriented. When the rock is reheated, all or part of its primary magnetization is lost and is replaced with a secondary magnetization (or overprint) oriented in the direction of the Earth's magnetic field with respect to where it is deposited after the second eruption (Figure 1). Since pumice is typically a juvenile material in PDC deposits, it is unlikely to have both a primary and secondary magnetization. Therefore, pumice usually only has a magnetization associated with the PDC emplacement. For the lithic fragments, by determining the temperature at which this secondary magnetization (most recent) is removed, it is possible to estimate the rock's emplacement temperature (Hoblitt and Kellogg, 1979). In principle, the emplacement temperature of the pumice would be found as the temperature at which its magnetization is completely removed.

The paleomagnetic technique of determining emplacement temperature has been called into question by recent observations that certain magnetic properties of titanomagnetite vary with the thermal history of the mineral (Bowles et al., 2013). The goals of this study are to (1) examine how the temperature at which magnetization is removed varies with thermal history; (2) determine to what extent this might bias emplacement temperature estimates; and (3) to examine how stratigraphic variations in magnetic properties might be used to estimate emplacement temperature. Because direct emplacement temperature measurements were made following the May 18th, 1980 eruption of Mount St. Helens (Banks and Hoblitt, 1996), this was the sampling location selected. It will allow for a direct comparison of paleomagnetic emplacement temperature estimates with direct temperature measurements.

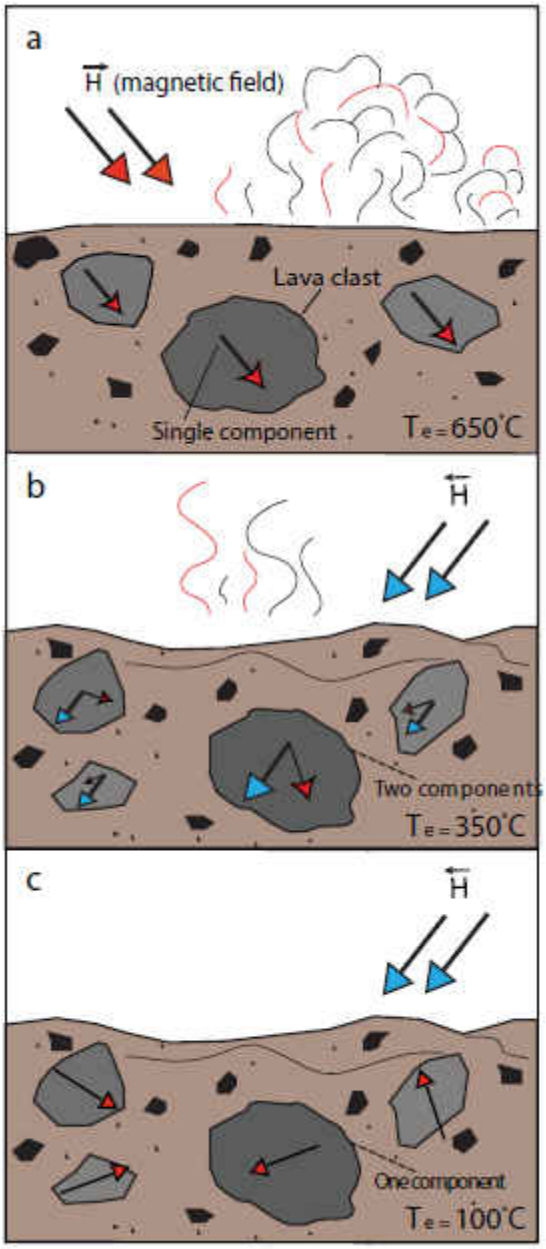

Figure 1. Paleomagnetic directions recorded by lithic fragments in a PDC: (a) emplacement temperature of 650°C was above the T_c of the magnetic minerals in the rock and thus they recorded the magnetic field at the time of their emplacement (primary magnetization) (red arrows); (b) after they are emplaced a second time at a lower emplacement temperature of 350°C, which led to a small loss of some of the primary magnetization and the acquisition of the secondary magnetization (blue arrows); and (c) after they have been emplaced by a lahar or in a colder setting where the clasts become randomized and no secondary magnetization is gained. The magnetic field arrows (blue and red) above the ground are representative of the Earth's magnetic field at the time of the deposits' formation (modified from Pensa et al., 2015).

1.1 Rock Magnetic and Paleomagnetic Background

As a sample is progressively heated, magnetization is usually removed incrementally, based on the blocking temperature distribution of the sample. The blocking temperature (T_b) is the temperature below which the magnetization of the rock can no longer change on geological or laboratory time scales. It is dependent on the size and composition of the magnetic mineral grains. Above the blocking temperature is the Curie temperature (T_c), below which a mineral becomes magnetic (Figure 2). A mineral's Curie temperature is traditionally considered to vary only with its composition.

Aramaki and Akimoto (1957) devised a method to determine whether a pyroclastic deposit was emplaced above its Curie temperature by measuring the thermoremanent magnetization (TRM) of individual lithic fragments. If the magnetic orientation of these fragments is aligned parallel to the geomagnetic field, then the deposit was emplaced above the Curie temperature of the magnetic minerals in the deposit. If it was not, then the deposit was emplaced below the Curie temperature (Aramaki and Akimoto, 1957; Chadwick, 1971; Wright, 1978). Hoblitt and Kellogg (1979) furthered this method to determine a sample's emplacement temperature via incremental thermal demagnetization. As the rock is reheated, the magnetization recorded by the rock (natural remanent magnetization) is removed bit by bit in a process called progressive thermal demagnetization. According to this method, if the sample has only one directional component of magnetization, then the maximum blocking temperature is equivalent to the minimum emplacement temperature of the sample. If the sample has more than one directional component, then the two components are compared to the direction of Earth's field at the time of emplacement of the PDC. If the magnetic orientation of the low-T_b component is parallel to the Earth's magnetic field and the higher-T_b component is not, then the emplacement

temperature is equal to the temperature at which the low-T_b component is removed. The high-T_b component is likely the result of a previous emplacement before the specimen in question was ejected and emplaced during the latest eruption (Hoblitt and Kellogg, 1979; Kent et al., 1981; Clement et al., 1993; Mandeville et al., 1994; Bardot, 2000).

Bardot and McClelland (2000) examined the reliability of thermal demagnetization and found that this method may be inaccurate if the low-T_b component of a sample's magnetization was not of thermal origin. For example, the low-T_b component could be viscous in origin, resulting from a lightning strike, or be due to growth or chemical alteration of magnetic minerals at temperatures less than T_c. Bardot and McClelland (2000) also addressed possible issues with multidomain (MD) grains. MD grains are magnetically more complex than single domain (SD) grains in that the temperature at which a magnetization is acquired is not necessarily equal to the temperature at which it is removed. In other words, the blocking temperature is not equal to the unblocking temperature ($T_b \neq T_{ub}$). MD grains may not completely demagnetize until the T_c, regardless of the emplacement temperature. The introduction of MD grains can therefore cause overestimations in paleomagnetic tests, although Bardot and McClelland (2000) argue that this is not the case where at least two magnetic components are present.

This paleomagnetic technique has been increasingly used in recent years. Paterson et al. (2010) used thermal demagnetization to identify different sources for layers in a flow based on differences (usually large) in emplacement temperatures. For example, samples with inconsistent paleomagnetic directions are usually emplaced cold (i.e. lahars). Paterson et al. (2010) also examined samples from Mount St. Helens and compared the paleomagnetically-determined emplacement temperatures to direct emplacement temperature measurements collected by Banks and Hoblitt (1996). Their emplacement temperature estimates were within range of the directly

measured emplacement temperatures (Banks and Hoblitt, 1996). The technique has also been used to distinguish debris flows from block and ash deposits for 1991-1995 Mt. Unzen (Japan) eruptions (Uehara et al., 2015). Rader et al. (2015) used progressive thermal demagnetization on samples from "boiling over" eruptions (strongly vesiculated magma erupted like a fountain without a plume) at Cotopaxi and Tungurahua in Ecuador in order to look at thermal heterogeneity.

The paleomagnetic method of determining emplacement temperatures is based on the assumption that Curie (and blocking) temperatures are constant for a given composition and grain size. However, new evidence suggests that the T_c of titanomagnetite ($Fe_{3-x}Ti_xO_4$; common in igneous rocks) is not constant with composition and can be influenced by its cooling rate and thermal history (Bowles et al., 2013; Jackson and Bowles, 2014). Samples from the 1980 eruption of Mt. St. Helens and the 1912 eruption of Novarupta were annealed at temperatures between 300°C and 450°C, resulting in an increase in T_c of up to 150°C. This was interpreted to arise from a cation reordering process. The cation reordering process occurs at high temperatures where cations in the mineral have enough energy to relocate to different crystallographic sites. The slower the mineral/rock cools, the more time these cations have to find more preferential sites, which results in a higher order and means higher Curie temperatures (Bowles et al., 2013; Jackson and Bowles, 2014).

If T_c increases during the natural annealing that takes place during slow cooling within PDCs, the method proposed by Hobblitt and Kellogg (1979) may result in an overestimate of emplacement temperature. It has already been shown that T_c increases with depth in a flow in at least one section from Mt. St. Helens (Jackson and Bowles, 2014). This is consistent with increased anneal time during slow cooling at depth. This study will focus on determining

whether T_b of samples from the 1980 eruption of Mt. St. Helens also varies systematically with depth and/or thermal history, allowing for an assessment of potential bias in the paleomagnetic method for determining emplacement temperature.

According to Bowles et al. (2013), the composition of titanomagnetite that has been observed to undergo cation reordering is a moderate-Ti titanomagnetite ($x \approx 0.3 – 0.4$) with minor Al- and Mg-substitution. These compositions are common in andesitic, dacitic, and rhyolitic rocks (i.e. most rocks in a PDC).

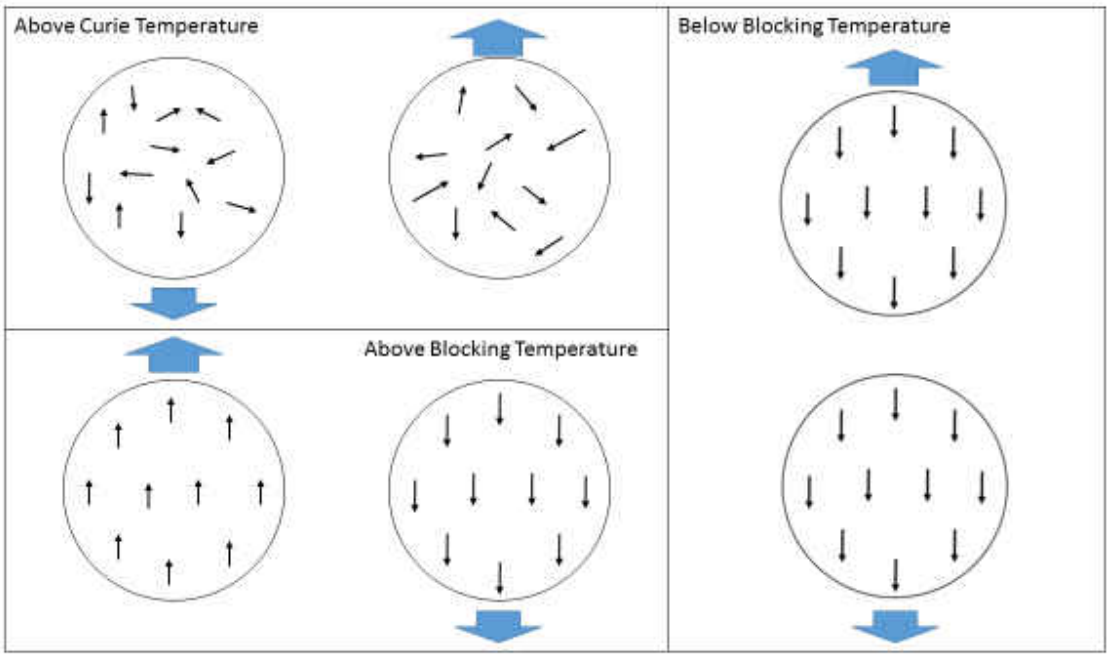

Figure 2. Schematic representation of magnetic moments (black arrows) in a magnetic mineral above the Curie temperature, and above and below the blocking temperature in a dominant magnetic field (blue arrows).

1.2 Geologic Background

On March 27th, 1980, Mount St. Helens, a composite volcano located in Washington State, became active after more than a century of inactivity (Figure 3). This activity resulted in a

new crater in the northern part of the old crater in the volcano and a bulge on the northern flank (Christiansen and Peterson, 1981). This bulge became increasingly prominent until May 18th, 1980. At 8:32 am local time, a landslide weakened and collapsed the northern slope of Mount St. Helens resulting in a violent blast as the volcano erupted (Christiansen and Peterson, 1981; Fisher, 1990). The May 18th eruption was classified into six phases. The first was the giant landslide that resulted in the subsequent lateral blast on the mountain's north face due to decompression. The second was the formation of a Plinian eruption column whose collapse signaled the third phase which was the early ash flow that generated most of the PDCs of which a large portion travelled north (where the mountainside collapsed). The fourth was the climactic phase, which consisted of the highest explosive intensity and mass flux. This is most likely due to the erosion and widening of the volcano's eruption conduit or vent (Criswell, 1987). About 77% of total erupted mass was from PDCs and co-ignimbrite (volcanic tuff) deposits and the rest was due to the collapse of the eruption column (Carey et al., 1990). The fifth phase was the late ash flow where fluctuating mass flux occurred, sometimes causing small PDCs. The sixth and last phase began at approximately 6:15 pm on May 18th and involved a low energy ash plume with occasional increases in intensity (Criswell, 1987).

Brand et al. (2014) examined the stratigraphy north of Mount St. Helens (pumice plain) that was formed on May 18, 1980, and they identified five flow units. The average thicknesses of each unit from bottom to top are ~6 meters (Unit I), ~4 meters (Unit II), ~7 meters (Unit III), and ~6 meters (Unit IV). Unit V is only exposed near the vent. There are varying amounts of ash, crystals, pumice, and lithics in the flow units, although it appears to be mostly nonwelded pumice and ash with minor lithics (Brand et al., 2014). Brand et al. (2016) looked at the influence of slope on flow dynamics of the PDCs during the May18th eruption and found that

slope and irregular topography can strongly influence flow dynamics of a PDC. For example, currents in the PDCs were partially confined in steep slot canyons and combined with the acceleration of the PDC and the surface roughness at the time, you can get an idea of roughly how much rock debris was picked up by the PDC on its way to the pumice plain (Brand et al., 2016).

Subsequent smaller eruptions on May 25th, June 12th, July 22nd, and August 7th all left additional PDC deposits of nonwelded dacitic pumice and ash (Christiansen and Peterson, 1981) These later PDCs were progressively hotter than the May 18th PDC (Banks and Hoblitt, 1996).

Banks and Hoblitt (1996) measured emplacement temperatures of all the 1980 PDC deposits by inserting temperature probes into the deposits in the days and weeks following the eruption. If the vertical temperature profile was isothermal over a "reasonable length" (e.g., Figure 4), this was taken to be the emplacement temperature. Otherwise, the maximum measured temperature was taken to be a lower bound on the emplacement temperature. In a few cases where more time had elapsed before the first measurement, emplacement temperature was mathematically modeled from the evolution of stratigraphic temperature over time. The emplacement temperature range for the May 18th PDCs found by Banks and Hoblitt (1996) is from 270°C to 418°C.

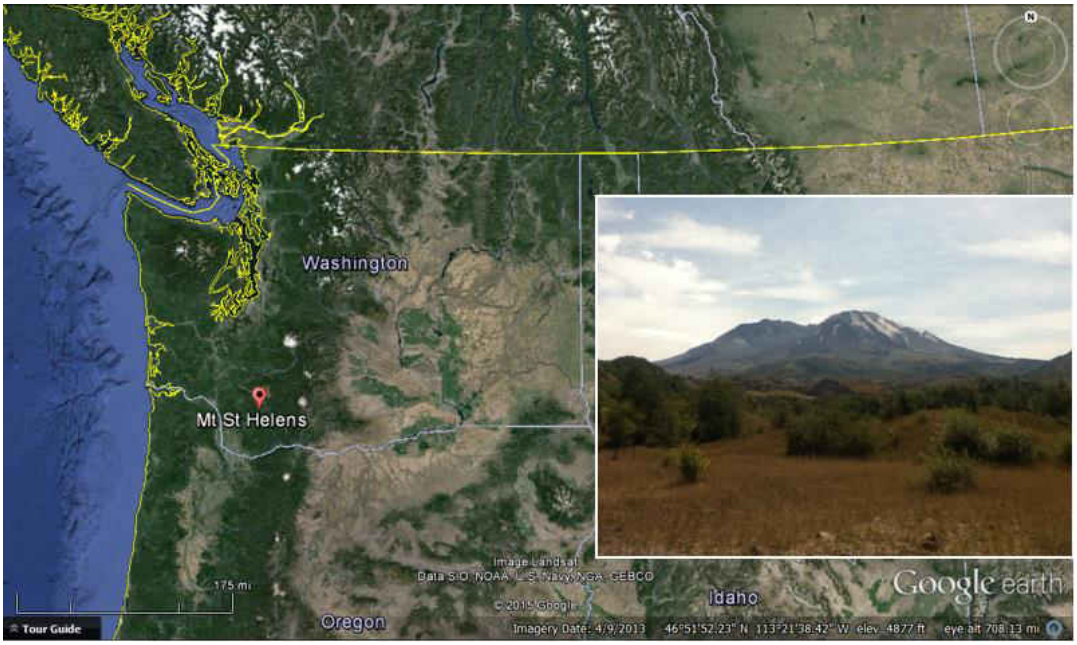

Figure 3. Location of Mount St. Helens in Washington State. A photo of Mt. St. Helens (lower right) shows the collapsed north side of the volcano.

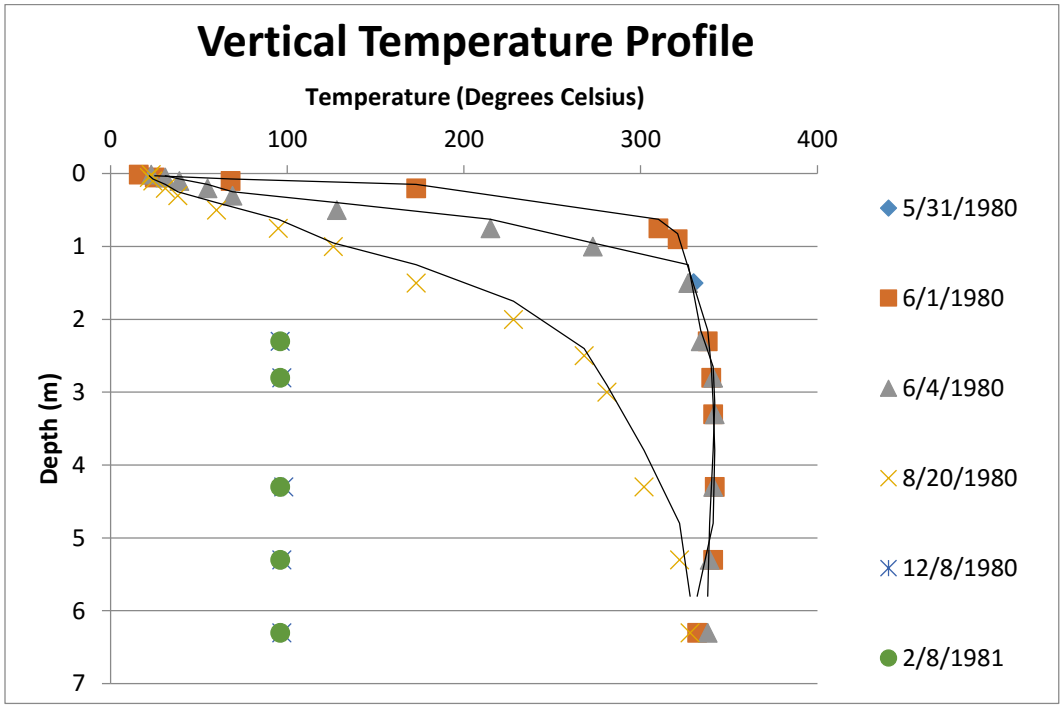

Figure 4. An example of vertical temperature profiles at different dates after the May 18, 1980 eruption (black lines are merely meant to guide the eye). Data are from Banks and Hoblitt (1996) station b, which is less than half a kilometer east of sites 1-4 of this study. The isothermal segments in the profiles up to June 4, 1980 are assumed to provide the emplacement temperature of 342°C. °C

Chapter 2: Methods and Samples

2.1 Field Sampling

Sampling at Mt. St. Helens took place in August 2014 (Table 1). We targeted pyroclastic flows with intact surfaces of capping ash in order to precisely measure depth within a flow. Unoriented pumice and ash samples were collected below these ash layers every five to ten centimeters down to a meter in depth (Figures 5, 6, 7, 8, 9, 10, 11, 12, and 13). In one case, pumice was drilled using a battery-powered drill which produced 1" diameter cores that were oriented using a magnetic or sun compass (site 4). A lithic layer was also drilled and oriented using a magnetic compass (site 5). Several oriented blocks (both lithics and pumice) from sites 2 and 6 were brought back to the University of Wisconsin-Milwaukee to be drilled and reoriented. Sites 1-4 were less than or equal to 0.5 km from Banks and Hoblitt (1996) station b (342°C). Sites 5-8 were less than 0.5 km from Banks and Hoblitt (1996) stations j and l (both 307°C).

Samples from site 8 were chosen based on previous work suggesting a relatively simple magnetic mineralogy: single-phase, multi-domain, homogeneous titanomagnetite ($Fe_{2.55}Ti_{0.26}Mg_{0.10}Al_{0.08}O_4$; Bowles et al., 2013; Bowles et al., 2015). This would allow experiments to isolate the magnetic mineralogy responsible for the time- and temperature-dependent magnetic properties. Samples from other locations at Mount St. Helens are known to also contain oxy-exsolved titanomagnetite with ilmenite lamellae (Jackson and Bowles, 2014). Another study by Kuntz et al. (1981) indicated two different oxides (titanomagnetites and titanohematites) where one was mostly homogeneous with some oxy-exsolved titanomagnetite with ilmenite lamallae, and the other had complex intergrowths and altered margins (xenolith fragments or xenocrysts). The Kuntz et al. (1981) study was not specific to the May 18th flow.

Oriented pumice and lithic cores were cut no more than an inch in length and labeled (i.e. msh140830b = Mount St. Helens 2014 at site 08 with sample depth of 30 cm and specimen b). Unoriented pumice blocks were cut into cubes less than 1 in^3 and were marked with a fiducial line to maintain orientation throughout the experiments. Samples were then stored in a magnetically shielded room.

Table 1. Site locations, descriptions, and samples collected at Mount St. Helens.

Site	Location (Decimal Degrees)	Site Description	Samples Collected
1	46.2453°N 122.1876°W	Unit is at least ~2 m thick; base not exposed. Mostly ash with small (< ~1 cm) pumice fragments. Infrequent lithics become more abundant and larger (up to ~15 cm) with depth. Separated from overlying pink block and ash unit by capping ash layer ~50 cm thick. (Figure 6)	-Ash (every 5 cm from 0 to 100 cm below the capping ash layer) -Unoriented pumice fragments (7.5 cm, 18 cm, 27 cm, and 95 cm)
2	46.2430°N 122.1857°W	5-8 m thick with numerous pumice lenses. Tentatively identified as Unit II from Brand et al. (2014). Capping ash layer at least 35 cm thick and grades into overlying pink block and ash layer. Stratigraphically above site 3. (Figures 6 and 7)	-Ash (every 5 cm from 0-50cm , every 10 cm from 50-150 cm, and above the sampled unit (1 cm, 7 cm, 10 cm, and 15-20 cm)) -Oriented lithic block sample -Unoriented pumice fragments (0 cm, 3-4 cm, 15 cm, 23-25 cm, 40 cm, 45 cm, and 103 cm)
3	46.2432°N 122.1860°W	Mostly ash matrix layer with small (< 2 cm) pumice fragments ≥ 2 m thick (base not exposed). Tentatively identified as Unit I from Brand et al. (2014). Capping ash layer is at least 15 cm thick. 30-40 m downstream from and stratigraphically below site 2. (Figure 8)	-Ash and unoriented pumice fragments (every 5 cm from 0-50cm and every 10 cm from 50-110 cm) -Unoriented lithics (12-13 cm, 35 cm, and 65 cm) -Unoriented pumice from overlying unit
4	46.2459°N 122.1880°W	Comprised of two units. The lower is a clast (pumice)-supported, poorly-sorted, pink-toned unit with abundant large (≤ 10 cm) pumice blocks. Variable thickness, but about 1 m thick where sampled. Tentatively identified as Unit III from Brand et al.	-Ash (every 5 cm from 0-50cm and every 10 cm from 50-100 cm) -Oriented pumice cores (15 cm, 19 cm, 20cm, 28 cm, 32 cm, 33cm, 39 cm, 40 cm, 42 cm, 43 cm, 44 cm, 67 cm, 72 cm, 75 cm, and 77

		(2014). Upper unit is a matrix supported, gray unit with occasional pumice and lithic fragments up to 5-10 cm. Tentatively identified as Unit IV from Brand et al. (2014). Overlain by ash layer ~2 cm thick. (Figure 9)	cm with two samples from above the sampled unit (2 cm and 42 cm) -Unoriented pumice fragments (4-8 cm, 15 cm, and 30 cm with many samples from the flow above (up to 50 cm))
5	46.2619°N 122.1905°W	In an incised gully roughly 20 m below site 8. No obvious contacts between sites 8 and 5. Sampled section is a 30-50 cm thick lithic lens, which is laterally continuous over at least a few tens of meters. (Figure 10)	-Oriented lithics (9 specimens at approximately same depth)
6	46.2608°N 122.1966°W	Massive, bedded ash with abundant small lithics and pumice increasing with depth. Base not exposed. Tentatively identified as Unit II from Brand et al. (2014). Overlain by ~ 2 cm ash layer, followed by ~1 m thick pumice lens that grades upwards into another massive ash bed (site 7). (Figure 11)	-Ash (every 5 cm from 0-50cm and every 10 cm from 50-150 cm) -Oriented pumice (4 samples above sampled flow) -Oriented lithic blocks (blocks from 55 cm and 155 cm)
7	46.2608°N a few tens of meters east of 122.1966°W	Roughly 3-4 m thick ash layer directly below a sand and gravel layer. Ash alternates between fines and coarser layers at about 5-10 cm scale with some fine-scale crossbedding in some layers. Tentatively identified as Unit III from Brand et al. (2014). Above and a few tens of meters east of site 6. (Figure 12)	-Ash (every 5 cm from 0-50cm and every 10 cm from 50-100 cm) -Unoriented pumice fragments (75 cm and 78 cm)
8	46.2615°N 122.1902°W	Ash matrix with abundant pumice pieces that become larger and more frequent upwards. Capped by an ash layer ~50 cm thick. Stratigraphically above site 5. (Figure 13)	-Unoriented pumice fragments (0-10 cm, 10 cm, 15 cm, 10-20 cm, 20 cm, 25 cm, 30 cm, 35 cm, 40cm, 45 cm, 50 cm, 58 cm, 60 cm, 65 cm, 70 cm, 80 cm, 90 cm, and 100 cm)

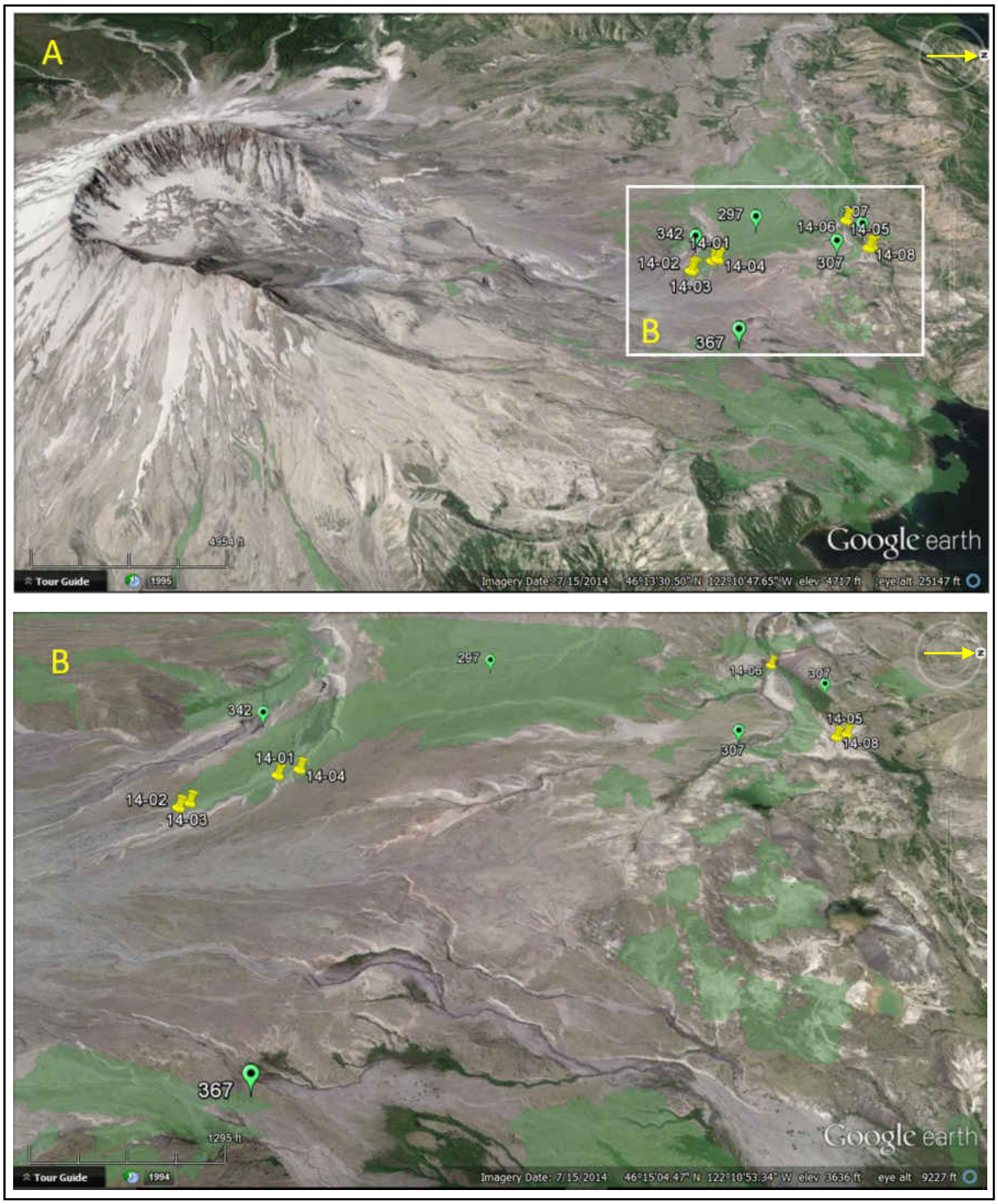

Figure 5. Sampling locations at Mount St. Helens can be seen in the pumice field to the north of the volcano in A. North arrow shown by yellow arrow in upper right corner. A closer look at the site locations can be viewed in B. The approximate outcropping extent of the May 18th, 1980 pyroclastic flow shown in green (from Kuntz et al., 1990). The sampled sites are labeled as 14-01, 14-02, 14-03, 14-04, 14-05, 14-06, and 14-08 and the sites closest to the sampled sites with the measured emplacement temperatures from Banks and Hoblitt (1996) are shown as green balloons.

Figure 6. Dr. Julie Bowles next to Site 1 (14-01 in Figure 5), which is capped by an ash layer approximately 50 cm thick. Ash layer overlain by pink block and ash unit.

Figure 7. Peter Solheid and Dr. Sophie-Charlotte Lappe sampling Site 2 (14-02 in Figure 5).

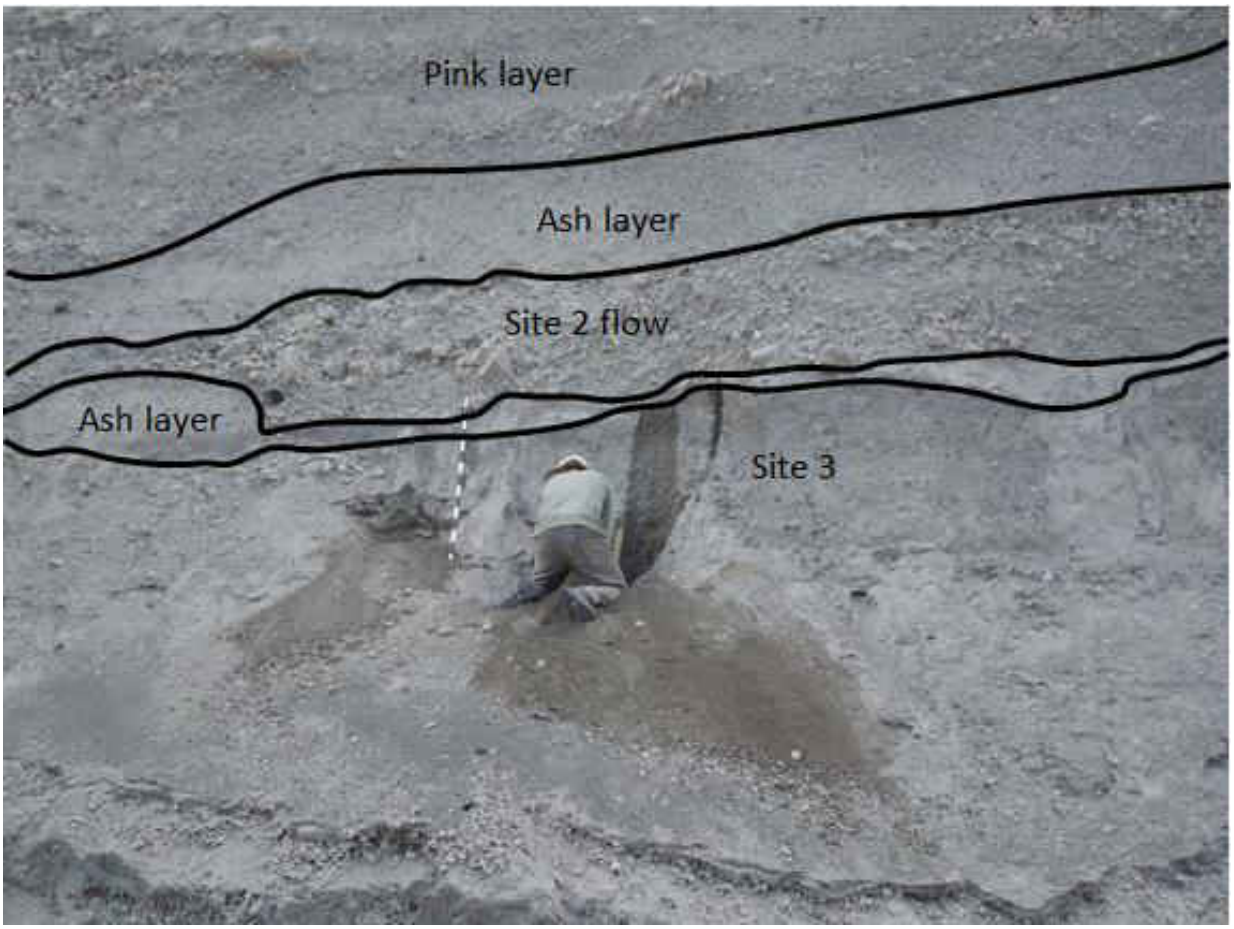

Figure 8. Peter Solheid digging into a PDC deposit at site 3 (14-03 in Figure 5). Scale provided by black and white rod, which has divisions every 10 cm. Site 2 is overlain by an ash layer at least 35 cm thick, which grades into overlying pink block and ash layer.

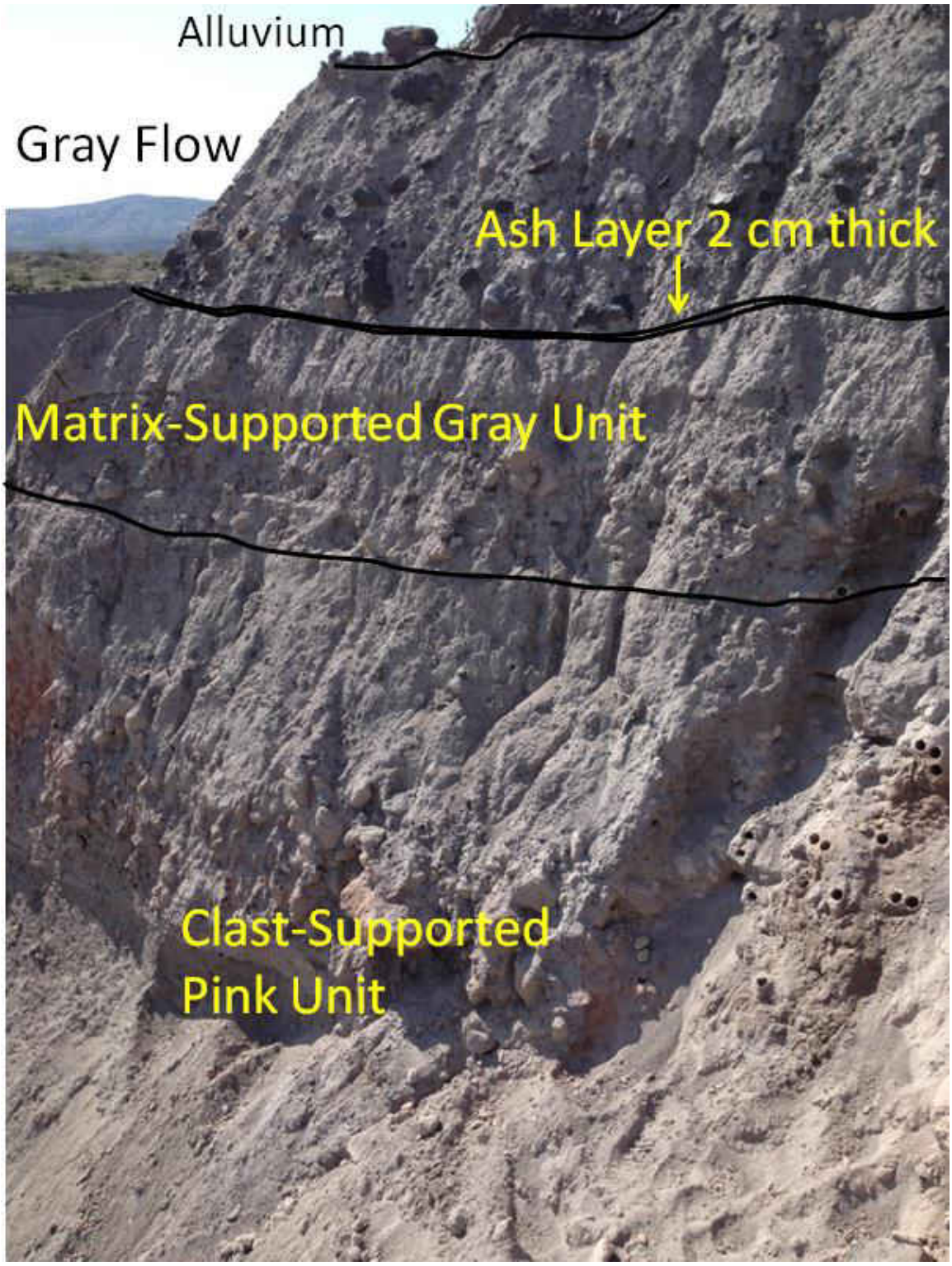

Figure 9. Site 4 sample site (14-04 in Figure 5) comprises two identifiable units: a lower pink, clast (pumice)-supported unit and an upper, matrix-supported gray unit. The gray unit is capped by a thin ash layer. Drilled pumice blocks can be seen in the bottom right corner.

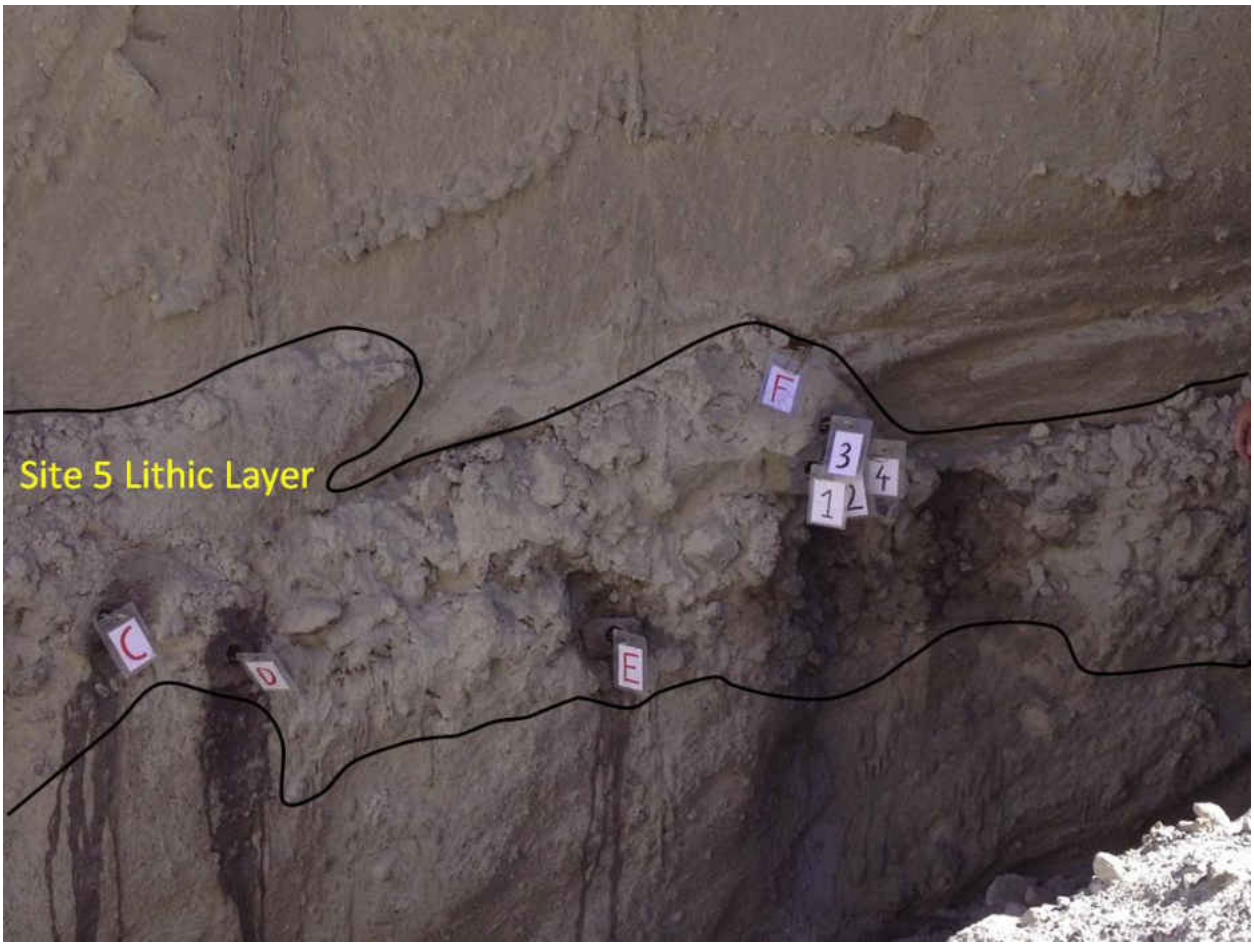

Figure 10. Site 5 lithic layer roughly 20 m below site (14-05 in Figure 5). Letters and numbers mark drilled locations.

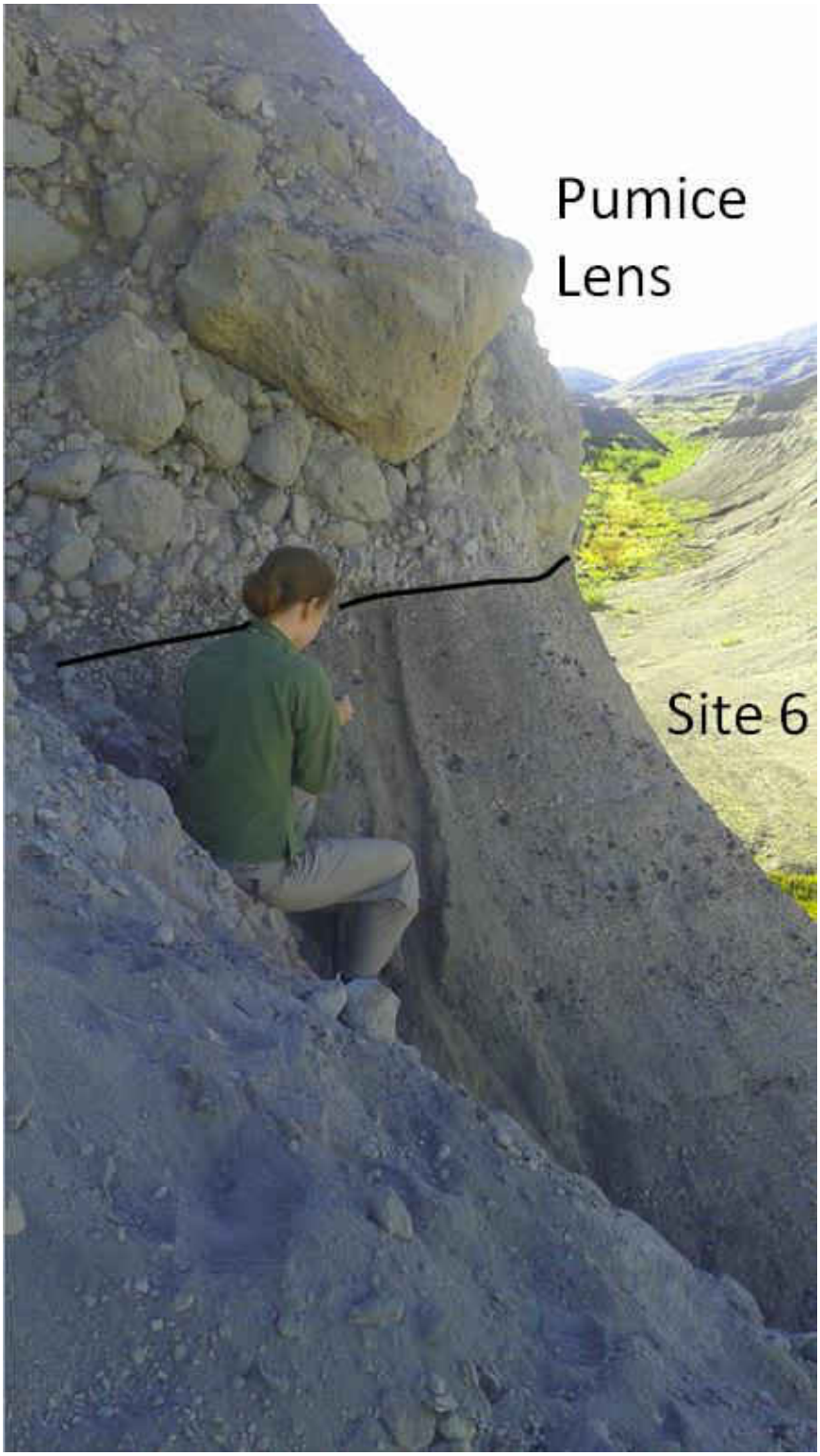

Figure 11. Dr. Julie Bowles next to site 6 sample site below (14-06 in Figure 5). Site 6 is overlain by a thin ash layer, followed by ~1 m thick pumice lens which grades upwards into massive ash bed, sampled as site 7.

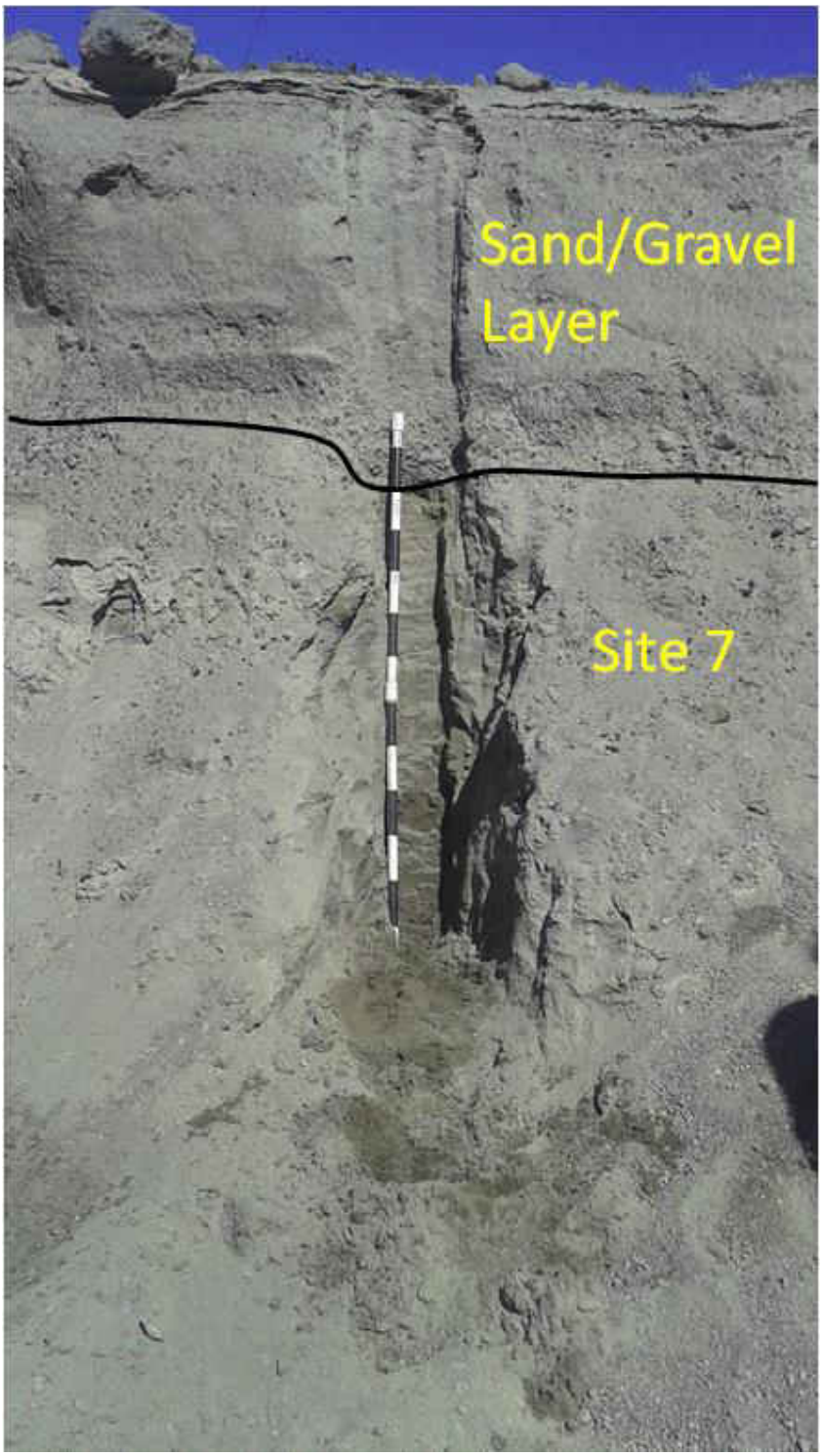

Figure 12. Site 7 ash layer below sand/gravel layer. Scale provided by black and white rod, which has divisions every 10 cm (14-07 in Figure 5).

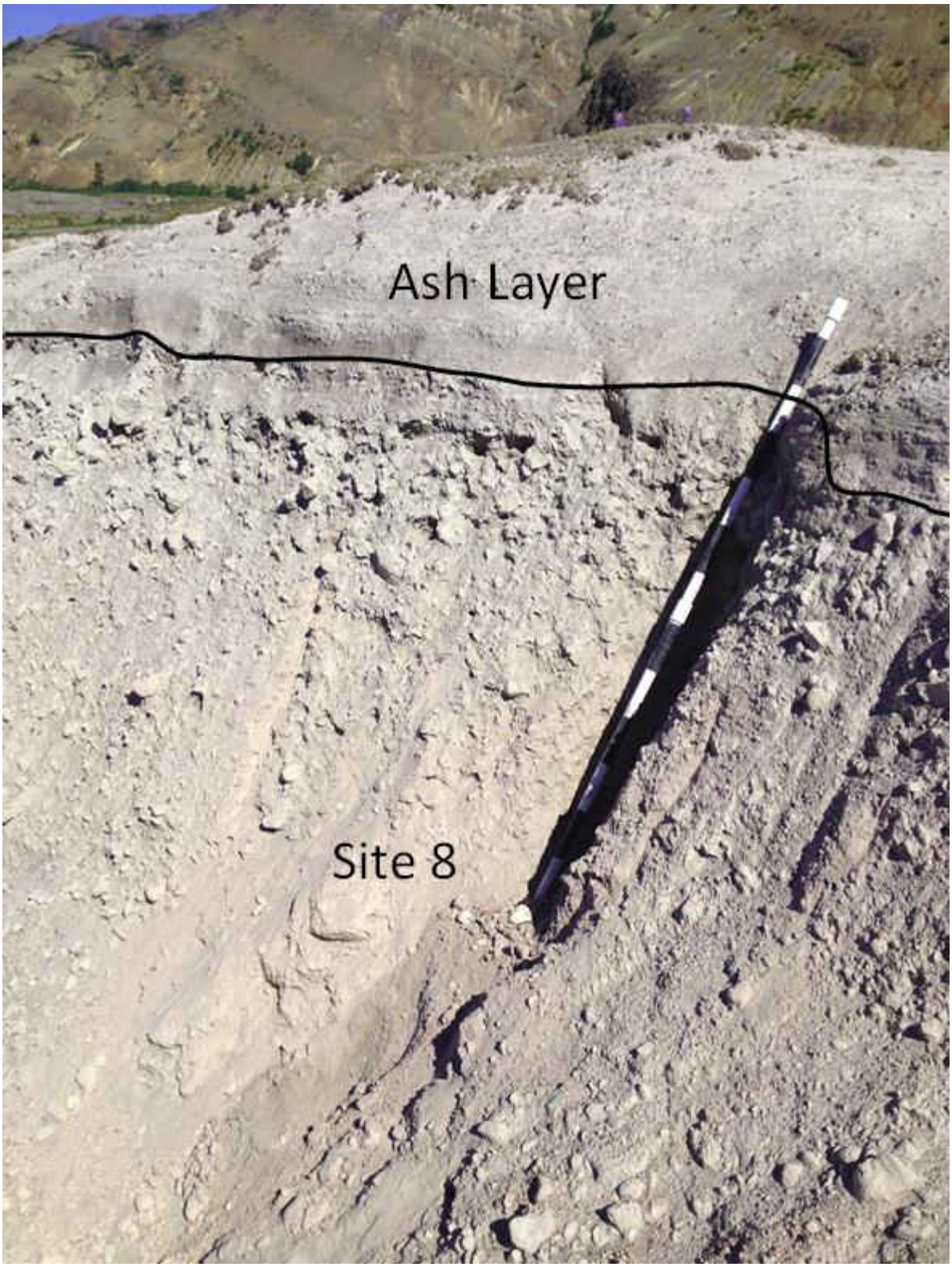

Figure 13. Site 8 ash and pumice layer below a capping ash layer (14-08 in Figure 5).

2.2 Laboratory Analyses

As noted above (Chapter 1), study goal #1 is to examine how blocking temperature varies with thermal history. If the Curie temperature depends on depth in the PDC (higher T_c for deeper samples due to slower cooling rate) (Bowles et al., 2013; Jackson and Bowles, 2014), then the blocking temperature should theoretically follow that same pattern (T_b increases with depth). Further, if blocking temperatures increase with anneal time at moderate temperatures (350°C-450°C), we would expect blocking temperatures to be higher following slow cooling compared to rapid cooling. Both of these hypotheses were tested by demagnetizing the natural remanent magnetization (NRM) of unoriented pumice cubes from sites 1 and 8 in steps of 50°C from 100°C to 200°C and 25°C steps from 200°C to 500°C. Moreover, Curie temperature as a function of flow depth was measured on ash matrix samples from every site except sites 4 and 8. An attempt to further test the hypothesis that blocking temperatures vary with thermal history was conducted by controlling the cooling conditions of these samples. Once the cubes were demagnetized, they were given a thermal remanent magnetization (TRM) by cooling quickly from 600°C in a field of 50 μT (about 28°C/min. at 344°C) to simulate the shallow cooling process. Afterwards, the process of thermal demagnetization as described above was repeated, but since there was evidence that the samples had acquired a self-reversed magnetization this part of the experiment was halted. Otherwise, the samples would have been reheated, given a TRM, and cooled slowly to simulate the cooling process of the deeper samples. This would have allowed a comparison of slow and fast cooling rates for the samples in a controlled environment, which then would have been compared to the results found in nature (the NRM demagnetization).

To test for self-reversing behavior, three fresh pumice samples (cubes) from site 8 at varying depths (0-10 cm, 30 cm, and 70 cm) from the top of the flow were subjected to a different experiment. The samples were demagnetized using an alternating field (AF) of increasing intensity. The peak AF fields used were 2.5 mT, 5 mT, 7.5 mT, 10 mT, 12.5 mT, 15 mT, 17.5 mT, 20 mT, 25 mT, 40 mT (70 cm only), 60 mT (70 cm only), and 100 mT until their magnetization was very close to zero. The orientation of the samples inside the demagnetizer was alternated between steps from +XYZ to –XYZ to detect spurious acquisition of an ARM (anhysteretic remanent magnetization). These samples were then given partial TRMs (pTRMs) by heating them up in steps of 50°C from 100°C to 200°C and 25°C steps from 200°C to 500°C in air and with a magnetic field of 50 μT (Doubrovine and Tarduno, 2004).

Study goal #2 was to determine whether and how blocking temperature variations arising from variable thermal history might bias emplacement temperature estimates. To determine this, paleomagnetic emplacement temperatures were determined for pumice and lithic samples from sites 2, 4, 5, 6, and 8, and the results were compared to measured emplacement temperatures from Banks and Hoblitt (1996). Samples underwent thermal demagnetization to estimate emplacement temperatures for the sites in question. The NRM thermal demagnetization of lithic and pumice cores followed the same demagnetization procedure as the first NRM thermal demagnetization. The first demagnetized boat included fourteen lithic cores from site 5 (six samples had two cores each) and site 6 (one sample had two cores), two lithic cubes from one sample from site 6, and four pumice cores from site 4. The second demagnetized boat included eleven pumice cores from site 4, four pumice cores from site 6, one lithic core from site 2, and two shallow (fresh) pumice cubes from site 8, which were subsampled after each demagnetization step to find T_c. For oriented samples, paleomagnetic directions were found

using principal component analysis (Kirschvink, 1980) and the PmagPy software package (Tauxe et al., 2016).

Study goal #3 was to evaluate whether or not stratigraphic variations in T_c can be used to provide rough estimates of emplacement temperature, independent of remanence directions. To test this, T_c was measured on ash matrix samples from sites 1, 2, 3, 4, and 6.

A summary of samples and the experiments each one underwent are located in Table 2. All thermal demagnetizations and TRM acquisitions were performed in an ASC furnace with a N_2 atmosphere except during the pTRM experiment and determination of emplacement temperature estimates, which were in air. Following each heating step, room-temperature susceptibility was measured using a Bartington MS2 susceptibility bridge to monitor potential changes in abundance or composition of magnetic minerals. Magnetic intensity and orientation were measured using a Molspin minispin magnetometer. Susceptibility as a function of temperature (up to 600°C) was measured on sample splits using an Agico MFK1-FA Kappabridge instrument with a CS-4 furnace in an Ar atmosphere. Curie temperatures of samples were determined by taking the peak in the first derivative curve (Petrovský and Kapička, 2006).

Table 2. A sample data table showing pumice (P), lithic (L), and ash (Ash) samples both oriented (O) and unoriented (U) from sites 1-8 that underwent one or more of the laboratory analyses described above in section 2.2.

Site	Sample	O or U	Type	NRM Demagnetization	TRM Acquisition I	TRM Acquisition II	pTRM	T_c ($\chi(t)$)
1	7.5 cm	U	P	X	X			
1	18 cm	U	P	X	X			
1	27 cm	U	P	X	X			
1	48 cm	U	P	X	X			
1	75 cm	U	P	X	X			

1	83 cm	U	P	X	X			
1	Every 10 cm		A					X
2	Every 10 cm		A					X
3	0 cm	U	P	X	X			
3	Every 5 cm up to 50 cm and every 10 cm afterwards		A					X
4	~every 5 cm		A					X
4	A1	O	P	X				X
4	A2	O	P					X
4	B1	O	P	X				X
4	C1	O	P	X				X
4	D1	U	P					X
4	D2	O	P	X				X
4	E1	O	P	X				X
4	F1	O	P					X
4	F2	O	P	X				X
4	G2	O	P					X
4	H1	O	P	X				X
4	I1	O	P	X				X
4	J1	O	P	X				X
4	J2	O	P	X				X
4	J3	O	P	X				X
4	K1	O	P					X
4	L1	O	P	X				X
4	M1	O	P	X				X
4	N1	O	P	X				X
5	A1	O	L	X				X
5	B1	O	L	X				X
5	C1	O	L	X				X
5	D1	O	L	X				X
5	E1	O	L	X				X
5	F1	O	L	X				X

6	Every 5 cm up to 50 cm and every 10 cm afterwards		A					X
6	B1	O	L	X				X
6	B2*	O	L	X				X
6	B3	O	P	X				X
6	B4	O	P	X				X
6	B5	O	P	X				X
6	B6	O	P	X				X
7	Every 5 cm up to 50 cm and every 10 cm afterwards		A					X
8	B1	U	P	X				X
8	0-10	U	P	X	X	X	X	X
8	15	U	P	X	X	X		X
8	20	U	P	X	X	X		X
8	30	U	P	X	X	X	X	X
8	35	U	P	X	X	X		X
8	58	U	P	X	X	X		X
8	65	U	P	X	X	X		X
8	70	U	P	X	X	X	X	X
8	90	U	P	X	X	X		X

* Results were excluded because of questionable orientation data.

Chapter 3: Results

3.1 Blocking Temperature vs. Depth

Study goal #1 was to examine how blocking temperature varies with thermal history (i.e. cooling or depth in a flow). Thermal demagnetization data from unoriented pumice cubes were used to assess whether and how unblocking temperatures (T_{ub}s) vary with depth in a flow. As observed previously (Jackson and Bowles, 2014), T_c measured on warming increases with depth

in the flow at site 8 (Figure 14). As hypothesized, we also see an increase in the maximum T_{ub} from ~415°C to ~465°C (Figure 15). Figure 16 shows that the temperature at which half of the site 8 samples' intensity is gone (NRM50) and the point at which 10% of the sample's intensity is left (NRM10) (maximum T_{ub}) are increasing as depth increases. The maximum unblocking temperature increases from about 400°C at the surface to 450°C at depth. Using all of this data, it was possible to compare T_c and T_{ub}, revealing a trend where T_{ub} approaches T_c as depth increases (Figure 14). Figure 14 shows that the maximum T_{ub} from the top of the flow at site 8 often exceeds T_c. In principle, this is a physical impossibility, and possible explanations are explored in the Discussion below.

In contrast to site 8, site 1 shows no apparent trend in the maximum unblocking temperatures (Figure 17). Here the dominant unblocking temperatures range from 200°C to 225°C and 400° to 425°C.

Room-temperature susceptibility measured following each temperature step hardly changes throughout the demagnetization process for both sites. At most there is a 14% decrease starting at 400°C in most of the deeper samples from site 8 (Figures 18 and 19), which suggests that the abundance and composition of the magnetic minerals in the samples hardly changed throughout the experiment.

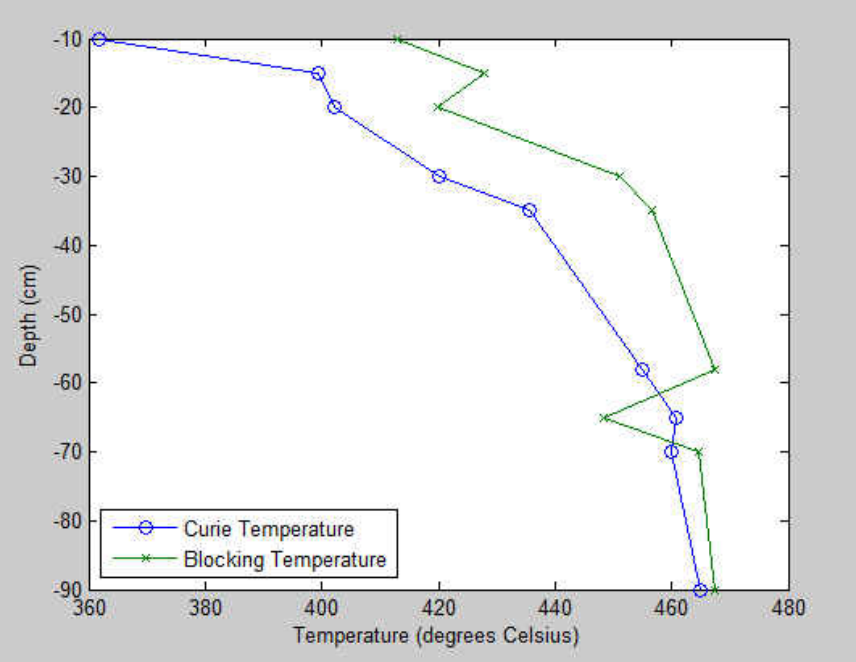

Figure 14. Maximum T_b (10% of NRM remaining) and T_c as depth increases for site 8. For the most part, the maximum T_b is higher than the corresponding T_c.

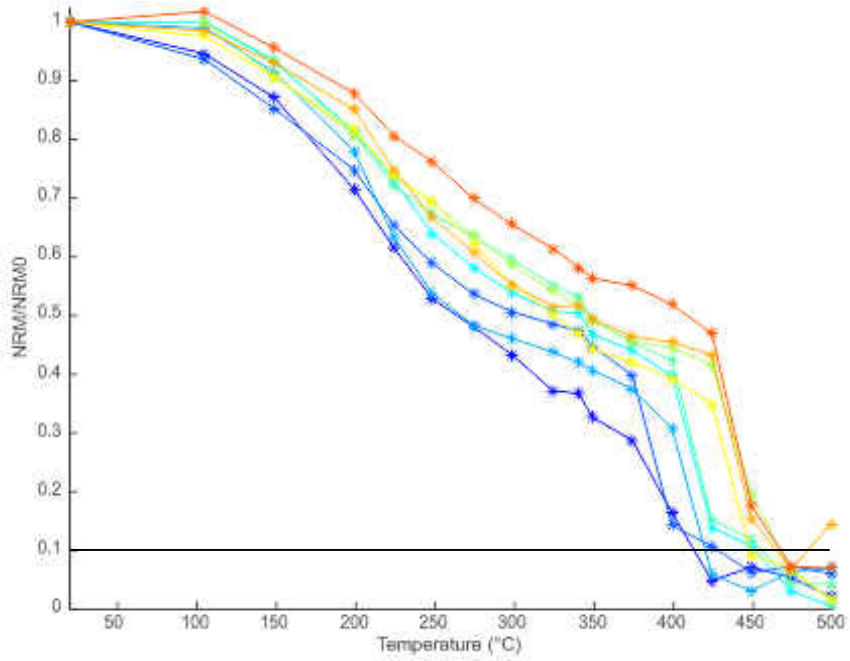

Figure 15. Results of the NRM demagnetization of the pumice cubes from site 8 (red is the deepest and blue is the shallowest). The large decreases in intensity indicate the dominant unblocking temperatures. For our purposes, the maximum unblocking temperature is 10% of original demagnetization (black line at 0.1 NRM/NRM0), which range from about 415°C to 465°C.

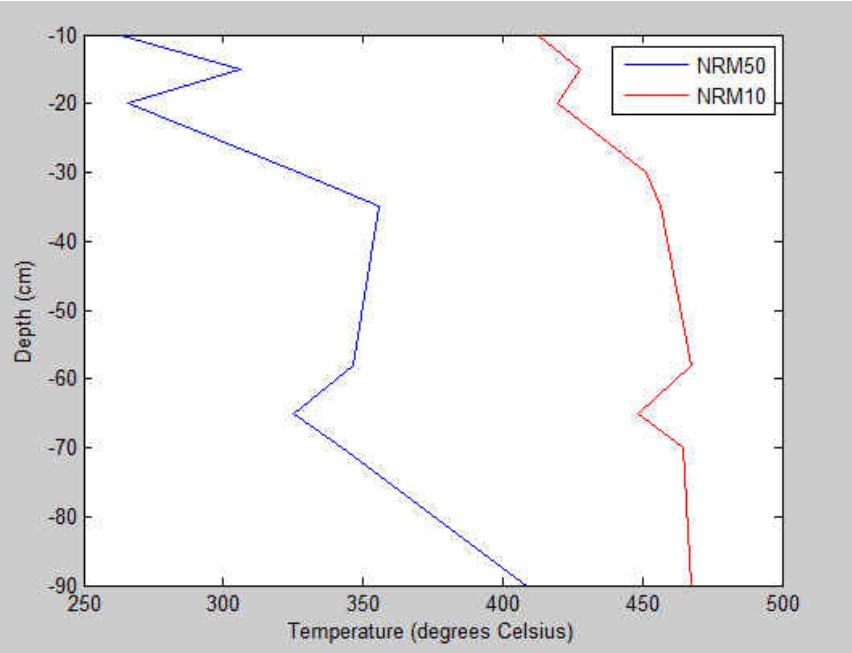

Figure 16. A comparison of NRM50 (50% of Natural Remanent Magnetization) and NRM10 (10% of Natural Remanent Magnetization) for each sample in site 8 as depth increases.

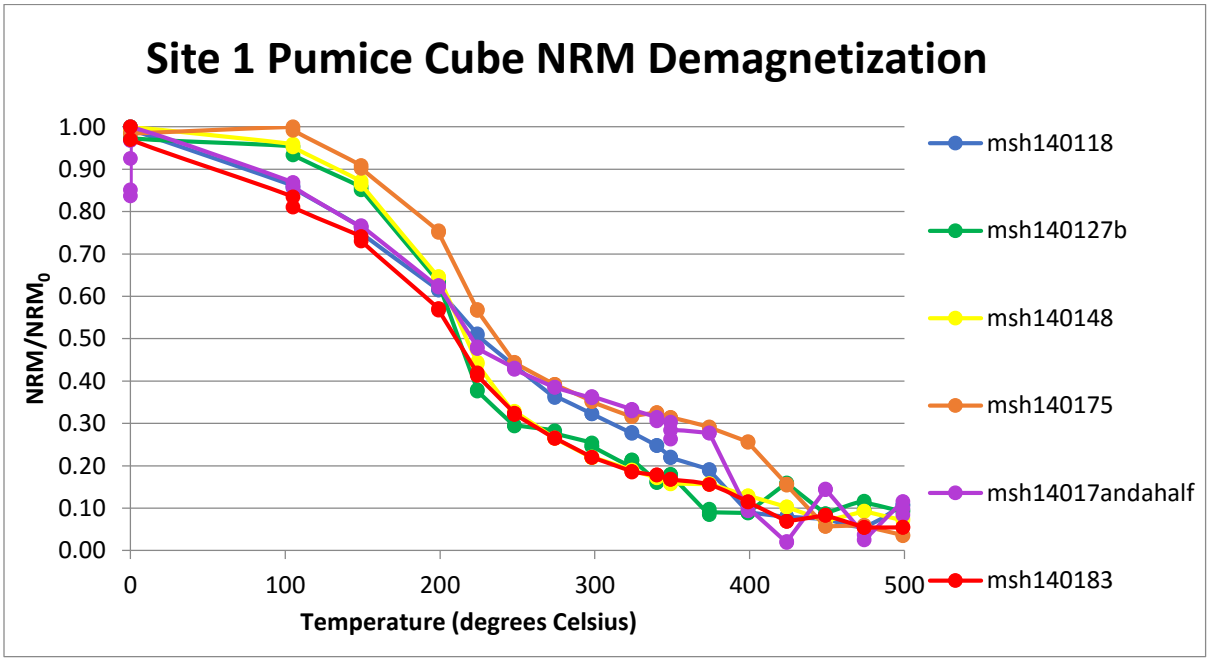

Figure 17. Results of the NRM demagnetization of the pumice cubes from site 1. The large decreases in intensity indicate the blocking temperature.

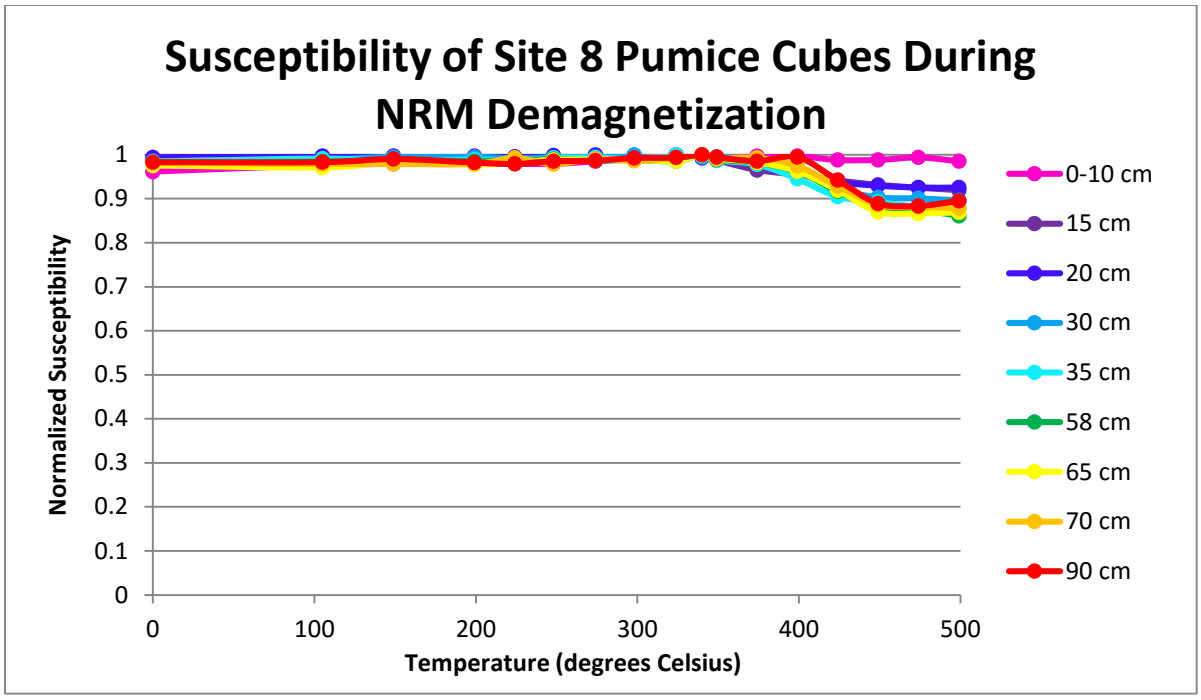

Figure 18. The susceptibility of the pumice cubes of site 8 after each NRM demagnetization step.

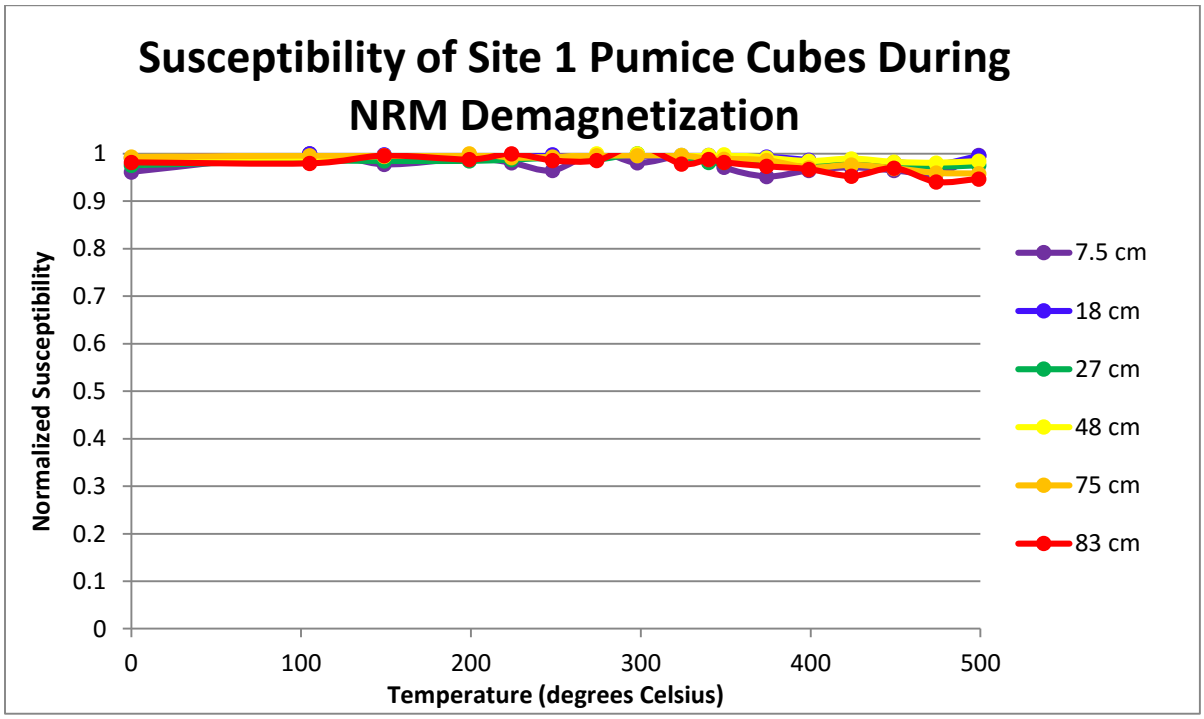

Figure 19. The susceptibility of the pumice cubes of site 1 after each NRM demagnetization step.

3.2 Self-Reversal Test

After the demagnetization of the NRM of the pumice cubes, the samples were given a total TRM as described above, and thermally demagnetized up to 250°C. At 250°C, several of the samples' magnetization intensity started to increase, which was a possible sign of self-reversal in the samples' magnetizations (Figure 20). Room-temperature susceptibility of the samples never changed, suggesting that the magnetization increase was not tied to a chemical alteration (Figure 21). A new sample holder was introduced at this point and the experiment was repeated in case the holder had affected the measurements. The site 8 pumice cube samples were again given a total TRM. This time the pumice cubes were fully demagnetized up to 600°C (Figure 22) with no change in the susceptibility of the samples (Figure 23). Magnetization intensities started to increase around 350°C, and an analysis of directions showed that this is linked to a high temperature component nearly antipodal to the lower temperature component. This phenomenon is sometimes called a "self-reversal" because the apparent reverse component is linked to rock magnetic phenomena as opposed to an actual change in the magnetic field direction.

Acquisition of a self-reversed component of magnetization has been previously linked to low temperature oxidation (Doubrovine and Tarduno, 2004). Oxidation of titanomagnetite to titanomaghemite is accompanied by an increase in Curie temperature. Therefore, after 450°C, I measured T_c of two representative samples (msh140858 and msh140890). Compared to fresh samples, T_c measured on warming in the treated samples is different because they have a different thermal history. However, there are no differences in the cooling T_c, which is not affected by past thermal history. The identical Curie temperatures in both fresh samples and heated samples that display self-reversal behavior suggest that significant oxidation has not taken

place during any of the laboratory heatings (Figure 24), but does not preclude maghemitization during low-temperature oxidation in nature.

I further investigated the capacity of the samples to acquire a self-reversed magnetization using the method proposed by Doubrovine and Tarduno (2004). Three unused samples from 0-10 cm (ms1408010b), 30 cm (msh140830a), and 70 cm (msh140870c) were demagnetized in an alternating field and given pTRMs. The pTRM acquisition data were analyzed to assess the direction of magnetization acquired at each temperature step. At low temperatures, magnetization was acquired parallel to the applied field, but at higher temperatures, the polarity of magnetization changed for two of the three samples. At 500°C, the magnetic orientation of sample msh1408010b had already changed by about 176°. At 525°C, the magnetic orientation of sample msh140830a changed by 151°C, but sample msh140870c did not change in magnetic orientation. This demonstrates that the samples are actually capable of acquiring a true self-reversed magnetization. As temperatures increased, susceptibility for all three samples started to decrease slightly by at most 18% around 400°C but then leveled out (Figure 25).

Afterwards, samples from the NRM and pTRM experiments that had self-reversed in magnetization, along with fresh material from the samples' corresponding host rocks, were thin sectioned. The thin sections were examined under reflected light and compared to each other, but no outstanding differences were noticed. There were some bright spots that could have been indicative of sulfides, but at the scale of observation, there were no signs of alteration or maghemitization in the samples that had self-reversed that could help to explain the self-reversal. Ultimately, it was not possible to determine the exact cause of the self-reverse behavior.

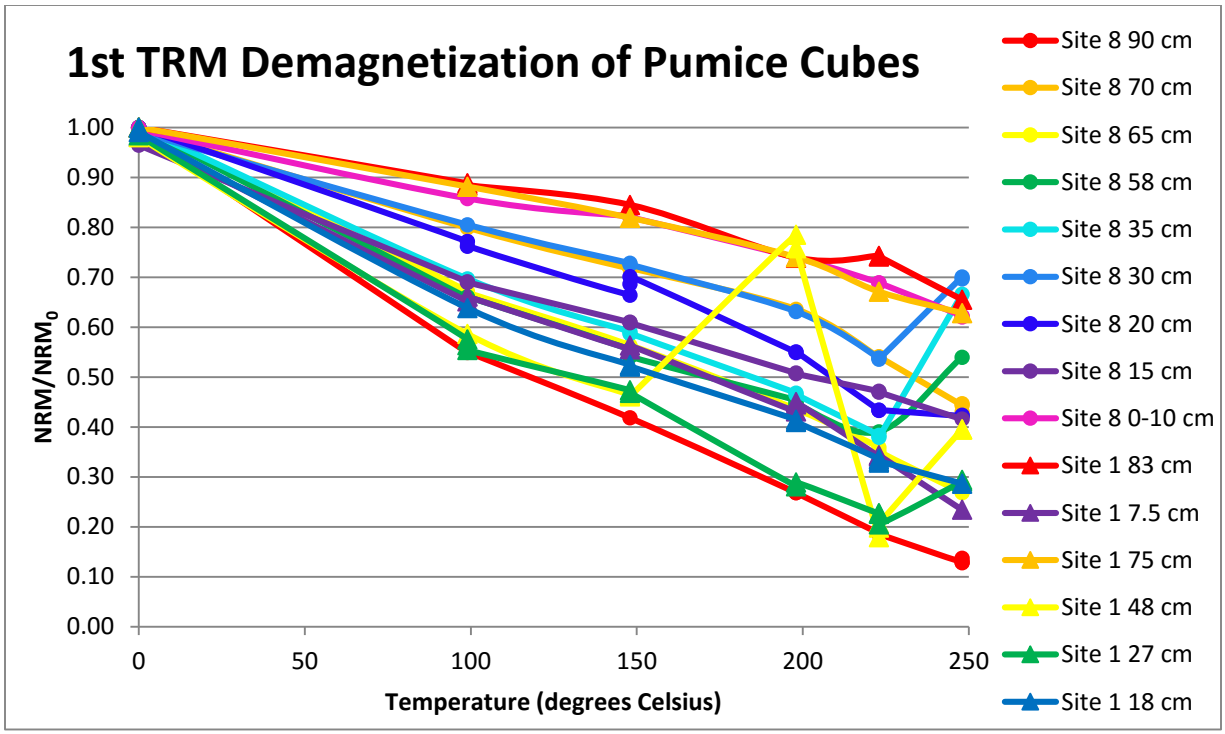

Figure 20. Results of the TRM demagnetization of the pumice cubes from sites 1 and 8. The increases in intensity indicate magnetic self-reversals.

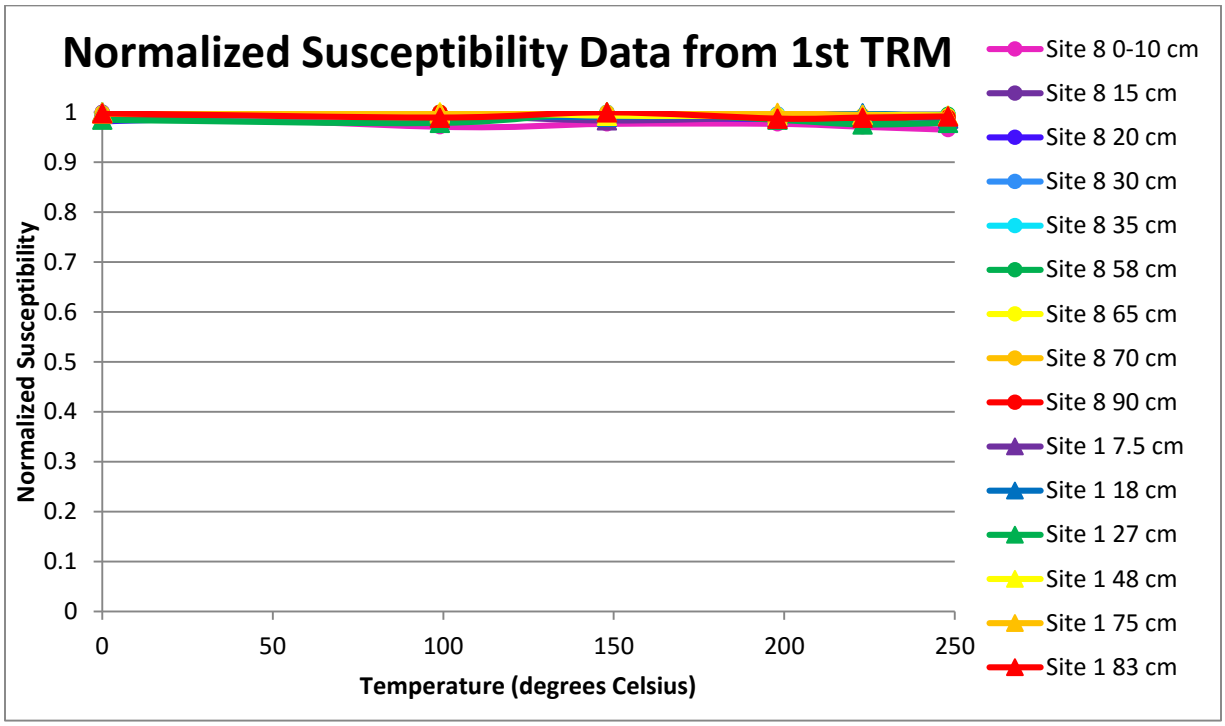

Figure 21. The susceptibility of the pumice cubes of sites 1 and 8 after each TRM demagnetization step.

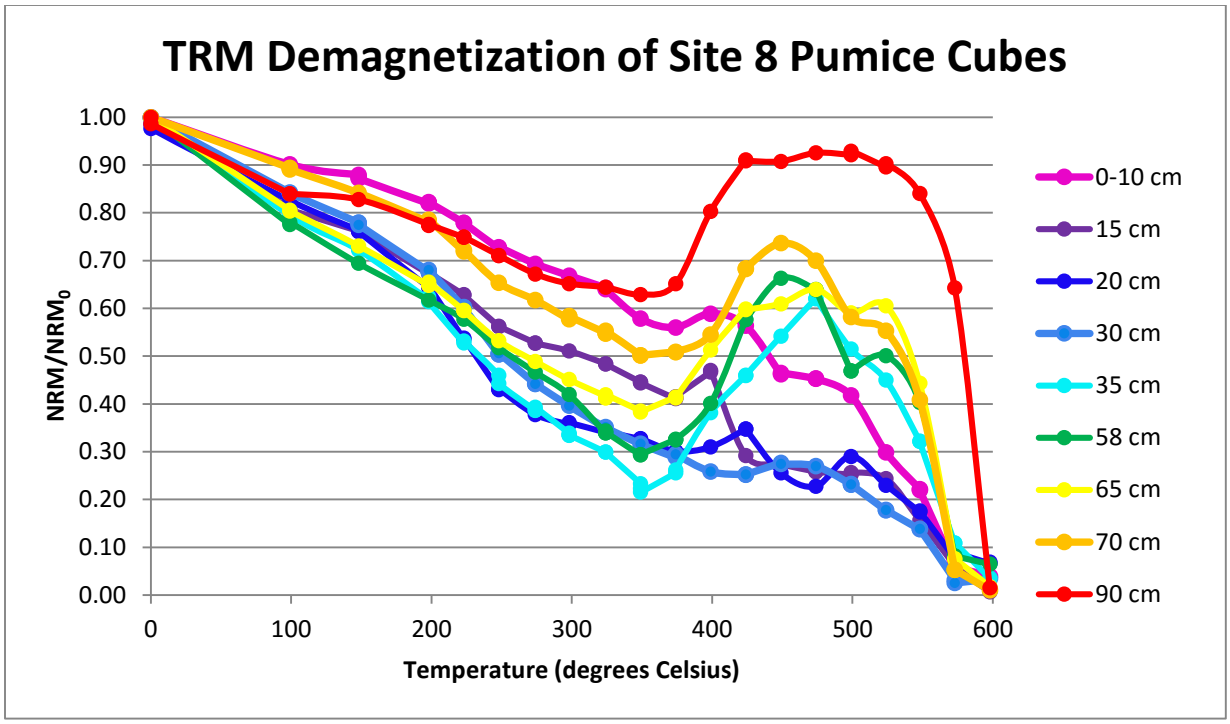

Figure 22. Results of the TRM demagnetization of the pumice cubes from site 8. The increases in intensity indicate magnetic self-reversals.

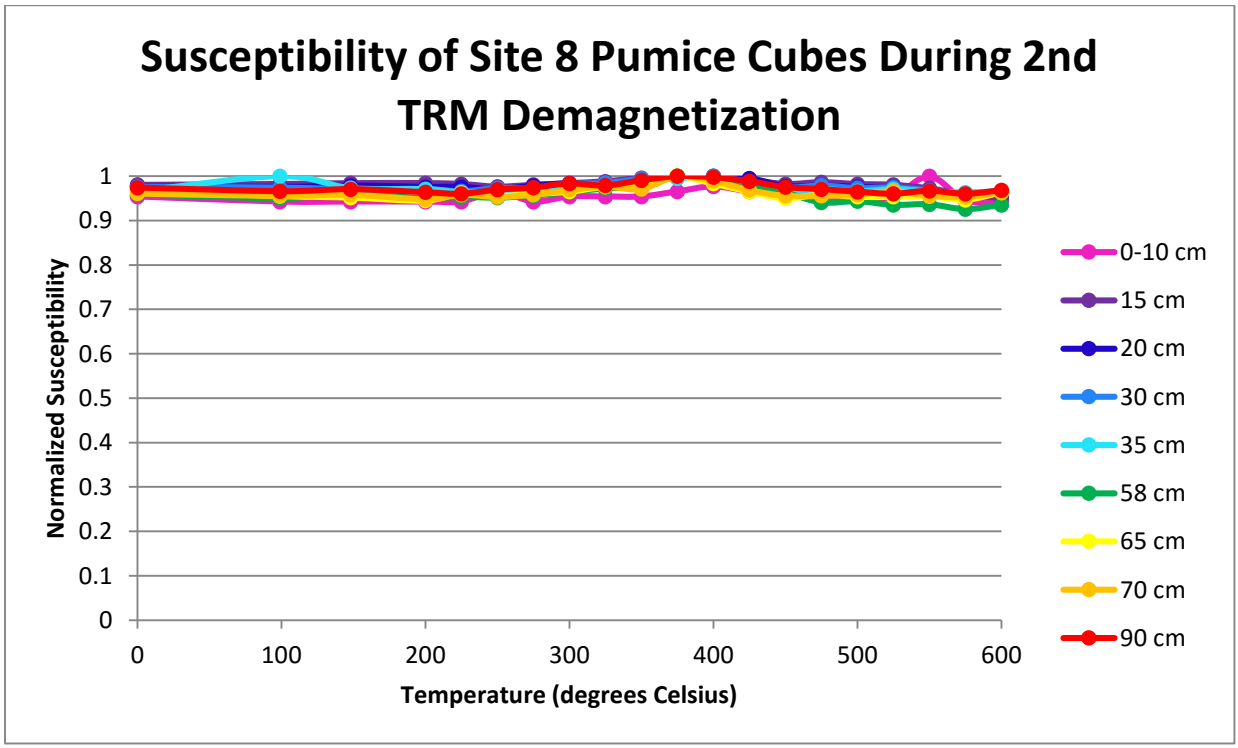

Figure 23. The susceptibility of the pumice cubes of site 8 after each TRM demagnetization step.

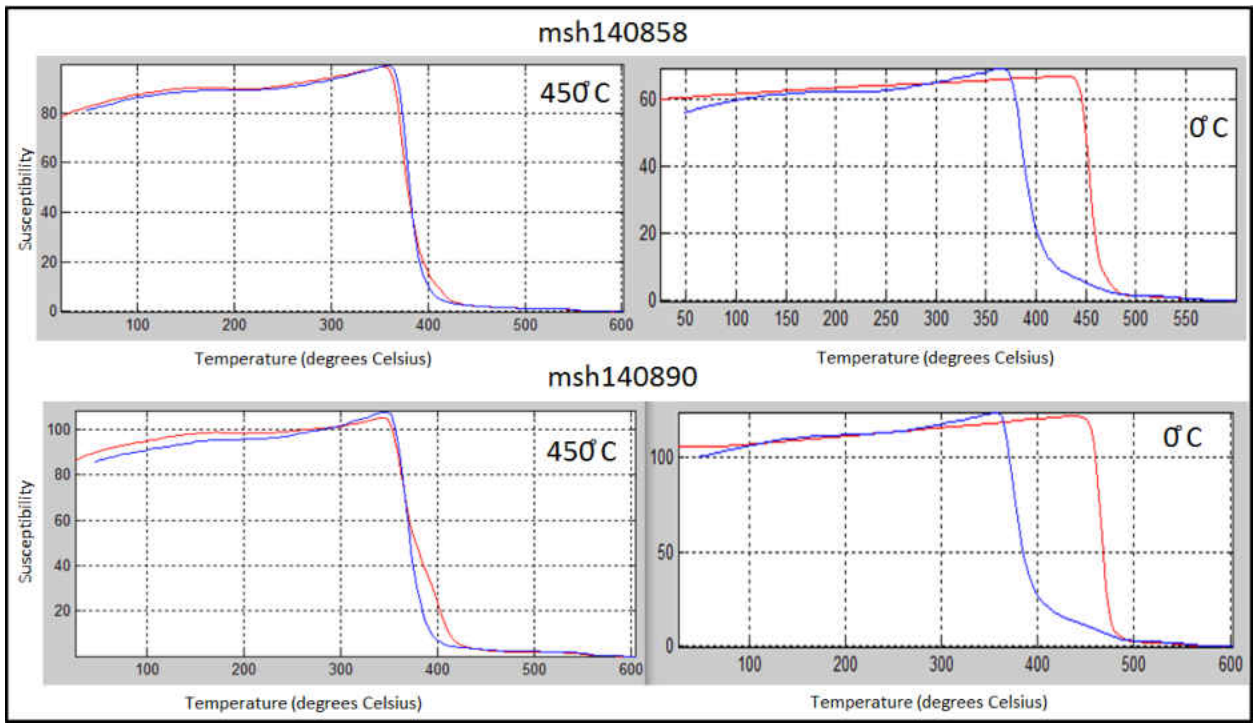

Figure 24. Susceptibility as a function of temperature for two representative samples (msh140858 and msh140890) that showed signs of possible self-reversal (after temperature step 450°C) and fresh samples (0°C) from the same pumice blocks, measured in Ar. The red curves represent heating curves and the blue curves represent cooling curves.

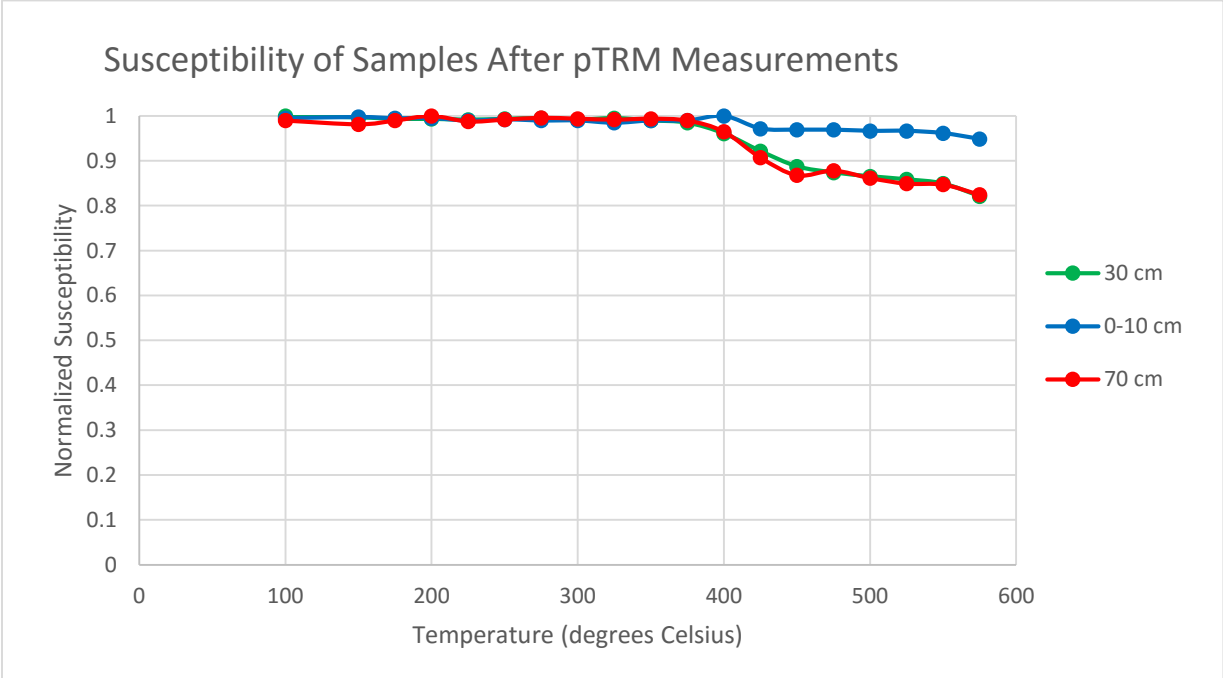

Figure 25. The susceptibility of the pumice cubes from site 8 after each pTRM acquisition step.

3.3 Paleomagnetic Emplacement Temperature Estimates

The previous experiments were designed to examine the extent to which T_{ub} varies with thermal history, and the results suggest that it may be up to ~50°C. This part of the study will apply the paleomagnetic method of finding emplacement temperatures using fresh samples to compare the results with the known magnetic orientation and emplacement temperature range at the time of the eruption of Mount St. Helens, and thus satisfy study goal #2 noted in Chapter 1. This will be done for lithic and pumice core samples collected from sites 4 and 5, with some samples from sites 2 and 6.

The lithic samples I demagnetized from sites 5 and 6 had two magnetic components, a low-temperature and high-temperature component, though two samples had three components (Figures 26 and 27; see also Appendix A). The lithic sample from site 2 had one magnetic component, unblocked at 500°C, and has a magnetic orientation close to the Earth's magnetic orientation on May 18th, 1980 (Figure 28). The low-temperature components for site 5 unblocked between 350°C (Figure 27) to 400°C (Figure 26) and have magnetic orientations a little deviated from the magnetic orientation of the Earth at the time of the Mount St. Helens eruption (Figure 29). The high-temperature magnetic components unblocked at about 625°C and have random magnetic orientations (Figure 30). The samples from site 6 are from two lithic fragments and have low-temperature components with unblocking temperatures that range from 400°C to 425°C. The magnetic orientations of the low-temperature components for samples from the same lithic fragment are also a little deviated from the magnetic orientation of the Earth at the time of the Mount St. Helens eruption (Figure 31). A summary of all best-fit low-temperature components, including magnetic orientation, can be found in Table 3 and low-and high-temperature components of the lithic samples can be found in Table 4. The check for changes in

the abundance and composition of the lithic samples from sites 2, 5, and 6 shows a brief dip in susceptibility of several samples from 425°C to 450°C by at most 22%, followed by a general decrease around 550°C by at most 28% (Figure 32).

The pumice from sites 4 and 6 were thermally demagnetized and the magnetic orientation of the samples from sites 4 and 6 are all comparable to the magnetic orientation of the Earth's magnetic field at the time of the eruption of Mount St. Helens (Figures 33 and 34). Unlike the lithics, all of the pumice samples have only one component of magnetization, as expected (Figures 35 and 36). The maximum unblocking temperatures for the site 4 and 6 cores range from 450°C to 625°C and 500°C to 600°C, respectively. Another difference between the lithics and the pumice is that the magnetization intensity of several pumice samples started to increase at higher temperatures and their magnetic orientation changed by about 180° (Figure 36). Evidence of any changes in abundance and composition of the magnetic minerals in the samples was checked using the susceptibility of the pumice from sites 4 and 6, which shows a similar pattern to the lithics boat with a brief dip in susceptibility of 20% to 25% from 450°C to 475°C followed by a general decrease in susceptibility around 575°C by at most 30% (Figure 37).

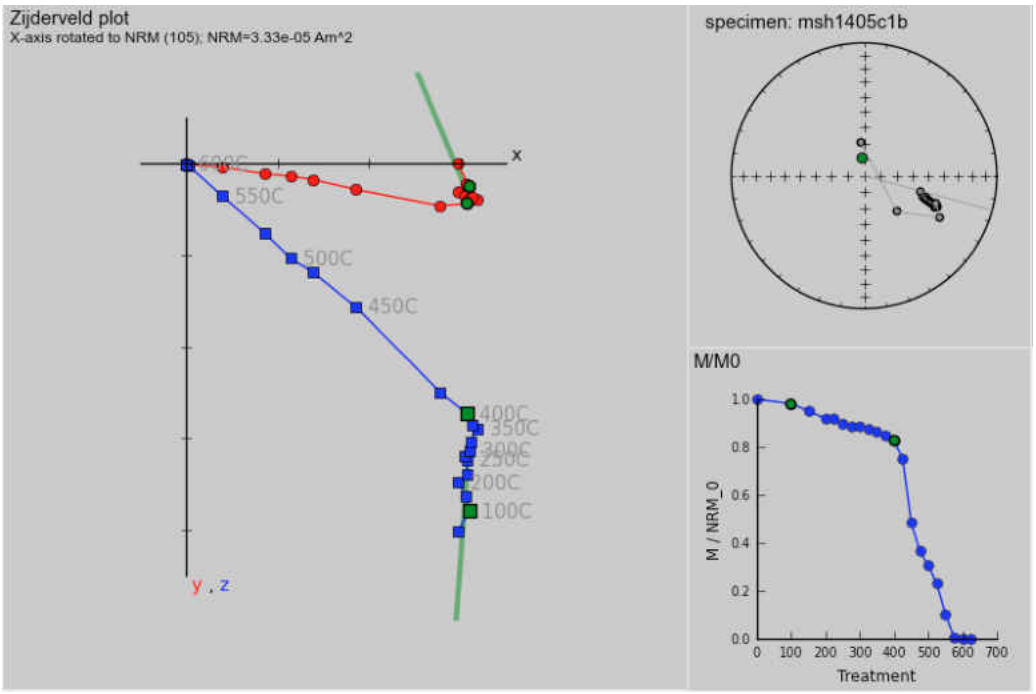

Figure 26. Sample C1b from site 5 has two magnetic components as seen in the Zijderveld plot at left. Green lines show best-fit to the low-T component from 100°C to 400°C. This direction is also shown by the green dot on the stereonet in the upper right, and its demagnetization curve is shown in the lower right (green dots show the demagnetization of the low-temperature component). The emplacement temperature is interpreted to lie at the break between the low-T and high-T components, ~400°C.

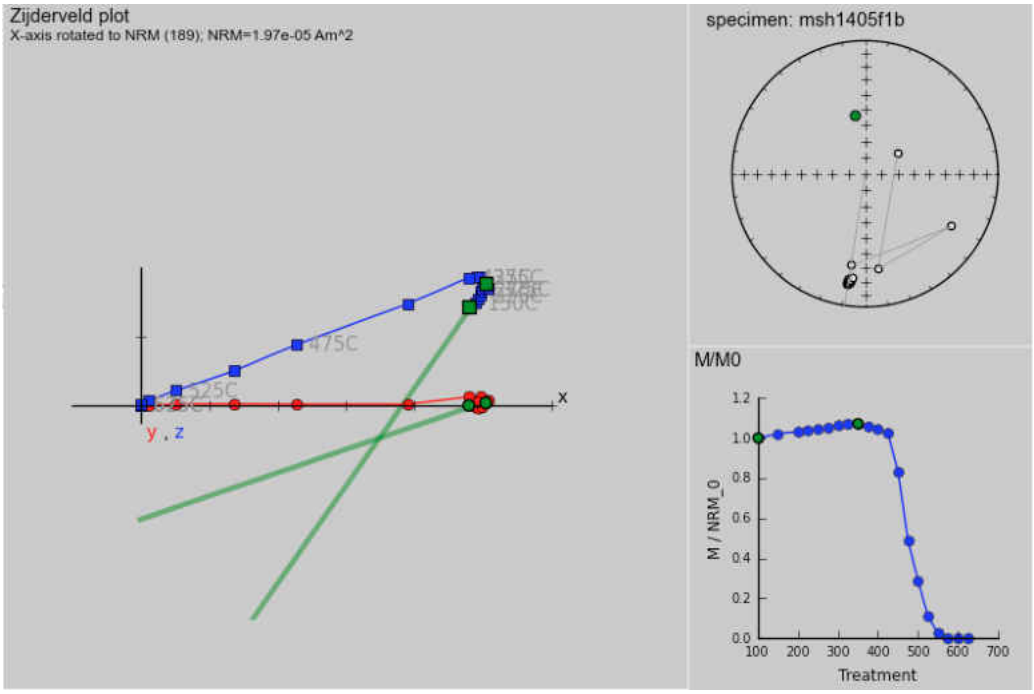

Figure 27. Sample F1b from site 5 has two magnetic components as seen in the Zijderveld plot at left. Green lines show best-fit to the low-T component from 100°C to 350°C. Symbols as in Figure 26. The emplacement temperature is interpreted to lie at the break between the low-T and high-T components, ~350°C.

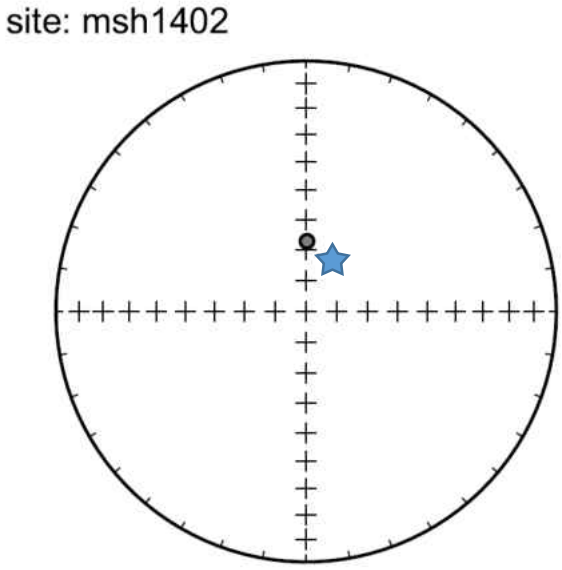

Figure 28. The orientation of the single magnetic component of the single site 2 lithic sample. The blue star is the magnetic orientation of the Earth during the May 18th, 1980 eruption of Mount St. Helens. It should be noted how close the orientation of the magnetic component is to the magnetic orientation of the Earth on May 18th, 1980.

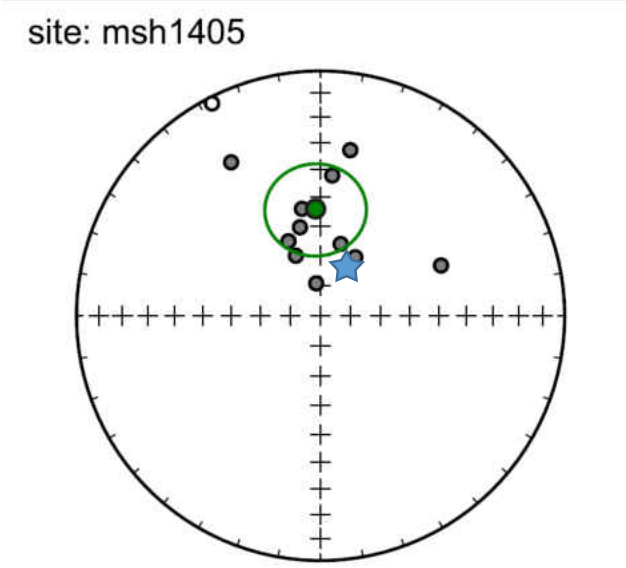

Figure 29. The orientation of the low-temperature magnetic components of the site 5 lithic samples with the green dot and circle showing the Fisher mean and α_{95} circle of confidence of the samples (Fisher, 1953). The blue star is the magnetic orientation of the Earth during the May 18th, 1980 eruption of Mount St. Helens. It should be noted how close the orientation of the low-T_b magnetic component is to the magnetic orientation of the Earth on May 18th, 1980, meaning the magnetization was acquired after the PDC deposit came to rest.

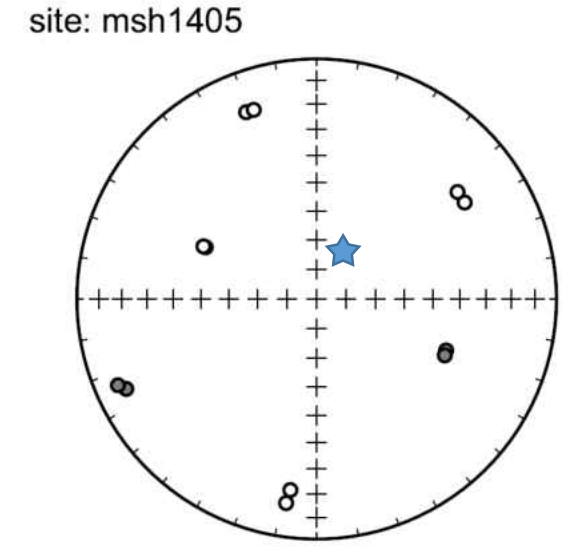

Figure 30. The orientation of the high-temperature magnetic components of the site 5 lithic samples. The blue star is the magnetic orientation of the Earth during the May 18th, 1980 eruption of Mount St. Helens. It should be noted how random the orientation of the high-T_b magnetic component is to the magnetic orientation of the Earth on May 18th, 1980, meaning the magnetization pre-dated the PDC.

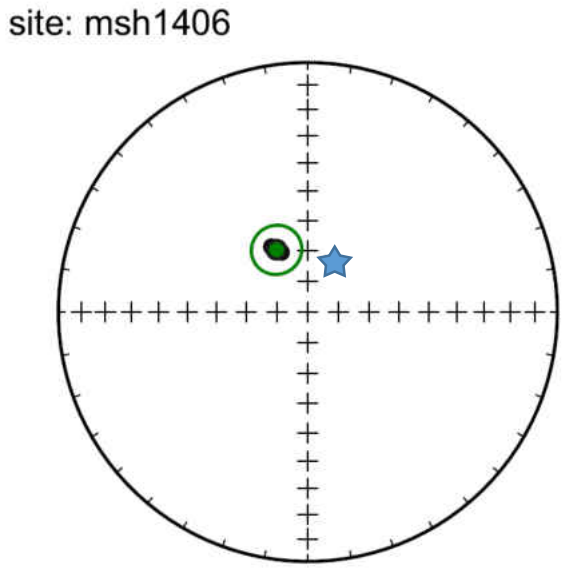

Figure 31. The orientation of the low-temperature magnetic components of the two site 6 lithic samples from the same lithic fragment. Symbols as in Figure 29. It should be noted how close the orientation of the low-T_b magnetic component is to the magnetic orientation of the Earth on May 18th, 1980, meaning the magnetization was likely acquired after the PDC deposit came to rest.

Table 3. Best-fit low-temperature directional data for all specimens.

	Sample Type	Sample Name	Specimen Name	Minimum Measurement Step	Maximum Measurement Step	Declination	Inclination	Deviation Angle	MAD	n	alpha95
Site 2	lithic	msh1402b1	msh1402b1a1	100	500	0.7	67.1	3.1	2.4	15	
Site 4	pumice	msh1404a1	msh1404a1a	100	625	25.9	63.7	0.2	3.4	20	
	pumice	msh1404a2	msh1404a2b	100	575	37.1	64.6	1	3.7	18	
	pumice	msh1404b1	msh1404b1a	100	450	35.1	72.5	1	2.7	13	
	pumice	msh1404c1	msh1404c1a	100	500	12.3	69.1	1.9	2.8	15	
	pumice	msh1404d2	msh1404d2a	100	525	23.1	69.5	0.9	2.2	16	
	pumice	msh1404e1	msh1404e1a	0	500	20	67.4	0.1	4	16	
	pumice	msh1404f2	msh1404f2a	100	450	25.6	70.1	3.1	5.4	13	
	pumice	msh1404h1	msh1404h1a	100	450	34	67	1.5	3.5	13	
	pumice	msh1404i1	msh1404i1a	100	450	40.7	72.4	0.7	3.9	13	
	pumice	msh1404j1	msh1404j1a	100	450	324.1	81.4	1.3	3.3	13	
	pumice	msh1404j2	msh1404j2b	100	550	8.5	71.5	1.6	2.7	17	
	pumice	msh1404j3	msh1404j3b	100	500	21.7	26.3	0.7	2.3	15	
	pumice	msh1404n1	msh1404n1a	100	575	145.1	59.5	0.7	2.9	18	
Site Mean						***29.5***	***69.7***				***9.7***
Site 5	lithic	msh1405a1	msh1405a1a	150	400	336.6	62.9	55.1	9.4	10	
	lithic	msh1405a1	msh1405a1b	150	400	346.9	59.6	68.8	8.9	10	
	lithic	msh1405b1	msh1405b1a	100	375	15.7	65.1	123.2	20.3	10	
	lithic	msh1405b1	msh1405b1b	0	350	329.7	28.2	75	12.2	10	
	lithic	msh1405c1	msh1405c1a	150	400	337.6	68.4	57.8	10.8	10	
	lithic	msh1405c1	msh1405c1b	100	400	352.4	79.2	49.9	8.7	11	
	lithic	msh1405d1	msh1405d1a	150	400	67.4	45.6	71.9	23.7	10	
	lithic	msh1405d1	msh1405d1b	100	400	332.9	-2.9	77.4	22.5	11	
	lithic	msh1405e1	msh1405e1a	100	350	4.8	42	62.7	24.3	9	
	lithic	msh1405e1	msh1405e1b	100	350	10.2	31.8	54.8	22.7	9	
	lithic	msh1405f1	msh1405f1a	0	350	30.7	67.3	123.5	10.3	10	
	lithic	msh1405f1	msh1405f1b	100	350	350.1	53.5	141.9	16.9	9	
Site Mean						***357.3***	***54***				***16.1***
Site 6	lithic	msh1406b2	msh1406b2a1	0	400	330.9	65.6	62.9	16.2	12	
	lithic	msh1406b2	msh1406b2a2	0	400	336.2	68.7	65.3	17.1	12	
Site Mean						***333.4***	***67.2***				***2.6***
	pumice	msh1406b3	msh1406b3a2	100	575	23.8	64.9	1.2	3	18	
	pumice	msh1406b4	msh1406b4a1	100	500	58.6	67.6	1.1	2.1	15	
	pumice	msh1406b5	msh1406b5a1	0	600	29.6	60.6	0.1	2.8	20	
	pumice	msh1406b6	msh1406b6a1	0	600	22.3	71.7	2	2.7	20	
Site Mean						***33.3***	***66.8***				***9.2***

Minimum and maximum measurement steps are the range included in calculating the best fit direction. Deviation Angle is the angle between the low-temperature component and the origin of the Zijderveld plot (Tauxe and Staudigel, 2004). For the lithic fragments, which have an additional high-temperature component, the deviation angle will be large. MAD (Maximum Angular Deviation) is a measure of the directional scatter in the measurement points included in the best-fit direction (Kirschvink, 1980). N is the number of measurement points included. Alpha95 represents the cone of 95% confidence about the best-fit direction (Fisher, 1953). For comparison, the May 1980 DGRF (Definitive Geomagnetic Reference Field) direction is 20.1° (declination) and 68.8° (inclination).

Table 4. A summary of the temperature ranges that encompass the magnetic components of the lithic samples from sites 2, 5, and 6.

	Specimen	Low-Temperature Component	High-Temperature Component	3rd (Highest) Temperature Component
Site 2	B1a1	100°C-500°C		
Site 5	A1a	150°C-400°C	400°C-500°C	500°C-625°C
	A1b	150°C-400°C	425°C-475°C	500°C-625°C
	B1a	100°C-375°C	425°C-625°C	
	B1b	0°C-350°C	400°C-625°C	
	C1a	150°C-400°C	400°C-625°C	
	C1b	100°C-400°C	400°C-625°C	
	D1a	150°C-400°C	400°C-625°C	
	D1b	100°C-400°C	425°C-625°C	
	E1a	100°C-350°C	375°C-625°C	
	E1b	100°C-350°C	350°C-625°C	
	F1a	0°C-350°C	350°C-625°C	
	F1b	100°C-350°C	375°C-625°C	
Site 6	B2a1	0°C-400°C	425°C-625°C	
	B2a2	0°C-400°C	425°C-625°C	

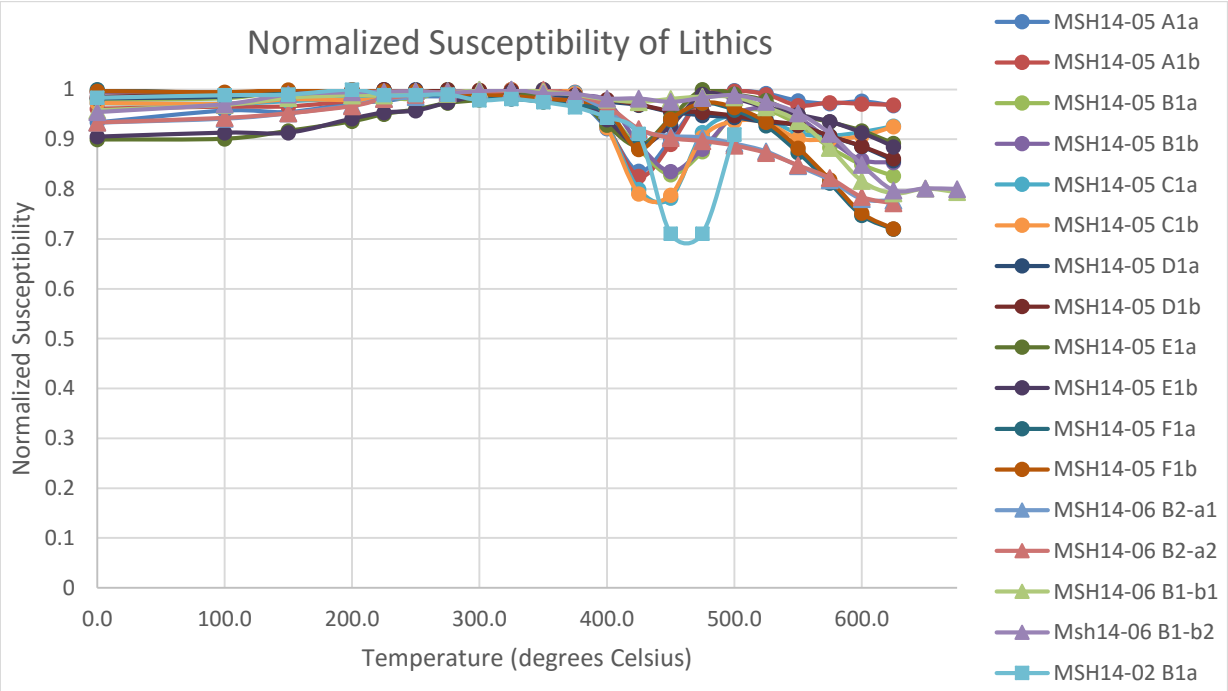

Figure 32. The susceptibility of the lithic cores from sites 2, 5, and 6 after each TRM demagnetization step.

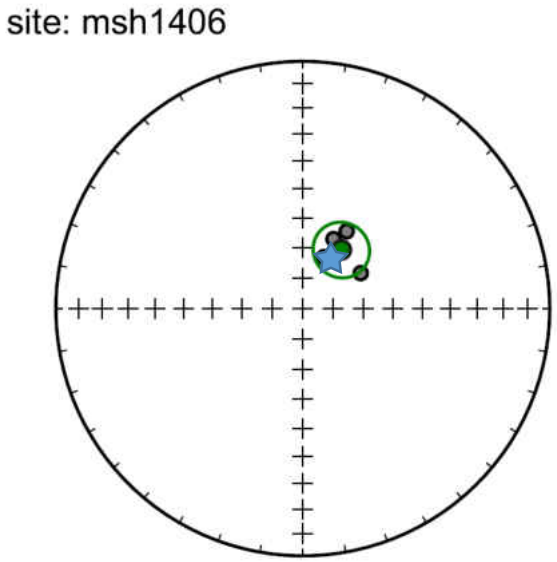

Figure 33. The orientation of the magnetic components of the site 6 pumice samples. Symbols as in Figure 29. As expected of juvenile material, the single magnetic component has a direction consistent with the field at the time of the eruption.

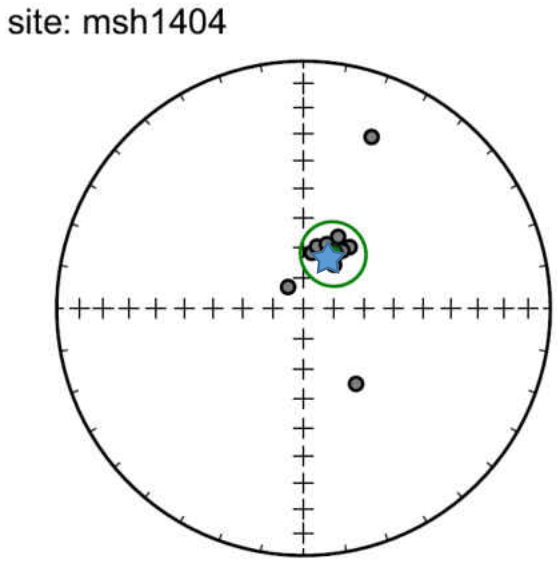

Figure 34. The orientation of the magnetic components of the site 4 pumice samples. Symbols as in Figure 29. As expected of juvenile material, the single magnetic component has a direction consistent with the field at the time of the eruption.

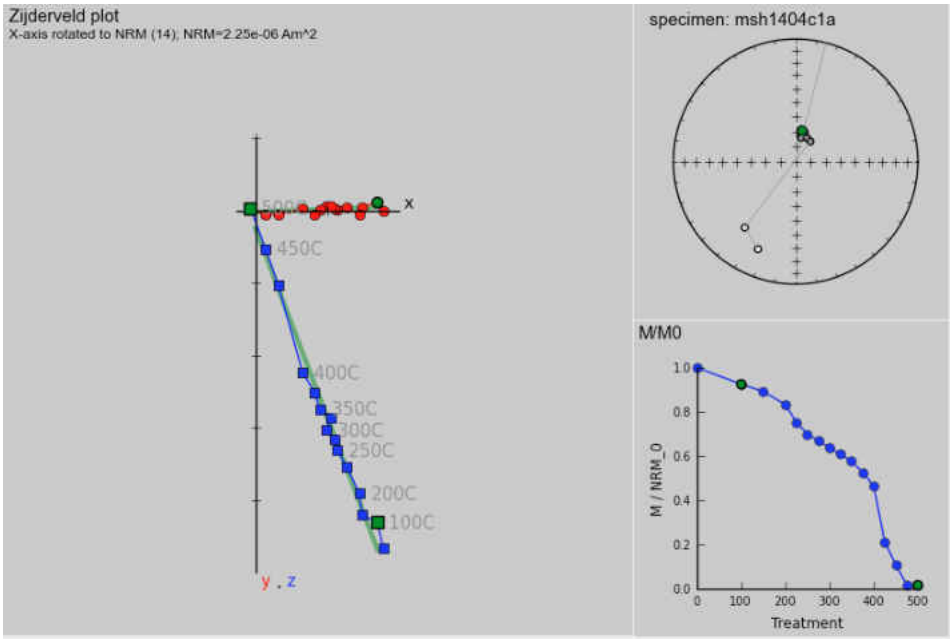

Figure 35. Pumice sample C1a from site 4 has one magnetic component as seen in the Zijderveld plot at left. Green lines show best-fit to the one temperature component from 100°C to 500°C. Symbols as in Figure 26. The emplacement temperature is interpreted to lie at 500°C.

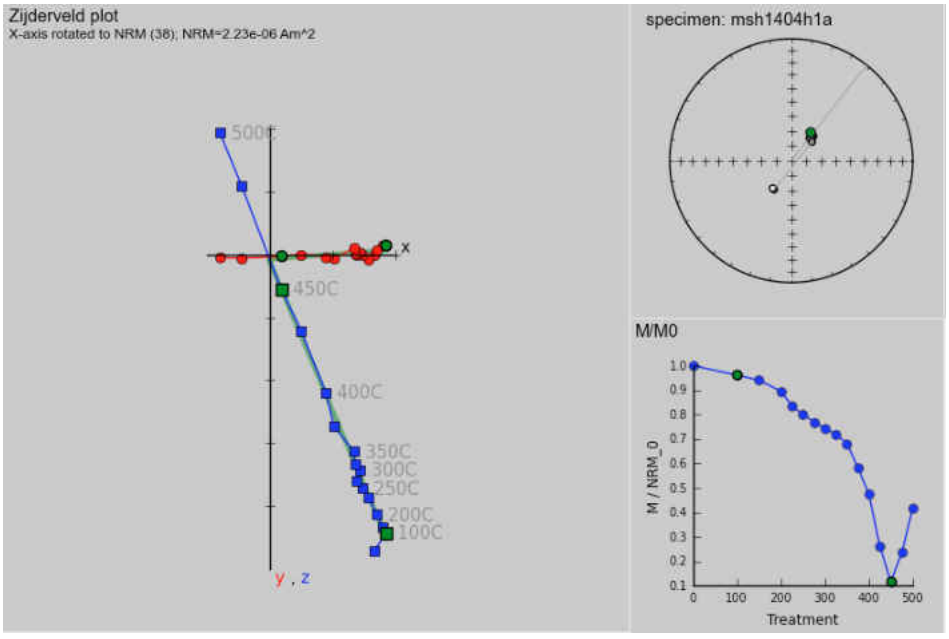

Figure 36. Pumice sample H1a from site 4 has one magnetic component as seen in the Zijderveld plot at left. Green lines show best-fit to the one temperature component from 100°C to 450°C. Symbols as in Figure 26. Past 450°C, the M/M0 graph shows the magnetic intensity of the sample increasing, accompanied by a ~180° change in magnetic orientation of the sample in the stereonet above it (white circles).

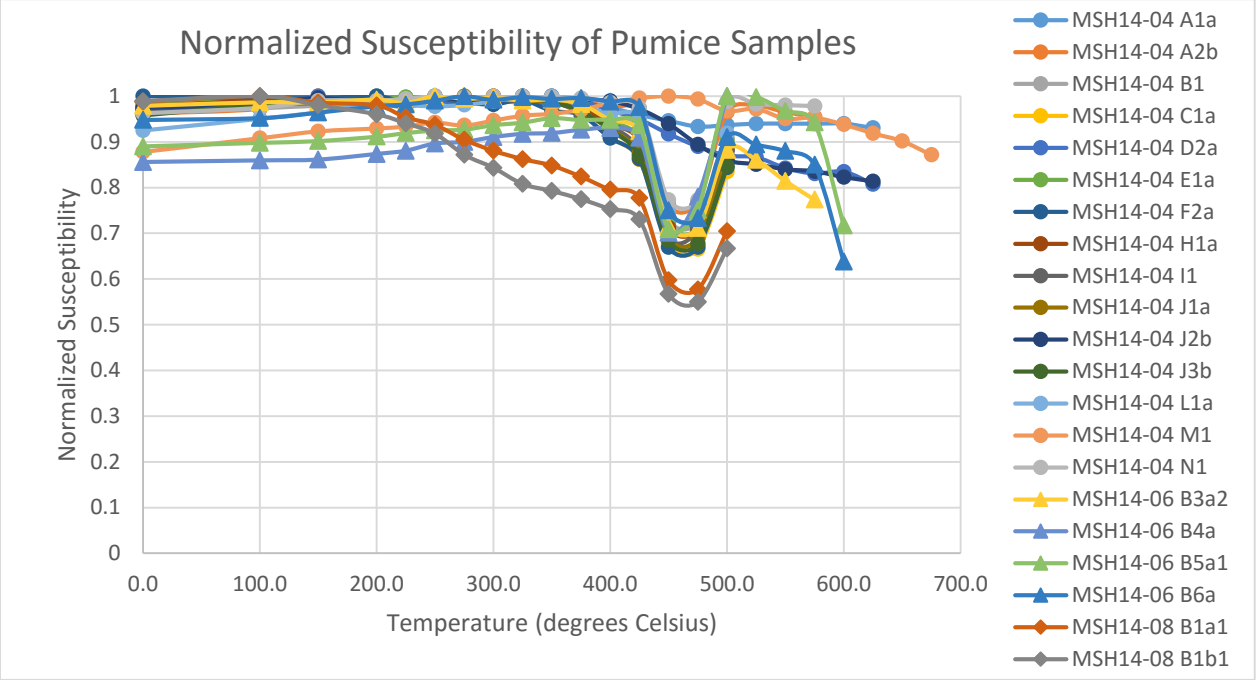

Figure 37. The susceptibility of the mostly pumice cores from sites 4, 6, and 8 after each TRM demagnetization step. The change in susceptibility signifies change in the abundance and/or composition of the magnetic minerals in each sample.

3.4 Curie Temperature Modification During Laboratory Heating

As shown above (Sec. 3.1, Figure 15), T_c increases with depth at site 8, presumably due to natural variations in thermal history. Two pumice samples from site 8 were used to test whether further laboratory heating may also modify T_c during the thermal demagnetization experiments. Results from splits taken from these samples following each demagnetization step are shown in Figure 38. The T_c measured on warming (T_c-heat) of the samples from site 8 stayed fairly consistent throughout the heating steps with a maximum difference of 27°C. If the laboratory heating steps were influencing T_c, one would expect a steady increase in T_c-heat. As this was not observed, this suggests that the time samples spend at elevated temperatures during thermal demagnetization experiments is not significantly modifying T_c or T_{ub}.

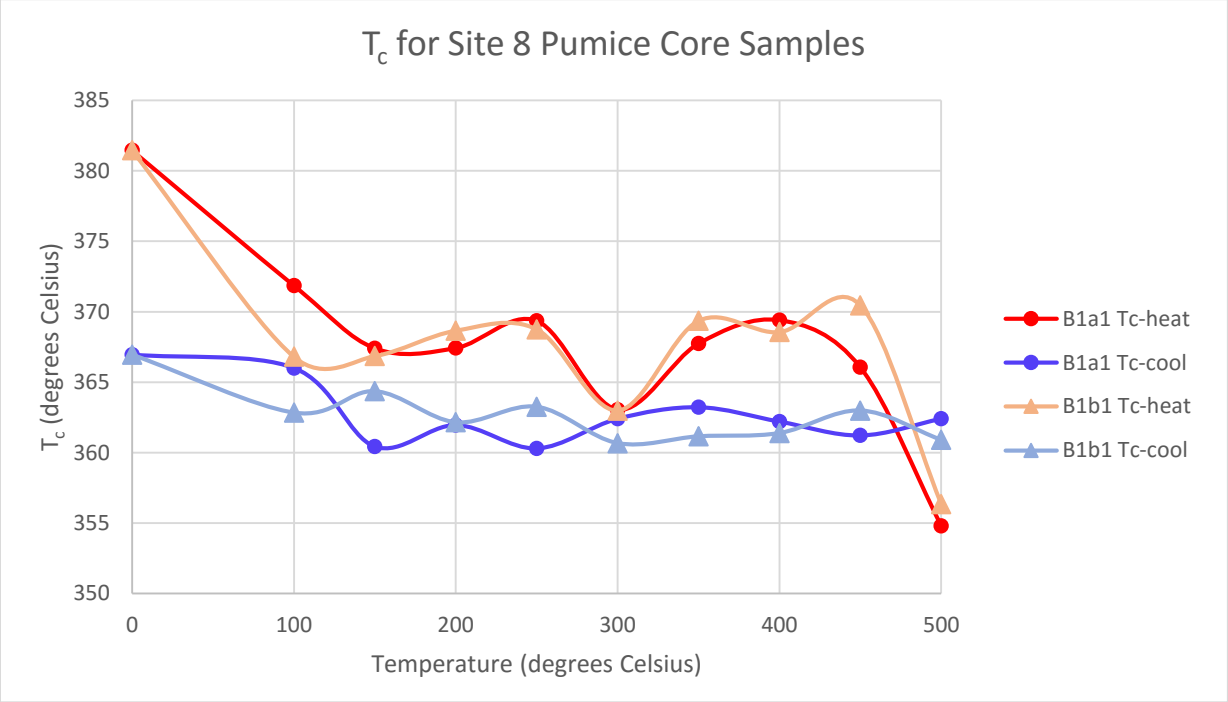

Figure 38. T_c of site 8 pumice core samples as heating steps increased during the TRM demagnetization. The lack of change in T_c shows that the thermal demagnetization steps were not altering T_c or T_{ub}.

3.5 Analysis of Curie Temperature Vs Depth

Curie temperature measurements were taken from ash matrices from sites 1, 2, 3, 4, and 6 and pumice from sites 4 and 8 (Figures 39, 40, 41, 42, 43, 44, and 45; also see Appendix B). These were then analyzed for patterns of Curie temperature vs. depth to examine any stratigraphic variations in T_c that could help to provide general estimates of emplacement temperatures (study goal #3). The ash samples from sites 1, 2, 3, 4, and 6 with some pumice samples from site 4 have one to two T_cs (Figures 39-45). As labeled in Figures 39-45, T_c-heat is T_c measured on warming and T_c-cool is T_c measured on cooling. T_c-cool is usually less than T_c-heat and does not change as much as T_c-heat with depth. This is because T_c-heat is influenced by

the prior thermal history of the sample, while all samples have the same thermal history for T_c-cool. T_c-cool predominantly reflects the compositions of the magnetic minerals in the sample.

T_{c1} is the dominant Curie temperature associated with the moderate-Ti, homogeneous titanomagnetite. This is the phase that will be most affected by any reordering process. T_{c2} is much higher in temperature and could indicate magnetite or low-Ti titanomagnetite. T_{c2} of sites 3 and 6 are quite varied, which could mean that these were titanohematites with complex growths and altered margins or oxy-exsolved titanomagnetites with some ilmenite lamellae that were observed by Kuntz et al. (1981). However, considering the large variances in the T_{c2} in the ash at sites 1, 3, 4, and 6 (Figures 39, 41, 42, and 43), the titanohematites with complex growths and altered margins seem more likely.

Ash from sites 2 and 6 show an increase in T_c-heat as depth increases similar to what is observed for site 8, which was addressed above and is shown in Figure 45 (Figures 40 and 43). However, ashes from sites 1 and 3 have relatively constant Curie temperatures below 400°C (~385°C and ~380°C, respectively) (Figures 39 and 41). Site 4 ash was different from the other sites in that it encompassed the base of one unit and the top of another (Figure 42). The upper part of the section was the base of a unit, and T_c-heat of these samples was relatively constant and considerably higher than T_c-cool measured on cooling. Below the boundary between the two units, the lower unit has relatively constant T_c-heat, but in this instance it is slightly less than T_c-cool. The pumice from site 4 shows a very general increase of T_c with depth, but the data are scattered and difficult to interpret.

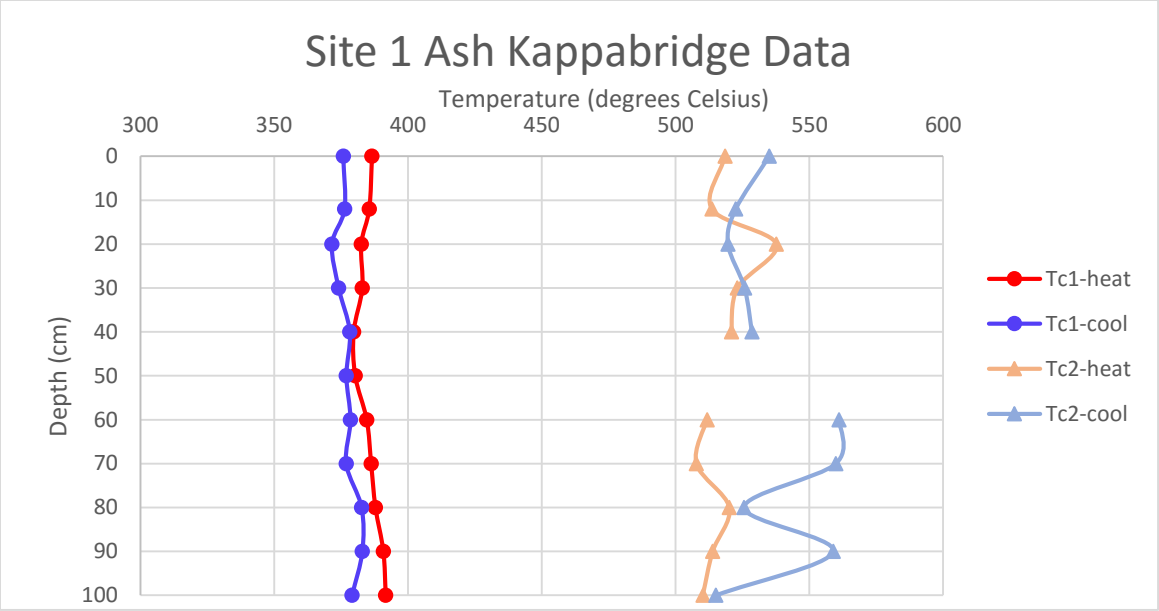

Figure 39. T_c of Site 1 ash matrix as depth increases during heating and cooling of samples. T_{c1} data points show dominant T_cs and T_{c2} indicates secondary T_cs much higher in temperature than T_{c1}. T_c-heat is T_c measured on warming. T_c-cool is T_c measured on cooling. The small difference between T_{c1}-heat and T_{c1}-cool suggests this flow was emplaced at temperatures less than ~300°C, and no cation reordering took place.

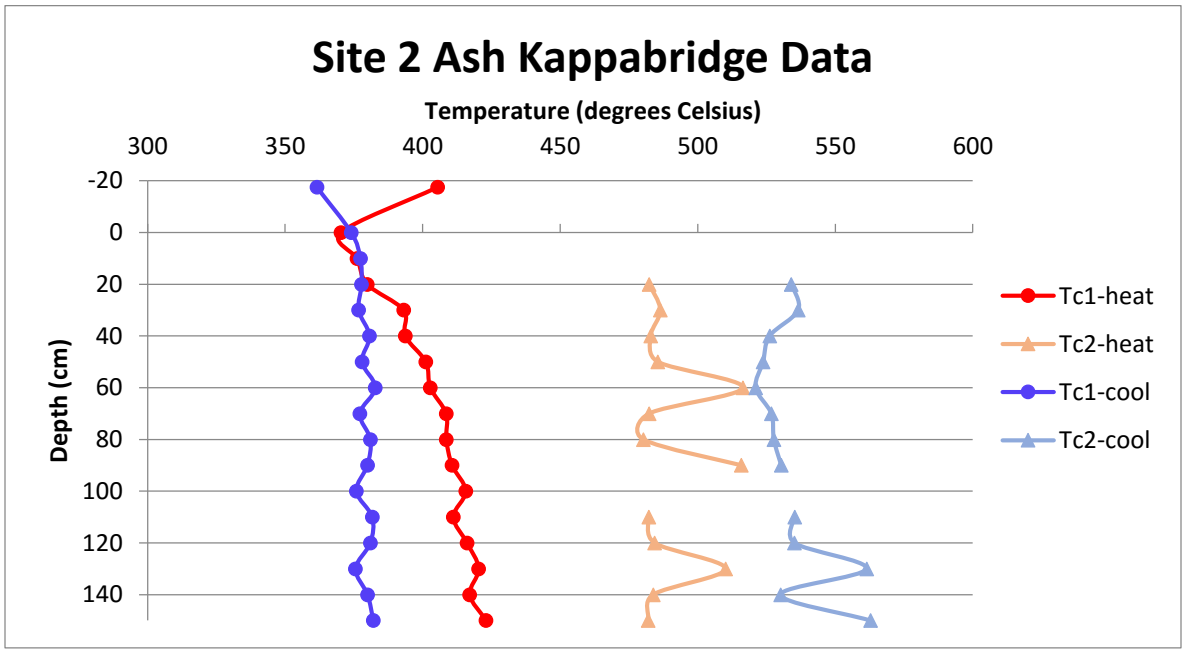

Figure 40. T_c of Site 2 ash matrix vs depth during heating and cooling of samples. Symbols as in Fig. 39. The gradual increase of T_c-heat with depth indicates that the emplacement temperature was > ~300°C, the approximate temperature at which reordering begins to take place. Slower cooling at depth led to greater reordering and higher T_c-heat.

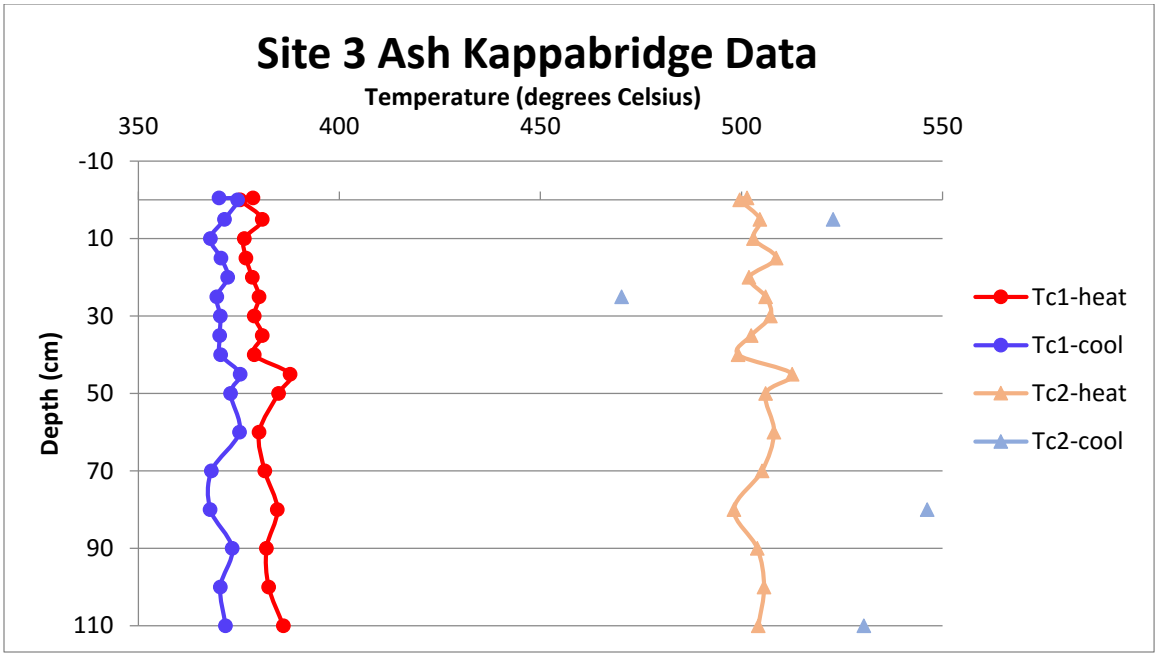

Figure 41. T_c of Site 3 ash matrix vs depth during heating and cooling of samples. Symbols as Figure 39.

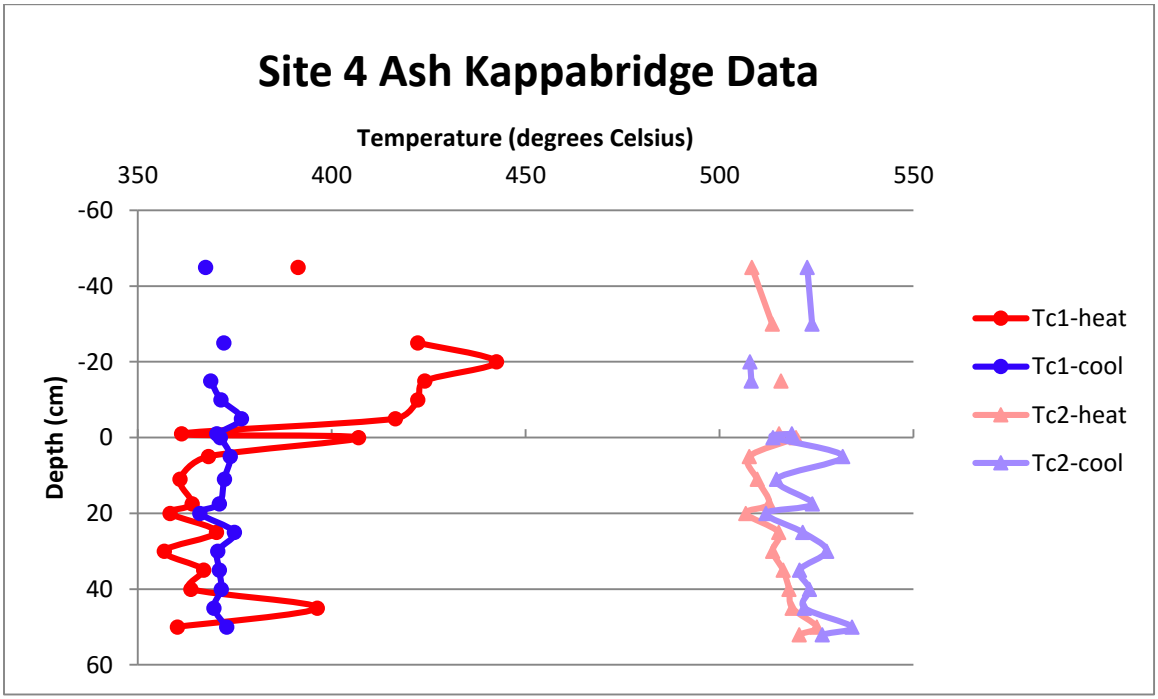

Figure 42. T_c of Site 4 ash matrix vs depth during heating and cooling of samples. Symbols as in Figure 39. This section is comprised of two units, with a boundary between them at 0 cm. The elevated T_c-heat in the upper unit suggests that it was emplaced at temperatures greater than 300°C, while the lower unit was emplaced at temperatures less than 300°C.

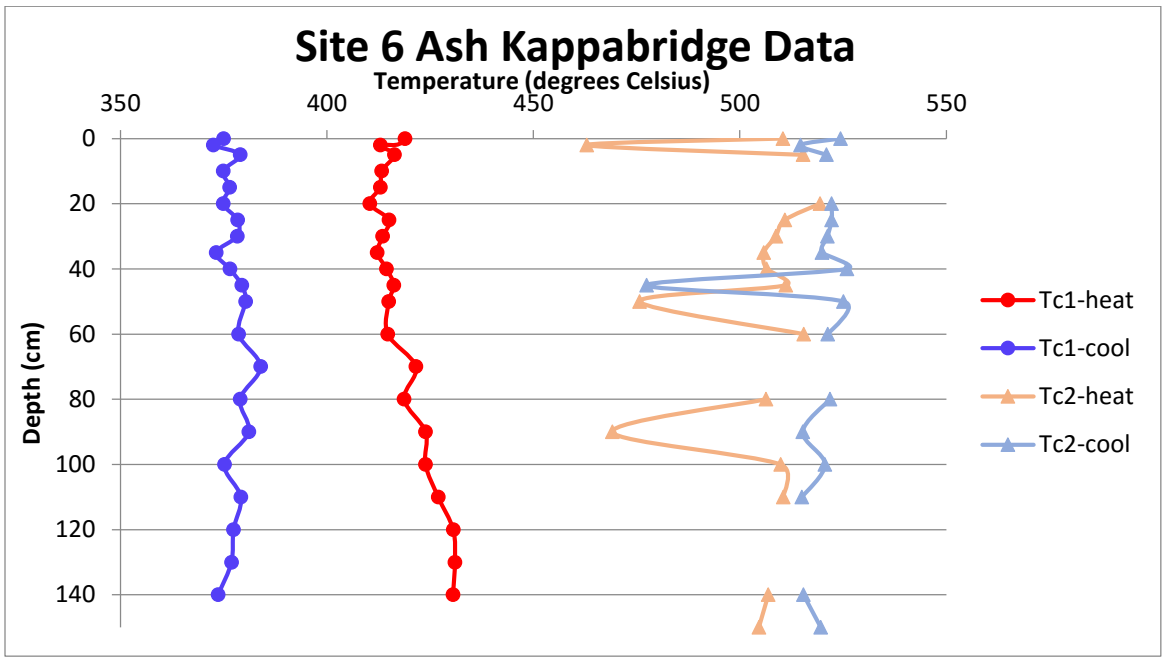

Figure 43. T_c of Site 6 ash matrix as depth increases during heating and cooling of samples. Symbols as in Figure 39. The gradual increase of T_c with depth signifies that cation reordering has occurred, which does not start until about 300°C.

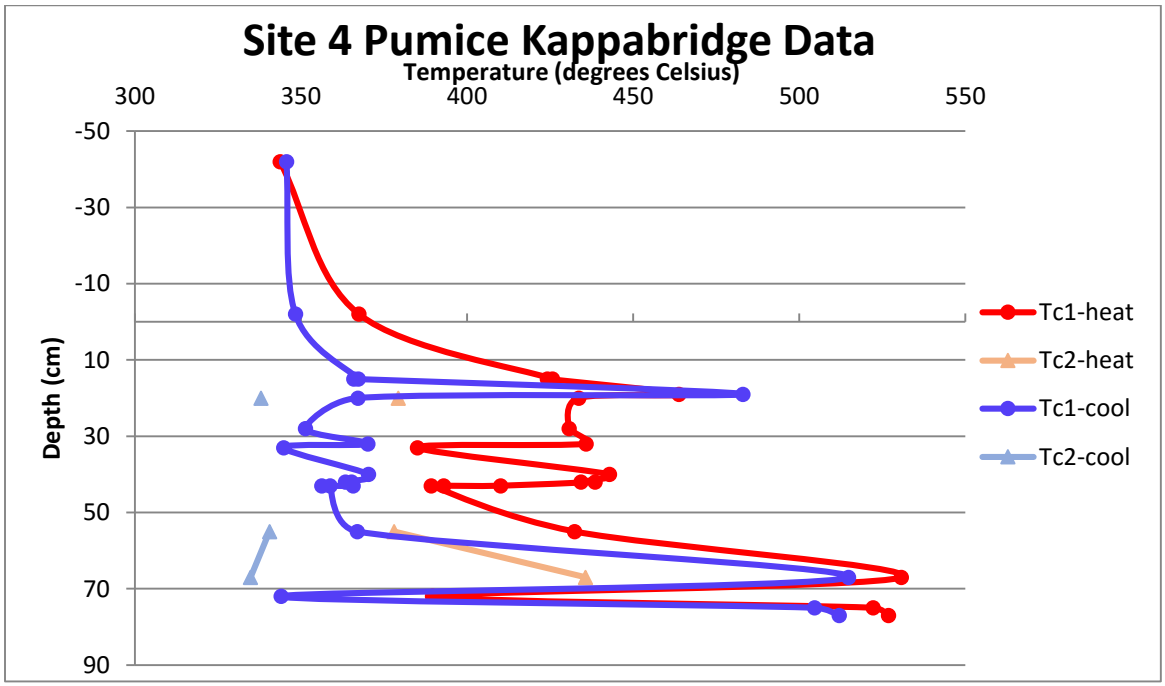

Figure 44. T_c of Site 4 pumice vs depth during heating and cooling of samples. Symbols as in Figure 39.

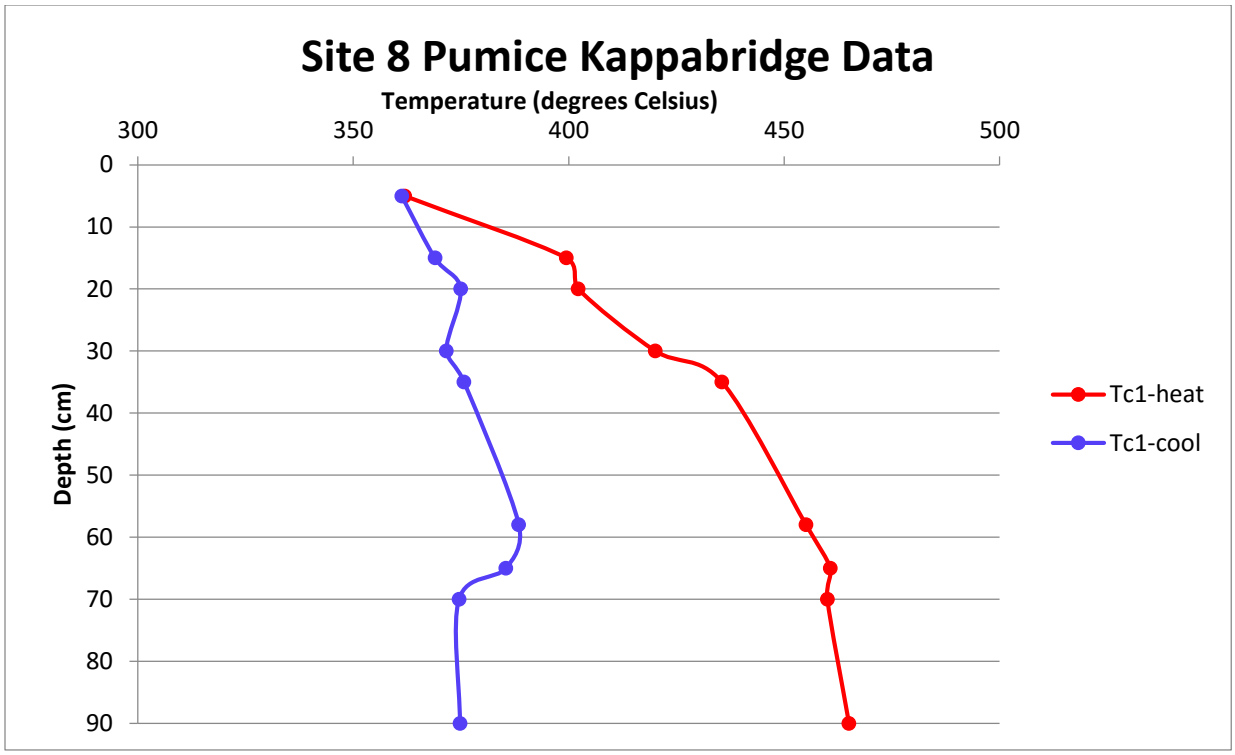

Figure 45. T_c of Site 8 pumice as depth increases during heating and cooling of samples.

Chapter 4: Discussion

Study goal #1 was to examine how blocking temperature varies with thermal history. Thermal demagnetization of pumice fragments from site 8 show that T_b-max increases with depth from ~415°C at the surface to ~465°C at 90 cm depth (Figure 15). This suggests that emplacement temperatures deeper in the flow may be biased high by as much as ~40-50°C.

Study goal #2 was to test paleomagnetically determined emplacement temperatures against direct temperature measurements to see if such a bias is actually observed. To examine the accuracy of the paleomagnetic method used for finding the emplacement temperature of PDC deposits, the estimated emplacement temperature will be compared to field measurements taken after the eruption of Mount St. Helens. The minimum directly measured emplacement temperature of the May 18th flow of Mount St. Helens is approximately 270°C with a maximum

measured emplacement temperature of 367°C. There was also an estimated emplacement temperature of 418°C, but that was less than a kilometer from the dome (not taking elevation into account), and far from our sampling sites (Banks and Hoblitt, 1996). The emplacement temperature estimates for this study show the lithic samples from sites 5 and 6 ranging from 350°C to 425°C and the pumice samples from sites 4 and 6 ranging from 450°C to as high as 625°C (Figure 46). Given the narrower emplacement temperature ranges and the closer emplacement temperature estimates, it is clear that the lithics provide more accurate results than the pumice. This makes sense as this paleomagnetic technique was designed for analyzing lithics which are most likely to have both primary and secondary magnetizations (e.g., Hoblitt and Kellogg, 1979; Paterson et al., 2010). When the unblocking spectrum of the low-temperature component exceeds the emplacement temperature (due, for example, to a multi-domain effect), this will not be detected if there is no overlapping high-temperature component.

According to Paterson et al. (2010), the lowest temperature in a range of emplacement temperatures found from samples taken from a single flow is the temperature of deposition for that flow. Using this definition, and focusing on the lithics, the temperatures of deposition for sites 2, 5, and 6 are 500°C, 350°C, and 400°C respectively. (Pumice results from sites 4 and 6 would give emplacement temperatures of 450°C and 500°C). Site 5 is likely the most robust, as it has six lithic clasts (12 total temperature estimates), while sites 2 and 6 only have one or two clasts each. The two Banks and Hoblitt (1996) temperature measurements closest to site 5 both gave temperatures of 307°C (Figure 5). This suggests the paleomagnetic estimates are biased high by ~40°C, consistent with the results from the thermal demagnetization of the site 8 pumice samples.

Paterson et al. (2010) also compared their paleomagnetic results of the deposits from the May 18, 1980 eruption to those of Banks and Hoblitt (1996). The directly measured emplacement temperatures that Banks and Hoblitt (1996) found for the sample sites in the study by Paterson et al. (2010) ranged from ~300°C to 367°C. The paleomagnetically-determined emplacement temperatures range from 330°C to 390°C. Their estimated emplacement temperatures are slightly higher than what was measured by Banks and Hoblitt (1996), suggesting an overestimate of approximately 20-30°C.

For the most part, the emplacement temperature estimates are higher than what was measured by Banks and Hoblitt (1996) by at most 58°C (lithics with two magnetic components), and this is likely due to the process of cation reordering. The mineral titanomagnetite is organized into a cubic lattice of oxygen anions and metal cations (Ti^{4+}, Al^{3+}, Mg^{2+}, and $Fe^{2+/3+}$). These cations can either occupy octahedral sites (ionically bonded with six oxygens) or tetrahedral sites (ionically bonded with four oxygens) (Figure 47). During the heating process, the cations and/or vacancies in the mineral titanomagnetite may obtain enough energy to be able to move to different interstitial sites. This movement of the cations can cause changes to the magnetic properties of the mineral. Bowles et al. (2013) have found that the higher the order of cations, the higher T_c becomes, which can occur during slow cooling. At temperatures greater than ~300°, the cations become mobile and will move towards equilibrium lattice locations and thus increase the degree of ordering. This appears to bias the emplacement temperature estimates because T_c and T_b are allowed to increase during natural cooling.

Other possible explanations for maximum unblocking temperatures that exceed the measured emplacement temperature include the presence of MD grains; alteration of magnetic minerals at temperatures less than T_{ub}, either in nature or in the lab; or the laboratory heating

steps themselves pushing T_{ub} up. We know that the homogeneous titanomagnetite present in these samples is multi-domain (Bowles et al., 2015), and that MD grains have unblocking temperatures that exceed the blocking temperature. Bardot and McClelland (2000) conclude that in lithic samples with two components of magnetization, the MD effect will not affect the emplacement temperature estimate. However, this is not the case for juvenile pumice with only one component. Therefore, MD grains can explain some of the overestimation in the pumice samples. It cannot explain the increase in blocking temperature with depth. MD grains should produce the same overestimation for each sample from the top of the flow to the bottom. Also, MD grains would not have fully demagnetized until the T_c was reached if the NRM was acquired at a temperature well below T_c, but would not have affected the susceptibility of the samples (Bol'shakov and Scherbakova, 1979). This is important to note, because the room-temperature susceptibility of many of these samples changed noticeably during the course of thermal demagnetization. This could suggest that at higher temperatures, new minerals were being created and/or destroyed, altering the amount and composition of the samples' magnetic minerals. Again, alteration is unlikely to produce the progressive increase in T_c or T_b with depth. The final possibility is that the paleomagnetic method itself was the cause of these alterations. As noted above, it was considered that T_c might increase with laboratory heating in the same way that it seems to increase when subjected to elevated temperatures in nature. If this were true, it might be expected that unblocking temperatures could increase during the course of the thermal demagnetization experiment. However, the two site 8 cores that were subsampled after each heating step to test this possibility had a consistent T_c throughout the experiment (Figure 38), showing that the heating steps themselves were not altering the T_cs of the samples and ruling out direct errors related to the laboratory heating itself.

As noted above (Sec. 3.1), the maximum unblocking temperatures exceed the Curie temperature in many samples from site 8 (Figure 15), a theoretical impossibility if the samples contain a single magnetic phase that remains unaltered during thermal demagnetization. There are several possible explanations for this observation: (1) alteration may be taking place during thermal demagnetization; (2) there may be additional magnetic phases present in addition to the homogeneous titanomagnetite; and (3) if T_c and T_{ub} are increasing during the experiment due to cation reordering, then it could in theory result in an apparent T_{ub} greater than T_c. The third explanation is disproved by the lack of change in T_c as demagnetization steps increased (Figure 38). If there had been any cation reordering, then T_c-heat should have increased with experimental temperature.

The decrease in susceptibility of some of the site 8 pumice samples after 400°C during the pTRM experiment and the thermal NRM demagnetization of the lithic and pumice cores (several of which also showed evidence of self-reversed magnetization) could have been linked to the inversion of low-Ti titanomaghemite to titanohematite, which has a higher T_c, but a lower susceptibility and saturation magnetization. This inversion could therefore produce an apparent T_{ub} higher than T_c. Titanomagnetite has a cubic structure, but when it is oxidized at low temperatures, the composition of the mineral becomes more akin to hematite (titanomaghemite), but the mineral retains its cubic structure. As a result, it can become unstable at high temperatures and inverts from cubic (titanomaghemite) to rhombohedral (titanohematite). The susceptibility of titanohematite is less than that of titanomaghemite, so this could explain the decrease in susceptibility. A fraction of the grains may have undergone low-temperature oxidization in nature or during the early, low-temperature steps in the lab. Doubrovine and Tarduno (2004) have suggested that the titanomaghemite can carry a self-reversed

magnetization. I looked for oxidation in the thin sections of used samples showing self-reversal and their unused counterparts but did not find any discrepancies. A possible explanation for this is that the oxidation was on a smaller spatial scale than what could be observed using a standard microscope. However, it seems unlikely that sample alteration would have produced a consistent, gradual increase in T_c with depth in samples from many sites. Alteration would have likely produced more erratic results as not every sample would have been altered in the same way.

The presence of other magnetic phases with high T_c in the fresh samples could result in unblocking temperatures that exceed the dominant T_c. A closer examination of the susceptibility vs. temperature data for the site 8 samples shows that this is likely the case. Although the dominant T_c (~375-450°C) is associated with the moderate-Ti titanomagnetite, susceptibility does not decrease to zero above this T_c. Instead, there is evidence of a secondary T_c much closer to 580°C, consistent with the presence of low-Ti titanomagnetite. Although subtle in the susceptibility vs temperature data, this magnetic phase can carry remanence above the dominant T_c (lower), leading to an apparent maximum T_{ub} greater than T_c.

Finally, study goal #3 was to evaluate whether stratigraphic variations in T_c could be used to provide rough constraints on emplacement temperature, in the absence of lithic fragments. I will now discuss the stratigraphic variations in T_c measured on the matrix ash in terms of emplacement temperature. In contrast to site 8, site 1 does not show an increase in maximum unblocking temperature with depth. A possible reason for this is that the top of the flow was not preserved. However, an examination of the Curie temperatures with depth (see Figure 39) shows that Curie temperature does not vary at all with depth and that the heating and cooling T_cs are nearly the same. This suggests that site 1 was emplaced at a temperature less than ~300°C and the titanomagnetite did not have the opportunity to reorder towards equilibrium. The same could

be said for site 3, which shows the same pattern as site 1. Sites 2 and 6 show a gradual and consistent increase in T_{c1}-heat, which is likely a result of cation reordering and suggests an emplacement temperature of ~300°C or higher. Site 4 ash shows two possible flows. The top flow has elevated T_c-heat, while the bottom flow does not appear to be increasing in T_c-heat, much like sites 1 and 3. Therefore, it is likely that the top flow was emplaced at or above ~300°C while the bottom flow was emplaced below ~300°C. Keeping in mind that site 2 is above site 3, this same sequence is observed in those two sites: a cooler flow is emplaced, followed by a somewhat hotter flow. If the tentative correlation between this study's sample sites and the flow units of Brand et al. (2014) is correct (Table 1), this suggests Brand et al.'s units I – IV were alternating cool-warm-cool-warm.

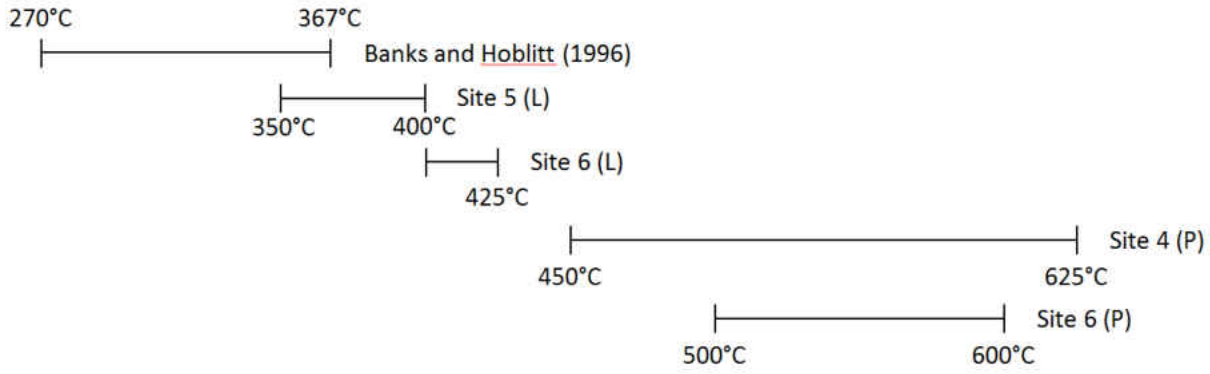

Figure 46. The range of emplacement temperature estimates from sites 4, 5, and 6 compared to range of minimum and maximum measured emplacement temperatures close to these sites by Banks and Hoblitt (1996) (top). It should be noted that the lithics (L) have a smaller range and are closer to the range of measured emplacement temperatures (Banks and Hoblitt, 1996) than the pumice (P).

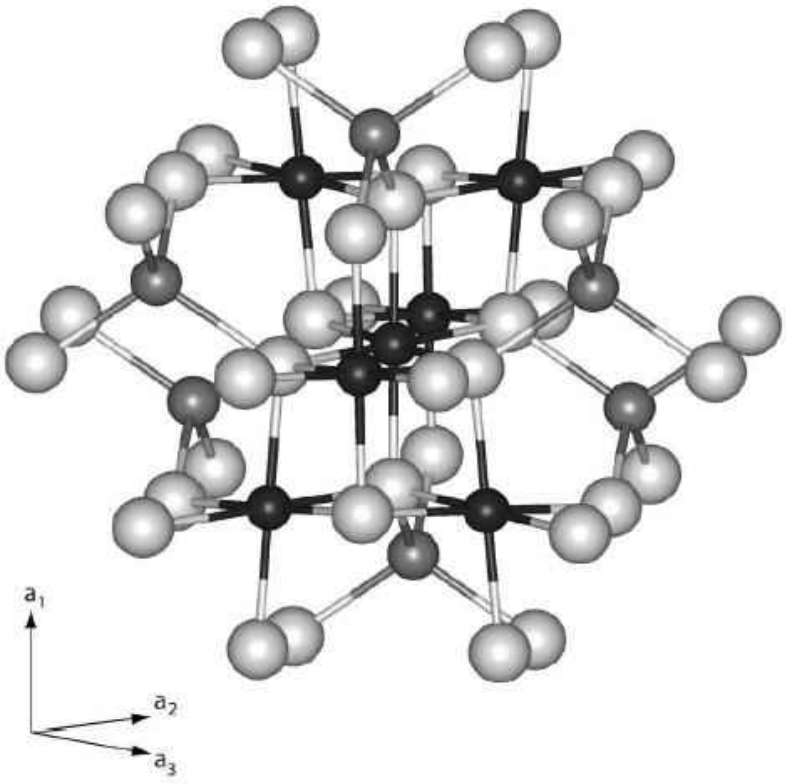

Figure 47. A ferrite spinel structure can be used as an analog for a titanomagnetite atomic structure (From Pattrick et al., 2002). The octahedral sites are the small black spheres, the tetrahedral sites are small gray spheres, and the oxygen atoms are the large light gray spheres.

Chapter 5: Conclusion

Goal #1 of this study was to examine how the temperature at which magnetization is removed varies with thermal history. Previously observed increases of T_c with depth were reflected in unblocking temperatures (Sec. 3.1). T_{ub}-max increased from 415°C to 465°C, which strongly indicated that this paleomagnetic technique could lead to overestimations of emplacement temperatures by up to ~40-50°C. The observed increase in T_b with depth is most plausibly explained by cation reordering during natural cooling.

Goal #2 was to determine to what extent this might bias emplacement temperature estimates. Titanomagnetite-bearing lithic and pumice fragments deposited during this eruption

were used to find the emplacement temperature of the 1980 flow using the paleomagnetic method of thermal demagnetization. Results were compared to emplacement temperatures measured by Banks and Hoblitt (1996). Where lithics are present they provide more accurate results than does pumice overestimating the measured emplacement temperature by ~40°C. Pumice provided the least accurate results due to MD effects and/or unidentified CRM and thus should be avoided. The current study demonstrates that the paleomagnetic method for determining emplacement temperatures of pyroclastic flows may lead to slight overestimates of up to 40-50°C.

Two likely reasons for the overestimation of emplacement temperatures include alterations and cation reordering. Although some samples may have altered during thermal demagnetization, this does not sufficiently explain all of the results. A model involving cation reordering during natural cooling is most consistent with the data.

Finally, examining how stratigraphic variations in magnetic properties might be used to estimate emplacement temperature was goal #3. It was shown that stratigraphic variations in T_c from matrix ash can provide crude estimates of emplacement temperature that may be useful, especially when no lithics are present. Using this technique, it was shown that the temperature of the first four May 18th PDC pulses oscillated between cooler and warmer temperatures.

References

Aramaki, S. and Akimoto, S., 1957, Temperature Estimation of Pyroclastic Deposits by Natural Remanent Magnetism: Am. J. of Science, v. 255, p. 619-627.

Banks, N.G. and Hoblitt, R.P., 1996, Direct Temperature Measurements of Deposits, Mount St. Helens, Washington, 1980-1981: U.S. Geol. Survey Prof. Paper, v. 1387, p. 1-76.

Bardot, L., 2000, Emplacement Temperature Determinations of Proximal Pyroclastic Deposits on Santorini, Greece, and Their Implications: Bull. Volcanol., v. 61, p.450-467.

Bardot, L. and McClelland, E., 2000, The Reliability of Emplacement Temperature Estimates Using Paleomagnetic Methods: A Case Study from Santorini, Greece: Geophys. J. Int., v. 143, p. 39-51.

Bol'shakov, A. S. and Shcherbakova, V.V., 1979, "Thermomagnetic Criterion of the Determination of Domain-Structure of Ferromagnetics": Izvestiya Akademii Nauk SSSR Fizika Zemli, v. 2, p. 38-47.

Bowles, J.A., Gee, J.S., Jackson, M.J., Avery, M.S., 2015, Geomagnetic Paleointensity in Historical Pyroclastic Density Currents: Testing the Effects of Emplacement Temperature and Postemplacement Alteration: Geochem. Geophys. Geosys., v. 16, p. 3607-3625, doi:// 10.1002/2015GC005910.

Bowles, J.A., Jackson, M.J., Berquó, T.S., Sølheid, P.A., and Gee, J.S., 2013, Inferred Time-and

Temperature-Dependent Cation Ordering in Natural Titanomagnetites: Nat. Comm., p. 1-9, doi:10.1038/ncomms2938.

Brand, B.D., Mackaman-Lofland, C., Pollock, N.M., Bendaña, S., Dawson, B., and Wichgers, P., 2014, Dynamics of Pyroclastic Density Currents: Conditions That Promote Substrate Erosion and Self-Channelization – Mount St Helens, Washington (USA): J. Volcanol. Geotherm. Res., v. 276, p. 189-214.

Brand, B.D., Bendaña, S., Self, S., and Pollock, N., 2016, Topographic Controls on Pyroclastic Density Current Dynamics: Insight from 18 May 1980 Deposits at Mount St. Helens, Washington (USA): J. of Volcanol. and Geotherm. Res., v. 321, p. 1-17.

Carey, S., Sigurdsson, H., Gardner, J.E., and Criswell, W., 1990, Variations in Column Height and Magma Discharge During the May 18, 1980 Eruption of Mount St. Helens: J. of Volcanol. and Geotherm. Res., v. 43, p. 99-112.

Chadwick, R.A., 1971, Paleomagnetic Criteria for Volcanic Breccia Emplacement: Geol. Soc. of Am. Bull., v. 82, p. 2285-2293.

Christiansen, R.L. and Peterson, D.W., 1981, “Chronology of the 1980 Eruptive Activity”: The 1980 Eruptions of Mount St. Helens, Washington: U.S. Geol. Surv. Prof. Pap., v. 1250, p. 17-30.

Clement, B.M., Connor, C.B., and Draper, G., 1993, Paleomagnetic Estimate of the

Emplacement Temperature of the Long-Runout Nevado de Colima Volcanic Debris Avalanche Deposit, Mexico: Earth Planet. Sci. Lett., v. 120, p. 499-510.

Criswell, C.W., 1987, Chronology and Pyroclastic Stratigraphy of the May 18, 1980 Eruption of Mount St. Helens, Washington: J. of Geophys. Res., v. 92, p. 10,237-10,266.

Denniss, A.M., Harris, A.J.L., Rothery, D.A., Francis, P.W., and Carlton, R.W., 1998, Satellite Observations of the April 1993 Eruption of Lascar Volcano: Int. J. Remote Sensing, v. 19, p. 801-821.

Doubrovine, P.V. and Tarduno, J.A., 2004, Self-Reversed Magnetization Carried by Titanomaghemite in Oceanic Basalts: Earth and Plan. Sci. Lett., v. 222, p. 959-969.

Fisher, R., 1953, Dispersion on a Sphere: Proceedings of the Royal Society of London, Series A, v. 217, p. 295-305.

Fisher, R.V., 1990, Transport and Deposition of a Pyroclastic Surge Across an Area of High Relief: The 18 May 1980 Eruption of Mount St. Helens, Washington: Geol. Soc. of Am. Bull., v. 102, p. 1038-1054.

Hoblitt, R. P., and Kellogg, K. S., 1979, Emplacement Temperatures of Unsorted and Unstratified Deposits of Volcanic Rock Debris as Determined by Paleomagnetic Techniques: Geol. Soc. of Am. Bull., v. 90, p. 633-642.

Jackson, M. and Bowles, J.A., 2014, Curie Temperatures of Titanomagnetite in Ignimbrites:

Effects of Emplacement Temperatures, Cooling Rates, Exsolution, and Cation Ordering: Geochem. Geophys. Geosys., v. 15, p. 1-26, doi:10.1002/2014GC0055

Kent, D.V., Ninkovich, D., Pescatore, T., and Sparks, S.R.J., 1981, Paleomagnetic Determination of Emplacement Temperature of Vesuvius AD 79 Pyroclastic Deposits: Nature, v. 290, p. 393-396.

Kirschvink, J.L., 1980, The Least-Squares Line and Plane and the Analysis of Paleomagnetic Data: Geophys. J. R. astr. Soc., v. 62, p. 699-718.

Kuntz, M.A., Rowley, P.D., and MacLeod, N.S., 1990, Geologic Maps of Pyroclastic-Flow and Related Deposits of the 1980 Eruptions of Mount St. Helens, Washington: U.S. Geol. Survey Pub., n. 1950.

Kuntz, M.A., Rowley, P.D., MacLeod, N.S., Reynolds, R.L., McBromme, L.A., and Kaplan, A.M., 1981, "The 1980 Eruptions of Mount St. Helens, Washington", Petrography and particle-sized distribution of pyroclastic-flow, ash-cloud, and surge deposits, v. 1250, p. 525-539.

Mandeville, C.W., Carey, S., Sigurdsson, H., and King, J., 1994, Paleomagnetic Evidence for High-Temperature Emplacement of the 1883 Subaqueous Pyroclastic Flows from Krakatau Volcano, Indonesia: J. Geophys. Res., v. 99, p. 9487-9504.

Mastrolorenzo, G., Petrone, P.P., Pagano, M., Incoronato, A., Baxter, P.J., Canzanella, A., and

Fattore, L., 2001, Herculaneum Victims of Vesuvius in AD 79: Nature, v. 410, p. 769-770.

Paterson, G.A., Roberts, A.P., Mac Niocaill, C., Muxworthy, A.R., Gurioli, L., Viramonté, J.G., Navarro, C., and Weider, S., 2010, Paleomagnetic Determination of Emplacement Temperatures of Pyroclastic Deposits: an Under-Utilized Tool: Bull. Volcanol., v. 72, p. 309-330, doi:10.1007/s00445-009-0324-4.

Pattrick, R.A.D., Van Der Laan, G., Henderson, C.M.B., Kuiper, P., Dudzik, E., and Vaughan, D.J., 2002, Cation Site Occupancy in Spinel Ferrites Studied by X-Ray Magnetic Circular Dichroism: Developing a Method for Mineralogists: European Journal of Mineralogy, v. 14, p. 1095-1102

Petrovský, E. and Kapička, A., 2006, On Determination of the Curie Point from Thermomagnetic Curves: J. Geophys. Res., v. 111, p. 1–10.

Pensa, A., Porecca, M., Corrado, S., Giordano, G., and Cas, R., 2015, Calibrating the pTRM and Charcoal Reflectance (Ro%) Methods to Determine the Emplacement Temperature of Ignimbrites: Fogo A Sequence, São Miguel, Azores, Portugal, as a Case Study: Bull. Volcanol., v. 77, p. 1-19, doi:10.1007/s00445-015-0904-4.

Rader, E., Geist, D., Geissman, J., Dufek, J., and Harpp, K., 2015, Hot Clasts and Cold Blasts: Thermal Heterogeneity in Boiling-Over Pyroclastic Density Currents: Geol. Soc. of London, v. 396, p. 67-86.

Sawada, Y., Sampei, Y., Hyodo, M., Yagami, T., and Fukue, M., 2000, Estimation of Emplacement Temperatures of Pyroclastic Flows Using H/C Ratios of Carbonized Wood: J. of Volcanol. and Geotherm. Res., v. 104, p. 1-20.

Sulpizio, R., Dellino, P., Doronzo, D.M., and Sarocchi, D., 2014, Pyroclastic Density Currents: State of the Art and Perspectives: J. of Vol. and Geotherm. Res., v. 283, p. 36-65, doi: 10.1016/j.jvolgeores.2014.06.014.

Tauxe, L., Shaar, R., Jonestrask, L., Swanson-Hysell, N.L., Minnett, R., Koppers, A.A.P., Constable, C.G., Jarboe, N., Gaastra, K., and Fairchild, L., 2016, PmagPy: Software Package for Paleomagnetic Data Analysis and a Bridge to the Magnetics Information Consortium (MagIC) Database: Geochem. Geophys. Geosys., v. 17, p. 1-14, doi:10.1002/2016GC006307.

Tauxe, L., and Staudigel, H., 2004, Strength of the Geomagnetic Field in the Cretaceous Normal Superchron: New Data from Submarine Basaltic Glass of the Troodos Ophiolite: Geochem. Geophys. Geosys., v. 5, p. 1-16, doi:// 10.1029/2003GC000635.

Uehara, D., Cas, R.A.F., Folkes, C., Takarada, S., Oda, H., and Porreca, M., 2015, Using Thermal Remanent Magnetisation (TRM) to Distinguish Block and Ash Flow and Debris Flow Deposits, and to Estimate Their Emplacement Temperature: 1991-1995 Lava Dome Eruption at Mt. Unzen Volcano, Japan: J. of Volcanol. and Geotherm. Res., v. 303, p.

92-111.

Voight, B., and Davis, M.J., 2000, Emplacement Temperatures of the November 22, 1994 Nuée Ardente Deposits, Merapi Volcano, Java: J. of Volcanol. and Geotherm. Res., v. 100, p.371-377.

Wright, J.V., 1978, Remanent Magnetism of Poorly Sorted Deposits from the Minoan Eruption of Santorini: Bull. Volcanol., v. 41, p. 131-135.

Appendix A

This appendix shows the demagnetization data from the lithic samples that underwent thermal demagnetizations to find emplacement temperature estimates.

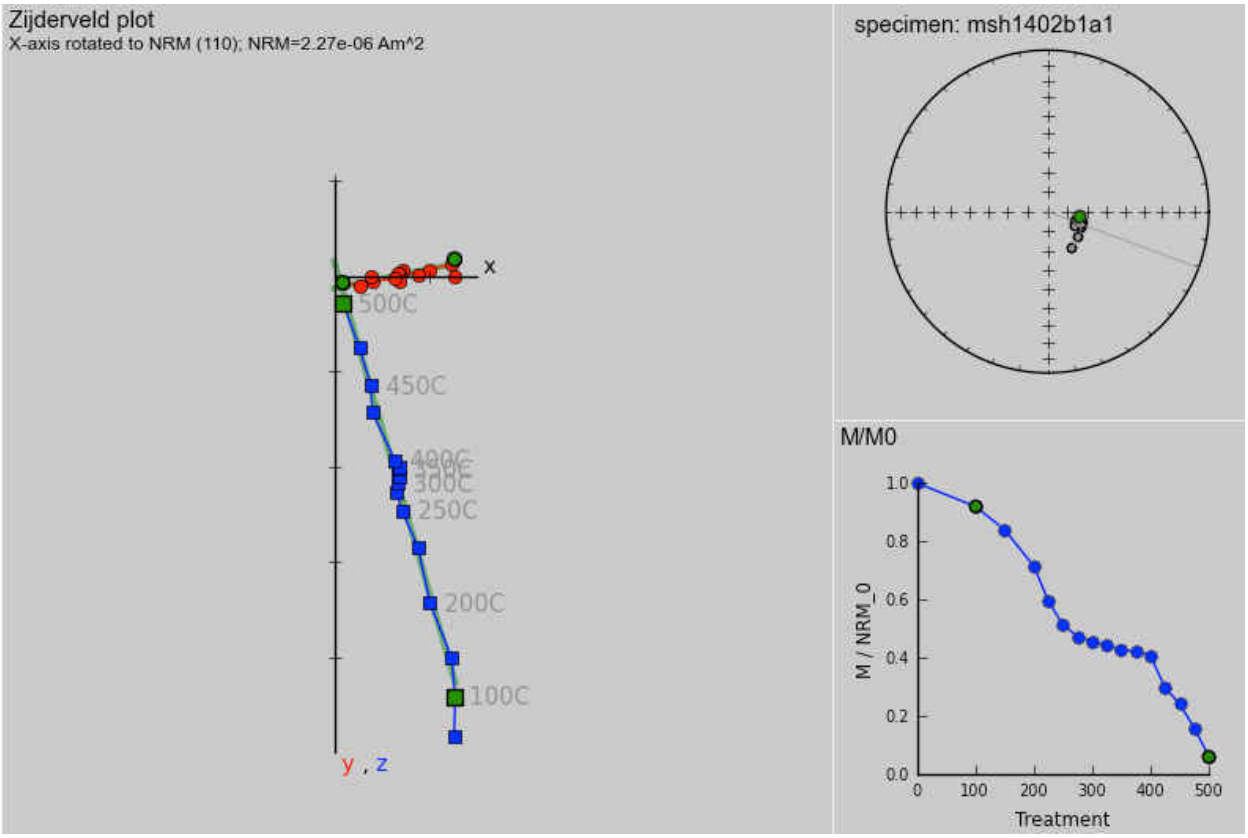

Figure A1. Sample B1a1 from site 2 has one magnetic components as seen in the Zijderveld plot with the emplacement temperature of the sample the temperature at which the one magnetic component is removed (500°C). The low temperature component's orientation is shown as a green dot on the stereonet, and its demagnetization curve is shown below the stereonet (green dots show the demagnetization of the low-temperature component).

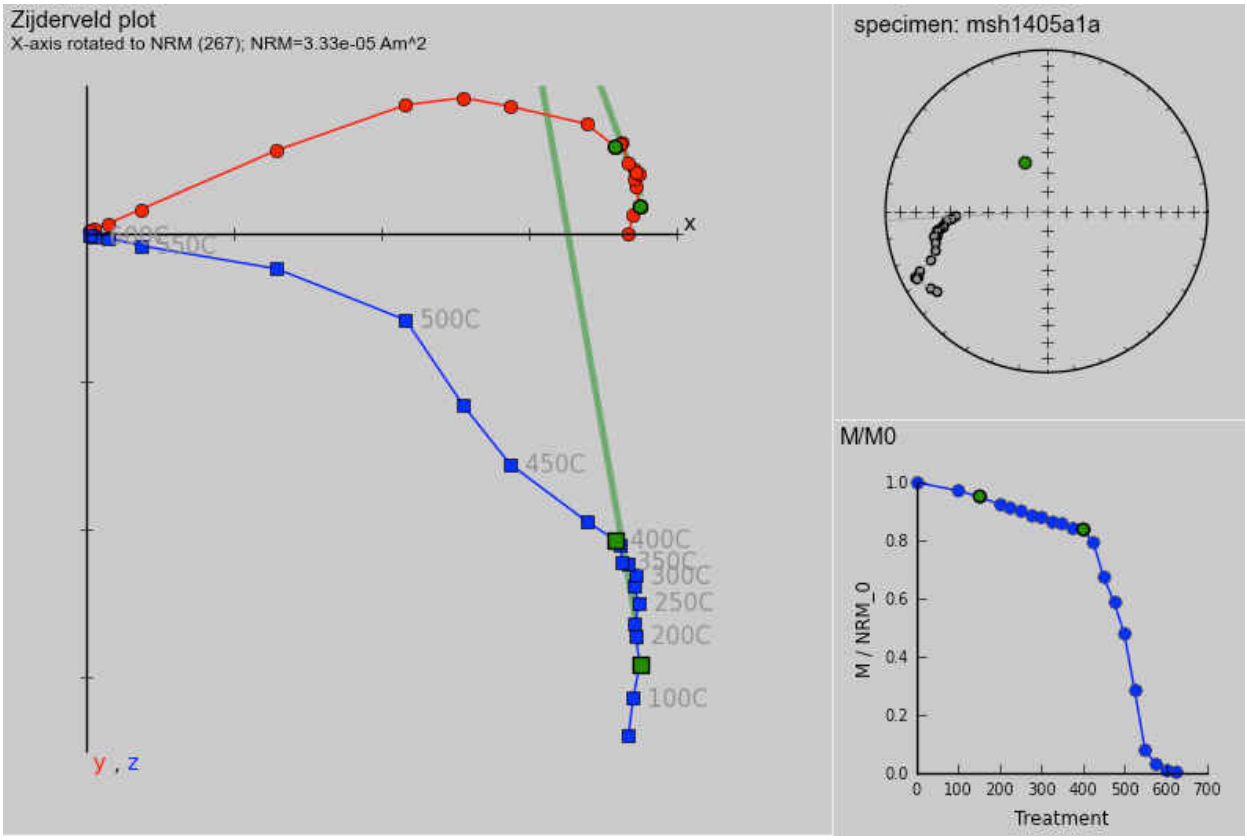

Figure A2. Sample A1a from site 5 has three magnetic components as seen in the Zijderveld plot with the emplacement temperature of the sample the temperature at which the low temperature magnetic component is removed (400°C). Symbols as in Figure A1.

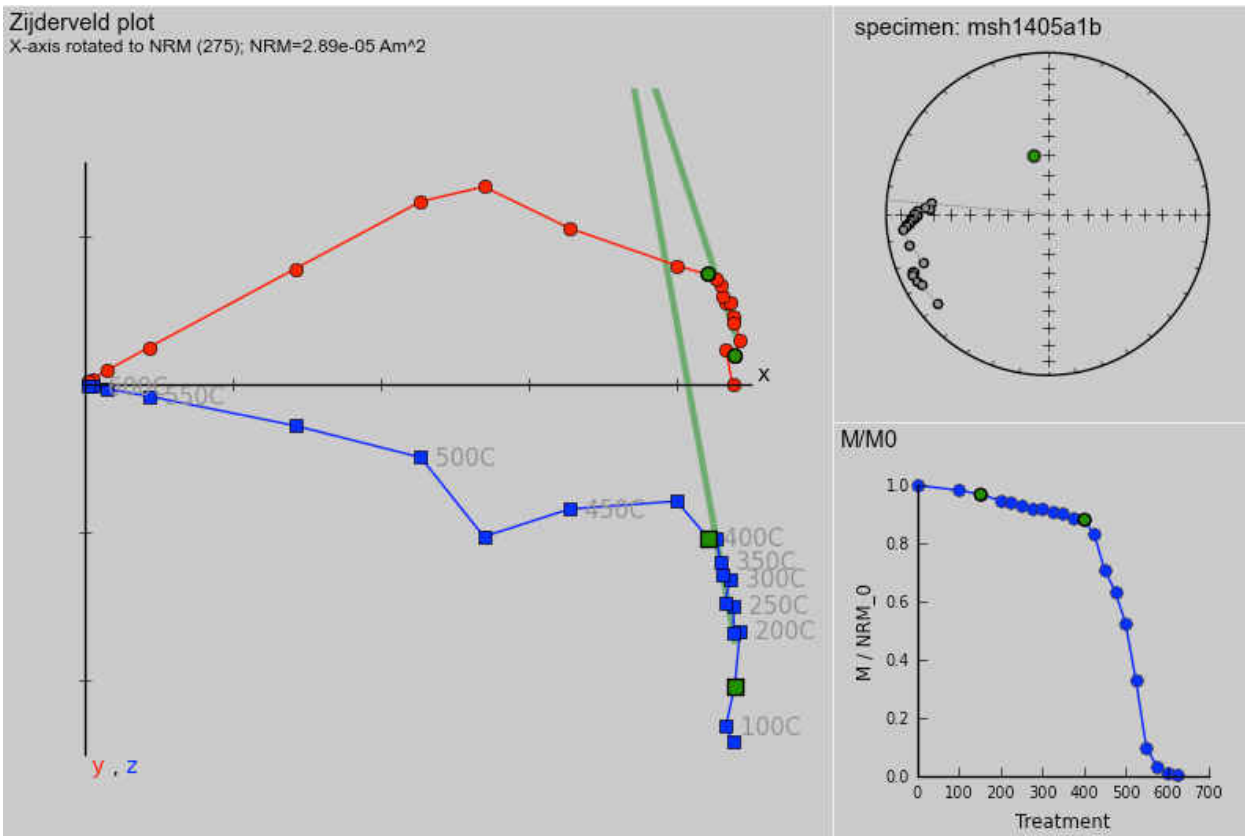

Figure A3. Sample A1b from site 5 has two magnetic components as seen in the Zijderveld plot with the emplacement temperature of the sample the temperature at which the low temperature component is removed (400°C). Symbols as in A1.

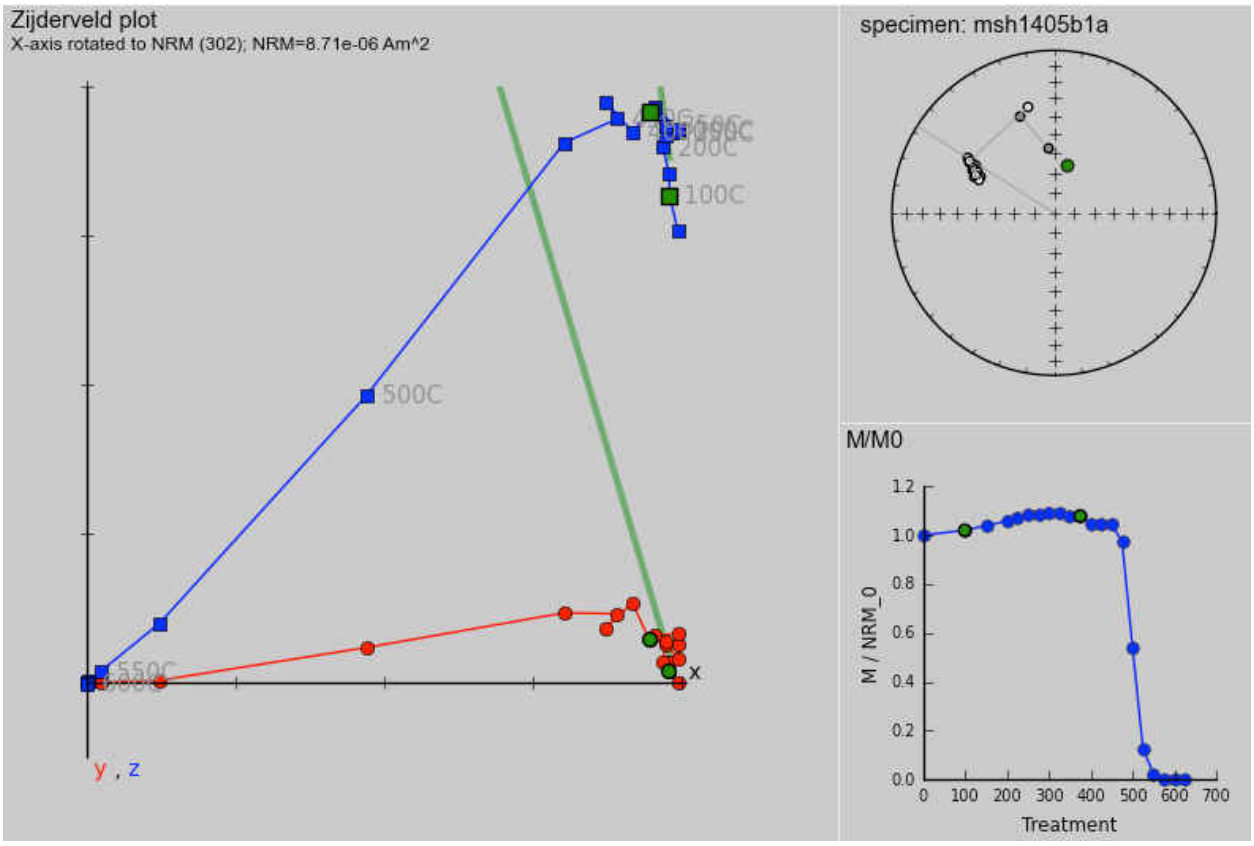

Figure A4. Sample B1a from site 5 has two magnetic components as seen in the Zijderveld plot with the emplacement temperature of the sample the temperature at which the low temperature component is removed (375°C). Symbols as in A1.

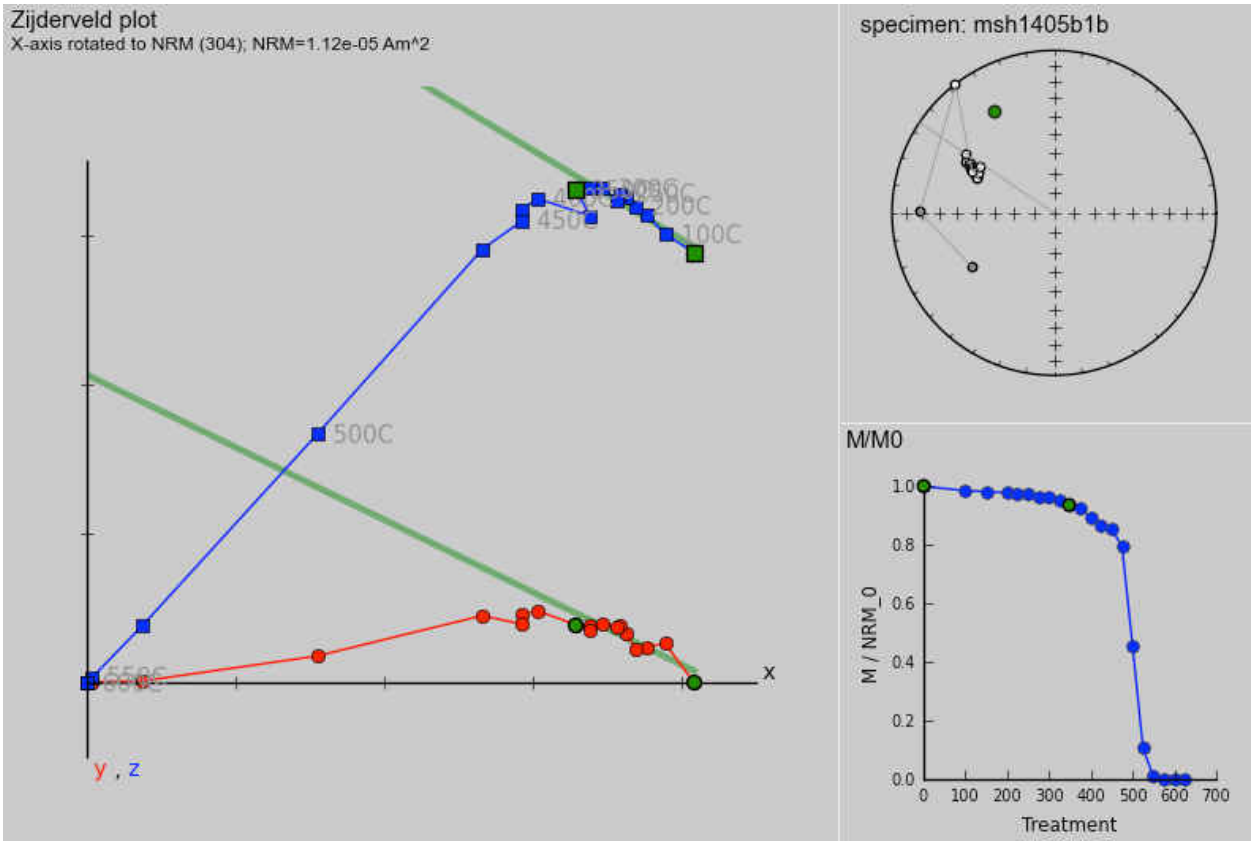

Figure A5. Sample B1b from site 5 has two magnetic components as seen in the Zijderveld plot with the emplacement temperature of the sample the temperature at which the low temperature component is removed (350°C). Symbols as in A1.

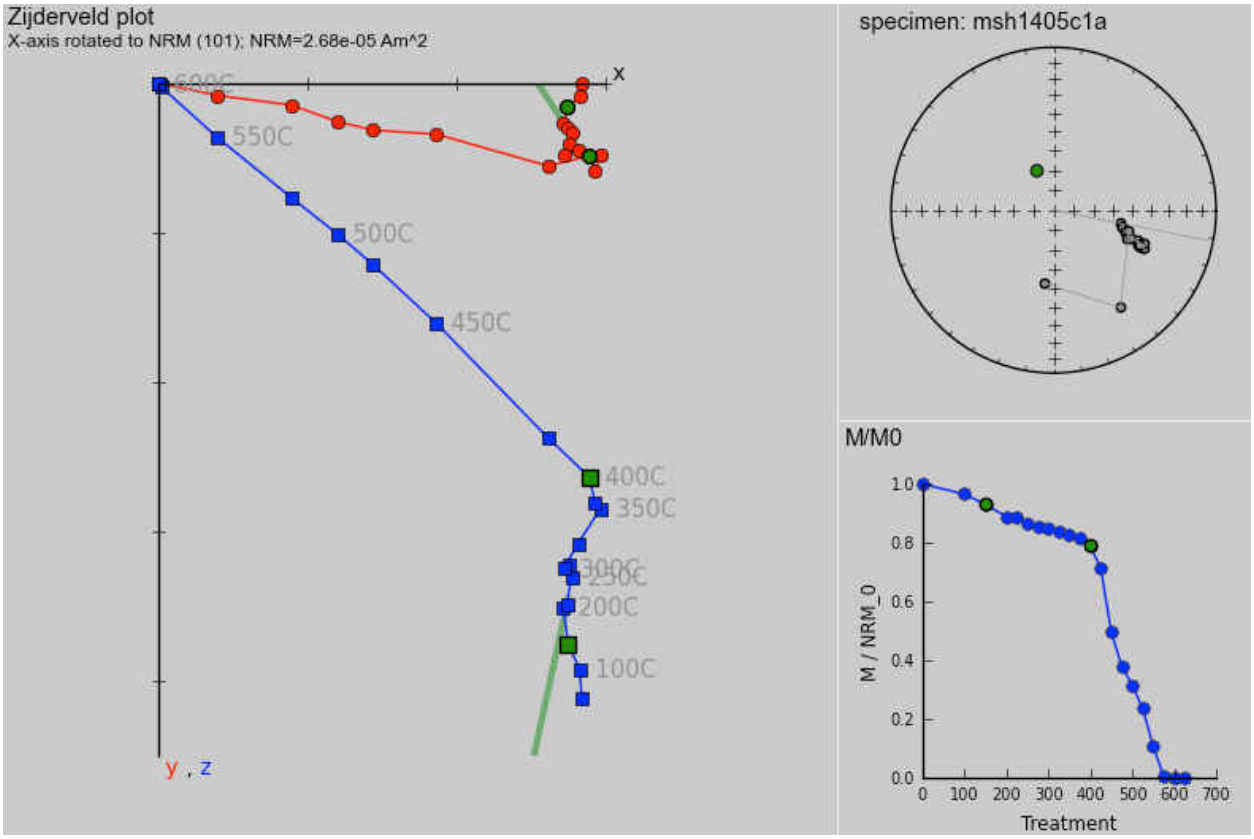

Figure A6. Sample C1a from site 5 has two magnetic components as seen in the Zijderveld plot with the emplacement temperature of the sample the temperature at which the low temperature component is removed (400°C). Symbols as in A1.

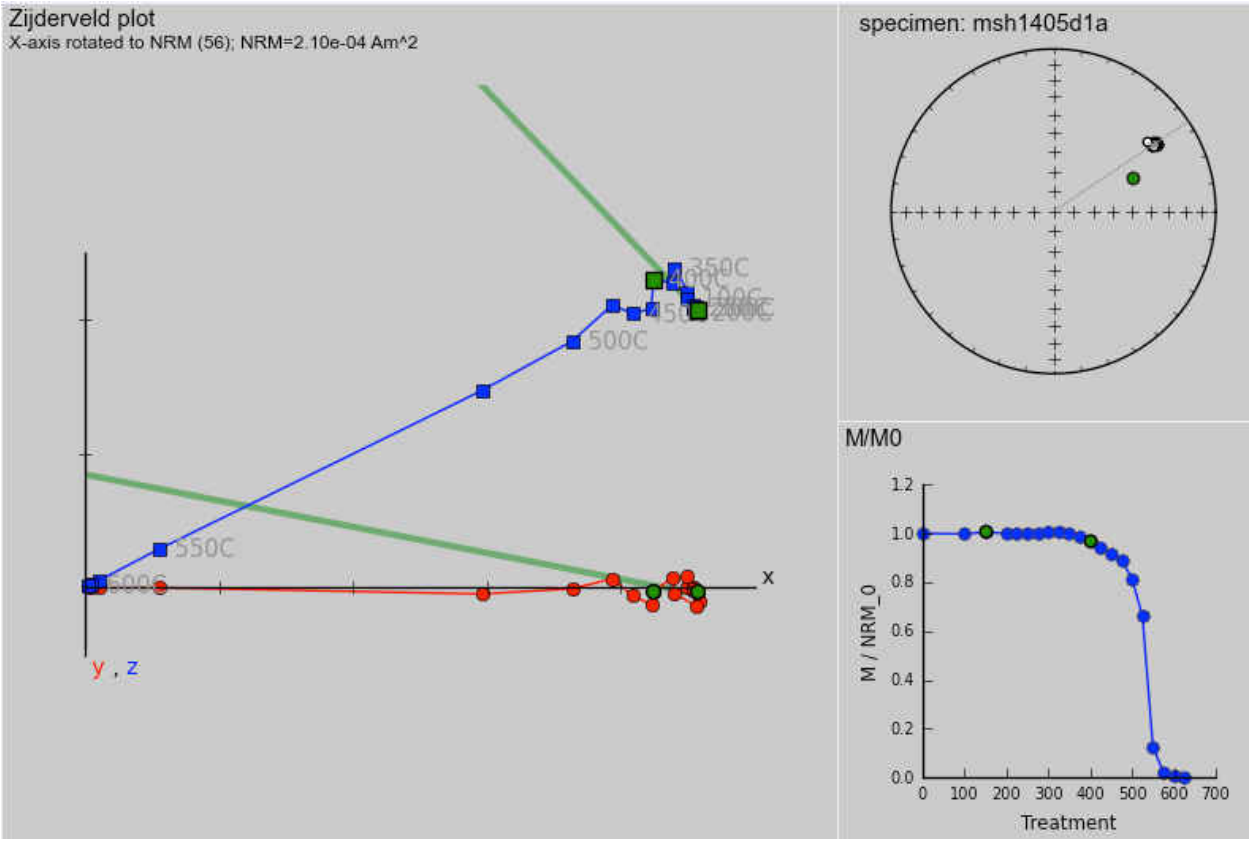

Figure A7. Sample D1a from site 5 has two magnetic components as seen in the Zijderveld plot with the emplacement temperature of the sample the temperature at which the low temperature component is removed (400°C). Symbols as in A1.

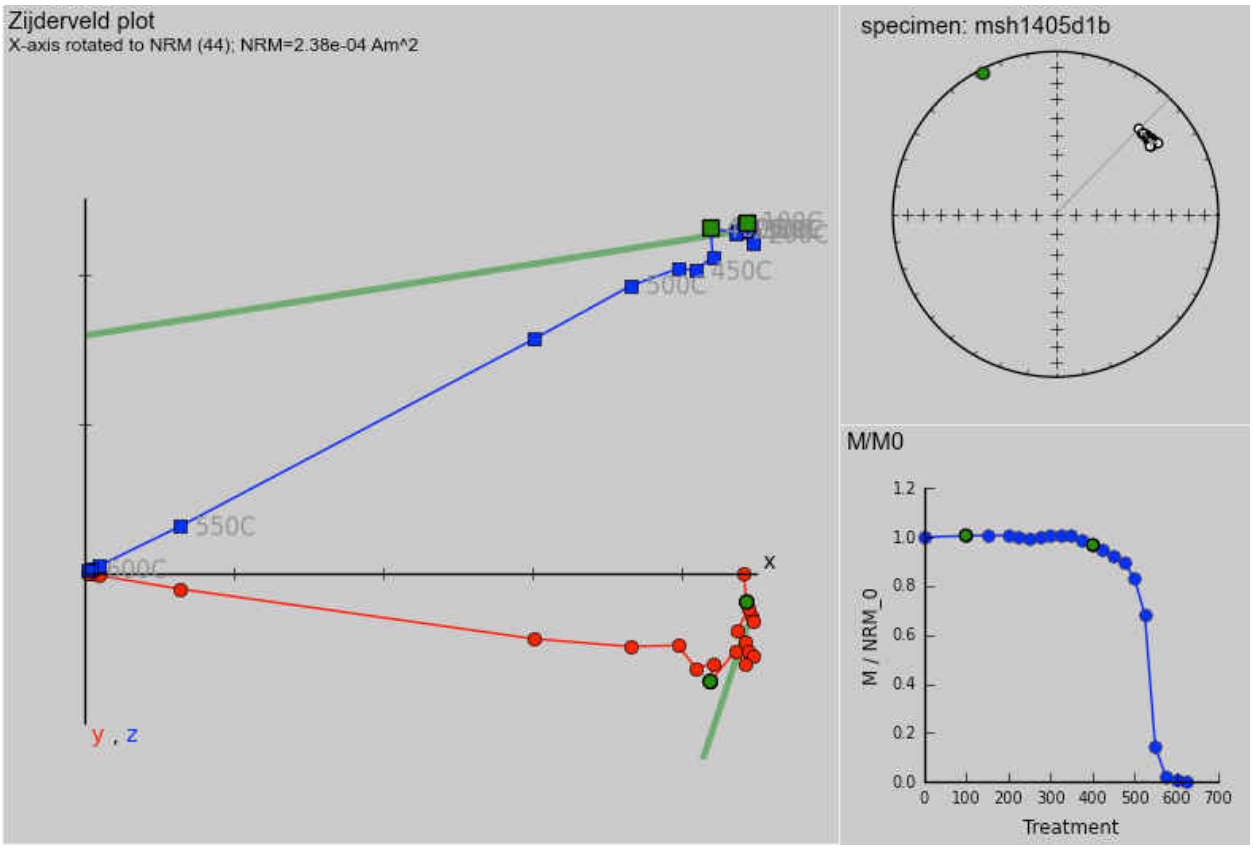

Figure A8. Sample D1b from site 5 has two magnetic components as seen in the Zijderveld plot with the emplacement temperature of the sample the temperature at which the low temperature component is removed (400°C). Symbols as in A1.

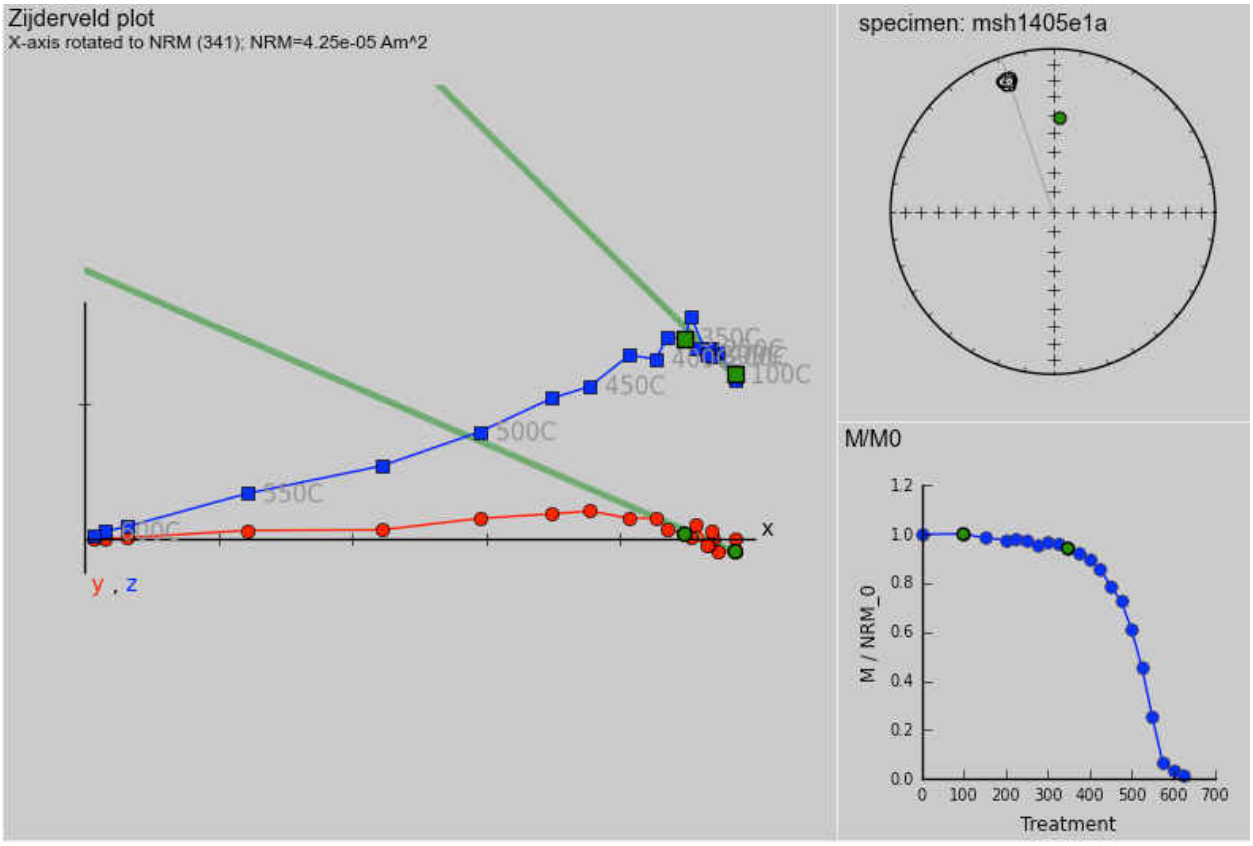

Figure A9. Sample E1a from site 5 has two magnetic components as seen in the Zijderveld plot with the emplacement temperature of the sample the temperature at which the low temperature component is removed (350°C). Symbols as in A1.

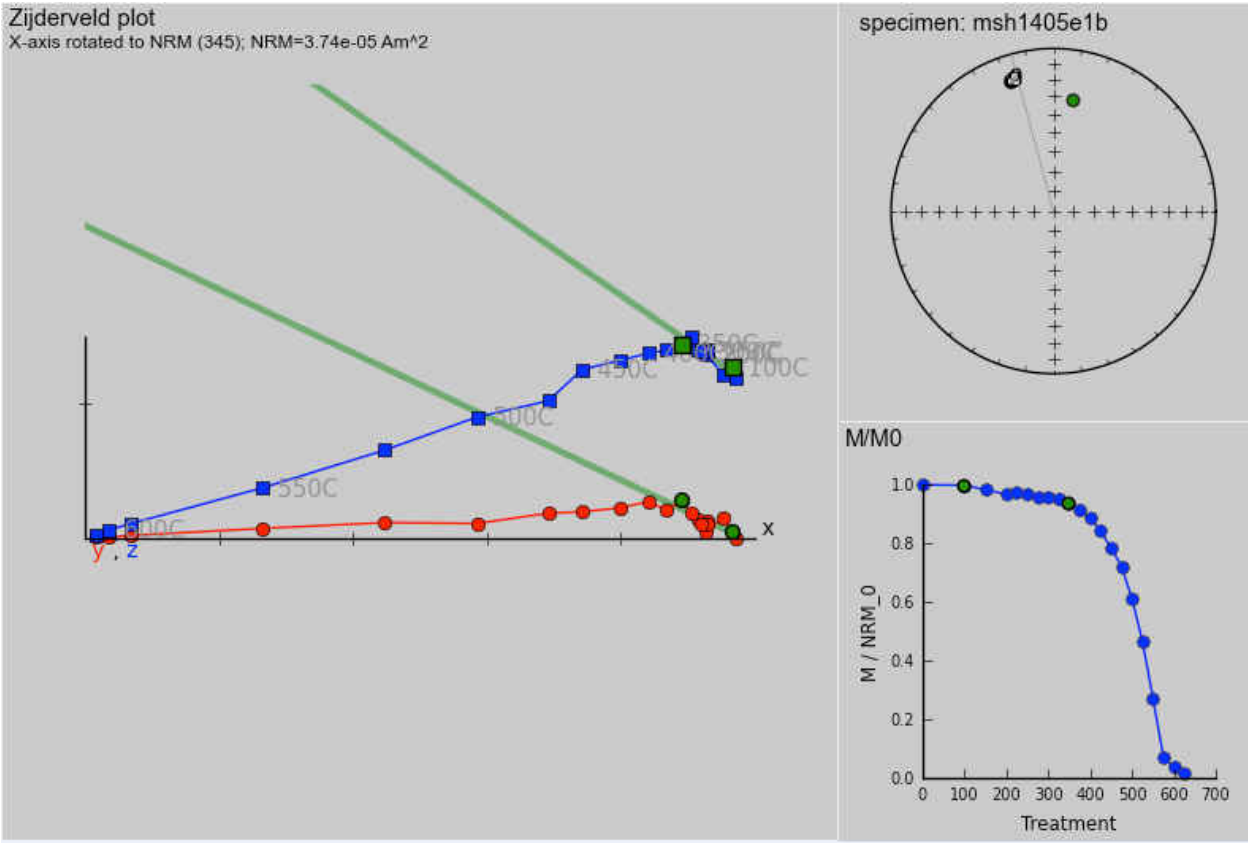

Figure A10. Sample E1b from site 5 has two magnetic components as seen in the Zijderveld plot with the emplacement temperature of the sample the temperature at which the low temperature component is removed (350°C). Symbols as in A1.

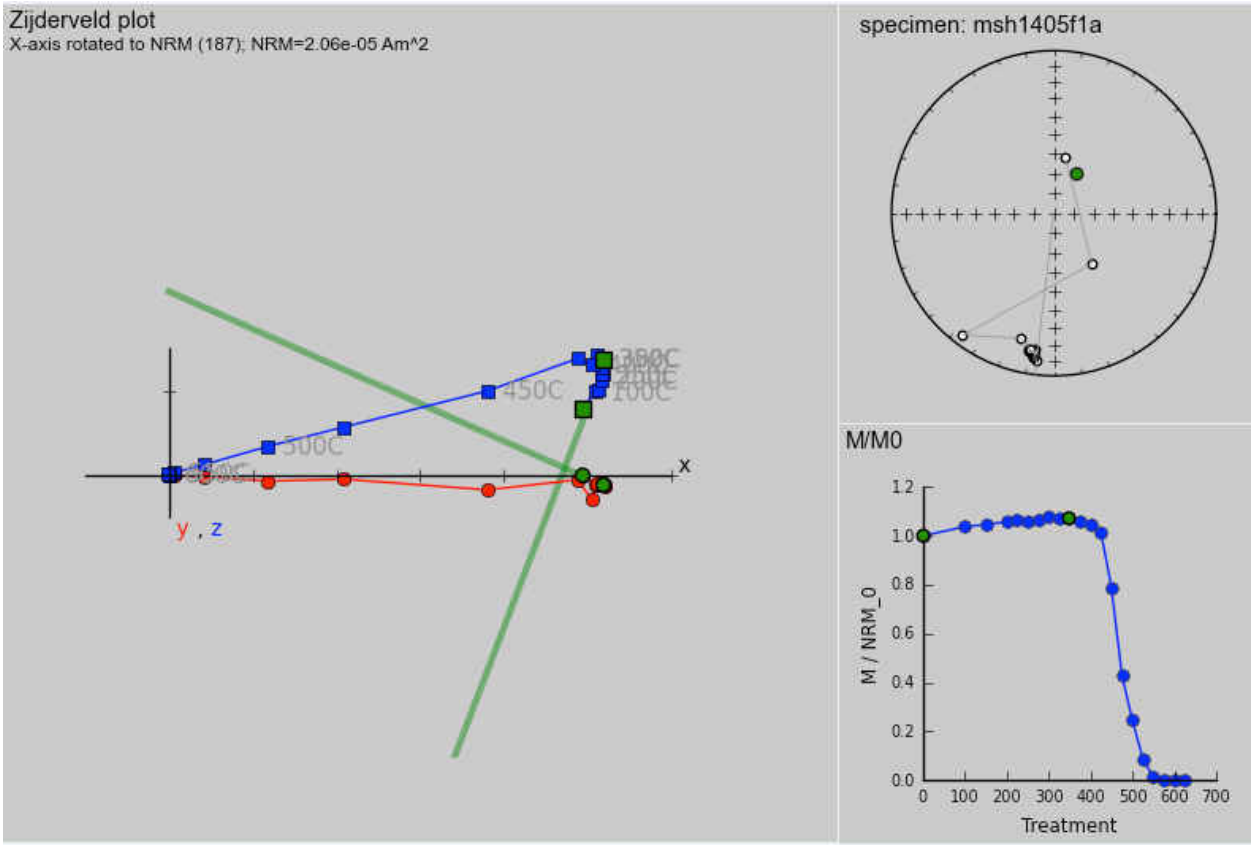

Figure A11. Sample F1a from site 5 has two magnetic components as seen in the Zijderveld plot with the emplacement temperature of the sample the temperature at which the low temperature component is removed (350°C). Symbols as in A1.

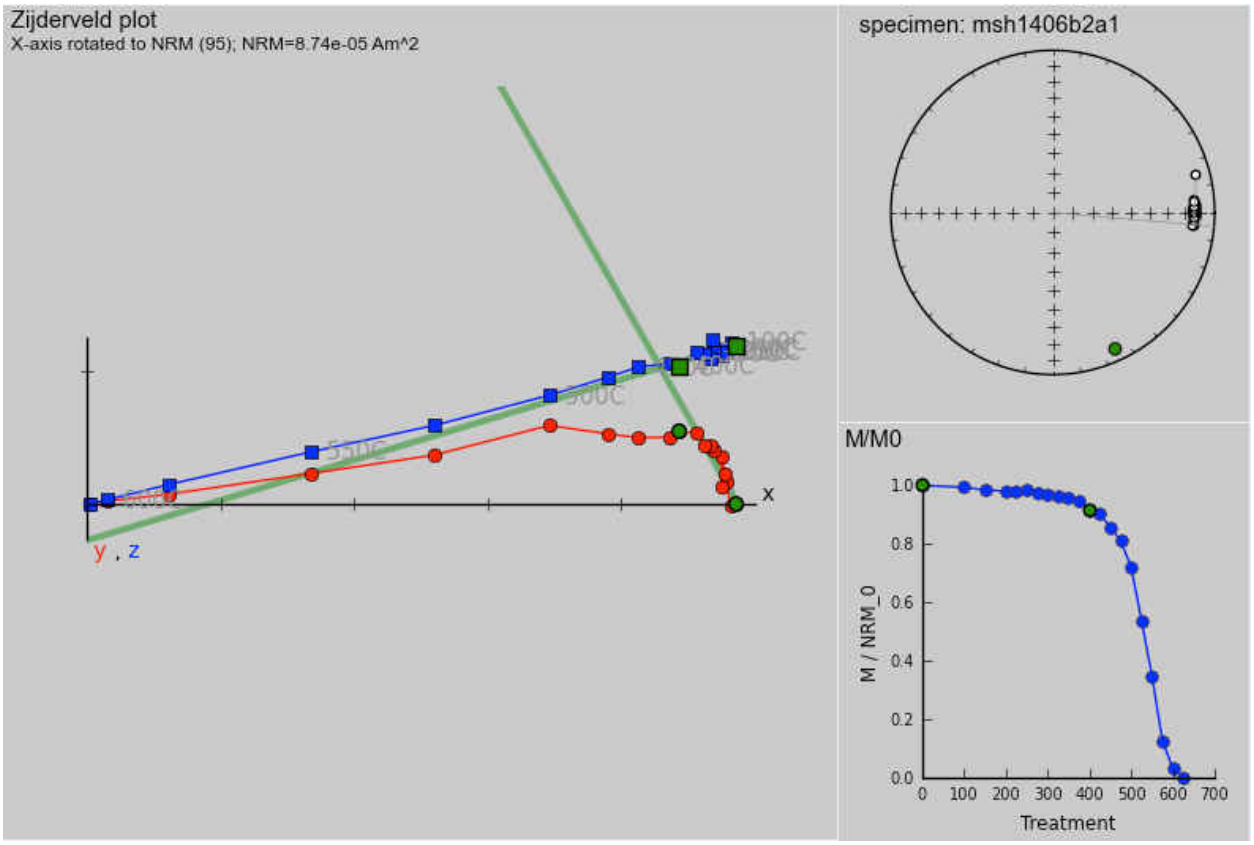

Figure A12. Sample B2a1 from site 6 has two magnetic components as seen in the Zijderveld plot with the emplacement temperature of the sample the temperature at which the low temperature component is removed (400°C). Symbols as in A1.

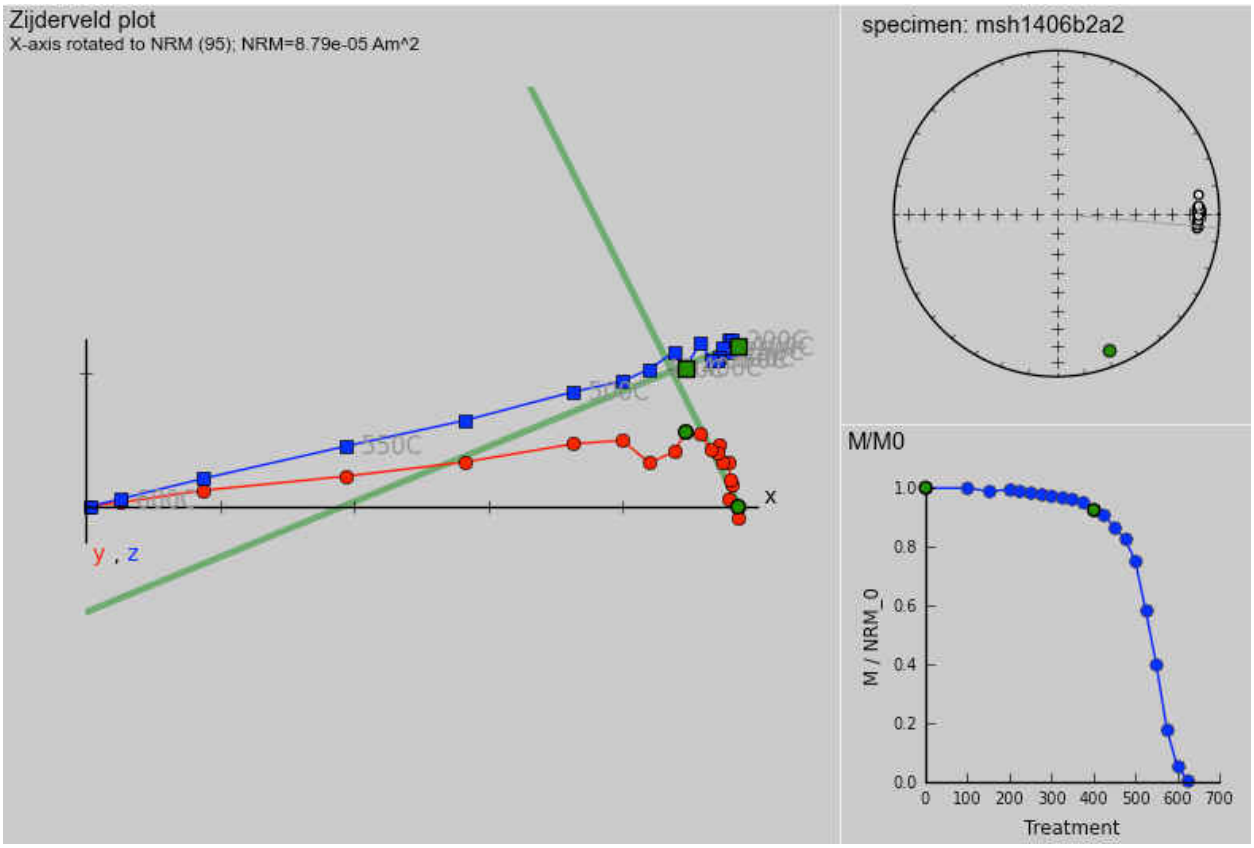

Figure A13. Sample B2a2 from site 6 has two magnetic components as seen in the Zijderveld plot with the emplacement temperature of the sample the temperature at which the low temperature component is removed (400°C). Symbols as in A1.

Appendix B

This appendix contains Curie temperature picks from Kappabridge measurements (susceptibility as a function of temperature) for Sec. 3.5. T_{c1} data points show dominant T_cs and T_{c2} indicates secondary T_cs much higher in temperature than T_{c1}. T_c-heat is T_c measured on warming. T_c-cool is T_c measured on cooling.

Table B1. Data for site 1 ash Kappabridge measurements.

Sample	Depth (cm)	Tc1-heat	Tc2-heat	Tc1-cool	Tc2-cool
0	0	386.5333	518.5	375.8	535
12	12	385.5167	513.6	376.3	522.5
20	20	382.5	537.7	371.6	519.6
30	30	382.9167	523.1	374.0833	525.8
40	40	379.6833	520.9	378.25	528.5
50	50	380.25		376.9667	
60	60	384.5667	511.8	378.5	561.1
70	70	386.2	507.8	376.9	559.9
80	80	387.8167	520.1	382.6667	525.6
90	90	390.7667	513.9	382.95	558.9
100	100	391.65	510.2	379.1	515.1

Table B2. Data for site 2 ash Kappabridge measurements.

Sample	Depth (cm)	Tc1-heat	Tc2-heat	Tc1-cool	Tc2-cool
15-20 above 0	-17.5	405.4333		361.55	
0	0	370.35		374.05	
10	10	376.15		377.3667	
20	20	379.85	482.3	377.8167	534
30	30	393.1	486.4	376.75	536.6
40	40	393.6667	482.9	380.7	526.2
50	50	401.15	485.5	377.95	523.8
60	60	402.8	516.4	382.8167	521.1
70	70	408.55	482.3	377.1667	526.8
80	80	408.6	480.2	381.0333	527.7
90	90	410.7	515.9	379.9167	530.4
100	100	415.6833		375.9	
110	110	411.1167	482.2	381.7	535.3
120	120	416.15	484.3	381	535.2
130	130	420.35	510.1	375.6	561.4
140	140	417.1167	483.8	379.9667	530.2
150	150	423.05	482	382.1	562.8

Table B3. Data for site 3 ash Kappabridge measurements.

Sample	Depth (cm)	Tc1-heat	Tc2-heat	Tc1-cool	Tc2-cool
ash overlay	-0.5	378.5	501.4	370.0667	
0	0	375.35	499.6	374.6667	
5	5	380.8	504.6	371.45	522.8
10	10	376.3333	503	367.9	
15	15	376.7833	508.6	370.6	
20	20	378.35	501.9	372.2167	
25	25	380	506	369.5	470.2
30	30	378.85	507.2	370.4	
35	35	380.85	502.4	370.25	
40	40	378.8	499.2	370.5	
45	45	387.7167	512.6	375.35	
50	50	384.8667	506	372.95	
60	60	380.0667	508.1	375.15	
70	70	381.4333	505.1	368.2	
80	80	384.5667	498.1	367.8833	546.2
90	90	381.8667	503.9	373.35	
100	100	382.4167	505.6	370.4	
110	110	386.05	504.2	371.7	530.4

Table B4. Data for site 4 ash Kappabridge.

Sample	Depth (cm)	Tc1-heat	Tc2-heat	Tc1-cool	Tc2-cool
-45	-45	391.3	508.3167	367.5	522.6
-30	-30		513.5833		523.85
-25	-25	422.2		372.1833	
-20	-20	442.45			507.8667
-15	-15	424.0167	515.8	368.8	508.2
-10	-10	422.2		371.45	
-5	-5	416.4		376.7	
-1	-1	361.3	515.3833	370.4	518.6667
0	0	406.95	519.7	371.3	513.8
5	5	368.2	507.6667	373.85	531.8
11	11	360.9	509.7	372.3167	514.7
17.5	17.5	364	512.7833	371.05	523.9
20	20	358.3	506.7667	366	512
25	25	370.3	515.2333	374.9	521.4167
30	30	356.8	513.7333	370.6	527.6
35	35	367	516.4	371	520.6167
40	40	363.7	517.9167	371.5	523.15
45	45	396.3	518.7667	369.65	521.9
50	50	360.2	525.05	372.9	534.15
52	52		520.5167		526.45

Table B5. Data for site 6 ash Kappabridge measurements.

Sample	Depth (cm)	Tc1-heat	Tc2-heat	Tc1-cool	Tc2-cool
0	0	418.9333	510.4	374.95	524.4
2	2	412.95	462.9	372.5167	514.7
5	5	416.35	515.3	379.0333	521
10	10	413.25		374.9167	
15	15	412.9167		376.45	
20	20	410.3667	519.4	374.9	522.2
25	25	415.0333	510.9	378.4	522.2
30	30	413.5167	508.7	378.3	521.2
35	35	412.2	505.8	373.2	519.9
40	40	414.45	506.5	376.5333	525.9
45	45	416.2	511.1	379.4	477.4
50	50	415	475.7	380.3	525.1
60	60	414.7	515.5	378.65	521.3
70	70	421.55		383.95	
80	80	418.7	506.3	379	521.8
90	90	423.9	469.1	381.0833	515.2
100	100	423.85	509.9	375.2333	520.6
110	110	426.95	510.5	379.2	515
120	120	430.6		377.4	
130	130	431		376.9167	
140	140	430.55	506.9	373.7	515.4
150	150	429.95	504.6	375.4	519.6

Table B6. Data for site 4 pumice Kappabridge measurements.

Sample	Depth (cm)	Tc1-heat	Tc2-heat	Tc1-cool	Tc2-cool
M1	-42	343.7167		345.6667	
L1	-2	367.45		348.35	
J2	15	425.75		367.2833	
J3	15	424.2167		365.9	
K1	19	463.8		483.0667	
J1	20	433.6	379.3	367.15	338
I1	28	430.75		351.3167	
G2	32	435.8		370.1167	
H1	33	385.1167		344.8	
E1	40	442.85		370.35	
F1	42	434.35		363.4167	
F2	42	438.55		365.2167	
D2	43	410.15		365.75	
D1a	43	392.95		356.3	
D1b	43	389.2333		358.8167	
C1	55	432.35	378	367	338.3
N1	67	530.75	435.7	514.8333	334.8
B1	72	389.6		344.0833	
A2-top	75	522.25		504.6667	
A1	77	526.9		512	

Table B7. Data for site 8 pumice Kappabridge measurements.

Sample	Depth (cm)	Tc1-heat	Tc1-cool
0-10	5	361.9	361.25
15	15	399.4167	368.95
20	20	402.2	374.9
30	30	420.1	371.6
35	35	435.55	375.7
58	58	455.05	388.4
65	65	460.7167	385.4167
70	70	460.0167	374.55
90	90	465.0333	374.7667